

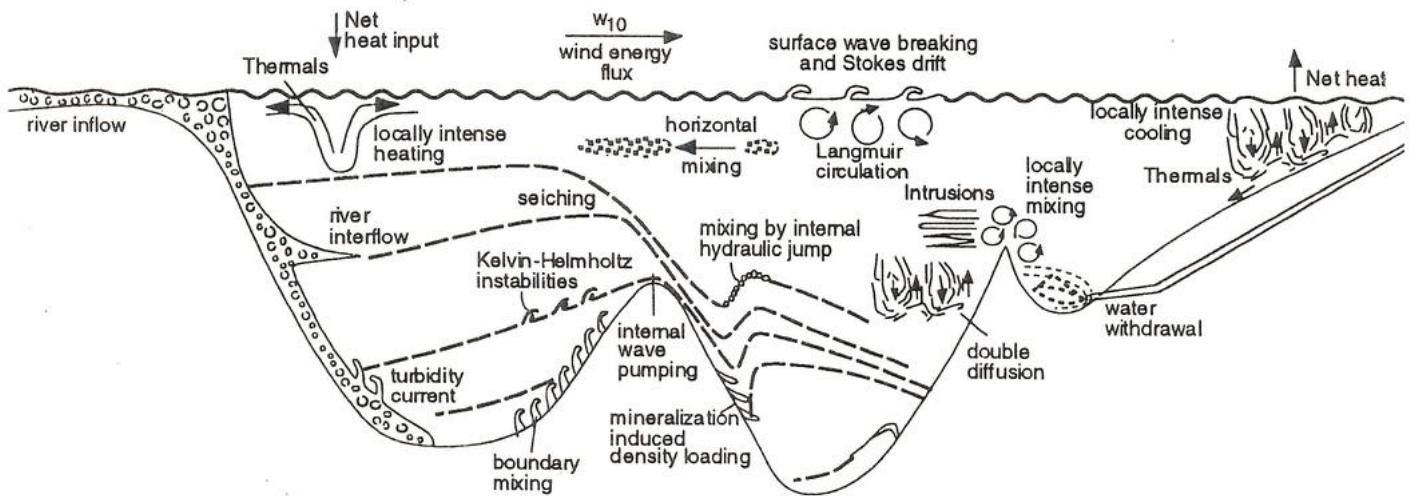


CEC Joint Research Centre

2nd Workshop on “Physical Processes in Natural Waters”

3-5 November 1997, JRC

I-21020 Ispra, Italy



Organisation: Anna Fontana, Francoise Thunis, Adolf Stips

2nd Workshop on “Physical Processes in Natural Waters”

3-5 November 1997, JRC

I-21020 Ispra, Italy

Program

Monday, November 3, 1997 10:45 - 18:00

Boundary Layer Processes and Turbulence

Chair: Alfred Wuest
Walter Eifler

Tuesday, November 4, 1997

Physical Dynamics in Natural Waters

Chair: Erich Baeuerle
Elena Roget

Wednesday, November 5, 1997

Coupling of Biological, Chemical, Optical and Physical Dynamics

Chair: Tom Osborn
Helmut Baumert

2nd Workshop on “Physical Processes in Natural Waters”

Final Program

15 October, 1997

Monday, November 3, 1997	10:45 - 18:00
Boundary Layer Processes and Turbulence	Chair: Alfred Wuest Walter Eifler
Tuesday, November 4, 1997	
Physical Dynamics in Natural Waters	Chair: Erich Baeuerle Elena Roget
Wednesday, November 5, 1997	
Coupling of Biological, Chemical, Optical and Physical Dynamics	Chair: Tom Osborn Helmut Baumert
Monday, November 3, 1997	
Boundary Layer Processes and Turbulence	
10:45	Opening of workshop by Director of Space Applications Institute (Rudolf Winter)
Chair:	Alfred Wuest
11:00	M. Thiele: Turbulence characteristics in a small river derived from in-situ measurements with a 3D-acoustic Doppler velocimeter
11:30	C. Zuelicke and E. Hagen Impact of the skin effect on the near surface temperature profile
12:00	W. Eifler: Fluctuating fields due to wave breaking
12:30 - 14:00	Lunch break
Chair:	W. Eifler
14:00	M. Regener, H. Baumert Simulating Flow, Turbulence, Waves, Seiches and SPM in Tidal and Inland Waters by 1D Models

14:30
A. Wuuest, A. Simon
Energy transfer efficiency from wind to waves and into the surface layer of natural waters

15:00
H. Burchard, A. Stips
A 1D reduction of a 3D estuarine model for simulating dissipation rate measurements in the Eastern Scheldt.

15:30 Coffee break

16:00
O. Kocsis, H. Prandke
Comparison of dissipation of turbulent kinetic energy determined by shear and temperature microstructure

16:30
B. Boehrer:
Modelling the salinity profile in the developing lakes of an open-cast mine under consideration of the lakes' dynamics and the groundwater flow

17:00 Short contributions and discussion/summary by conveners

18:00 End of first day

Tuesday November 4, 1997
Physical Dynamics in Natural Waters

Chair: Elena Roget

09:00
R. Jiang, S. Thorpe, U. Lemmin:
On progressive internal waves in Lake Geneva

09:30
A. Lorke
Horizontal distribution of mixing and stratification in a shallow lake

10:00 **O. Malve, M. Virtanen**
Water Renewal of Pojo Deep Waters

10:30 Coffee break

11:00
M. Lilover, U. Lips, J. Laanearu
Periodic components in the flow of the Irbe strait and their contributions to the water exchange

11:30
E. Baeuerle
Circulation patterns in lake Constance induced by local wind fields

12:00 E. Hollan:
Lateral renewal of deep water in Lake Constance by convective cooling in winter over ascending bottom

12:30 **Lunch break**

Chair: Erich Baeuerle

14:00 S. Dobrocić, W. Eifler
Modelling the Adriatic Sea under consideration of the orographic peculiarities

14:30 E. Roget, J. Colomer, R. Juanola
Second-step inhomogeneities in a lake due to differential cooling

15:00 B. Rasmussen, A. Stips
Upper Water Column Dissipation and Stability in the View of External Forcing

15:30 Coffee break

16:00 M. Shimaraev, V. Domisheva, L. Gorbunova
Limnic role of exchange processes in lake Baikal

16:30 N. Granin:
Nonlinear effects of buoyancy near the temperature of maximum density and examples of thermobaric instability

17:00 P. Sherstyankin, L. Kuimova, V. Potemkin
Main features in the T/S regime of deep water zone in Lake Baikal

17:30 Short contributions and discussion/summary by conveners
P. Sherstyankin, L. Kuimova
The frontogenesis in the deep water reservoirs of Lake Baikal

18:30 End of second day

20:00 **Joint Dinner**

Wednesday, November 5, 1997

Coupling of Biological, Chemical, Optical and Physical Dynamics

Chair: Tom Osborn

- 09:00
T. Osborn:
Microstructure, Finestructure and Thin Layers; Physics, Chemistry and Biology
- 09:30
H. Baumert:
Photoadaptation of Phytoplankton in Turbulent Water Bodies: Modelling the Coupling of Hydrophysics and Biology
- 10:00
E. Marmefeldt
SCOBI - the Swedish coastal/ocean biogeochemical model
- 10:30 Coffee break
- 11:00
S. Semovski, M. Grachev, P. Sherstyankin, M. Shimaraev
Bio-optical model of Lake Baikal phytoplankton: its application to paleolimnological studies
- 11:30
U. Franke
A physical-biological model for algal dynamics in lakes
- 12:00
S. Tassan
A procedure to determine shallow water quality from thematic mapper data
- 12:30 **Lunch break**
- Chair: Helmut Baumert
- 14:00
D. Pierson, N. Stroembeck
Estimation and Direct Measurement of Remote Sensing Reflectance in Stratified and Mixed Water Bodies
- 14:30
N. Stroembeck, D. Pierson
Measurement of lake water absorption coefficients in order to support modelling of remote sensing reflectance and primary production
- 15:00
A. Reinart
Algorithms for estimating some optically active substances and apparent optical properties from subsurface irradiance reflectance measurements in lakes
- 15:30 Coffee break
- 16:00
R. Kopmann, M. Markofsky
Averaging Techniques in Multi-Dimensional Water Quality Modelling of Vertical Stratified Lakes

16:30

M. Schimmelle

Influence of dissolved substances on the physical properties of lignite mining lakes

17:00

C. Mattenberger

Nutrient Fluxes and two dimensional advection in the density stratified Lake Lugano

17:30

Short contributions and discussion/summary by conveners

18:00 Drinks and End of Workshop

Turbulence characteristics in a small river derived from in-situ measurements with a 3D-acoustic Doppler velocimeter

Michael Thiele

Department of Ecohydrology, Institute of Freshwater Ecology and Inland Fisheries,
Rudower Chaussee 6a, D-12484 Berlin, Germany, email: m-thiele@igb-berlin.de

Abstract

Measurements and analysis of the 3D turbulence structure in a straight lowland river reach are presented. Accurate measurements of velocity profiles were taken at five verticals with the use of a sophisticated acoustic Doppler Velocimeter (ADV). The analysis is focused on properties related to turbulence intensity and on the effect of flow boundaries on turbulence structure. The data obtained allow the detection and preliminary analysis of turbulence driven secondary currents. The applicability of available approaches to prescribe this phenomenon is discussed. A quantitative comparison of empirical parameters between river and laboratory flows is given.

Experimental Site and Instruments

Turbulence measurements were carried out in the river Spree near the village Freienbrink, 10 km east of Berlin, Germany. The river channel at the considered reach is straight with stone-armoured banks and with bed covered by sands forming ripples and dunes (Figure 1). Relatively constant hydraulic characteristics occurred during the measurements: water discharge was $13.4 \text{ m}^3/\text{s}$, mean velocity: 0.49 m/s , river width: 21.3 m , average depth: 1.28 m , water surface slope: 0.000144 , corresponding shear velocity: 4.2 cm/s , Froude number: 0.019 , Reynolds number: $6.25 \cdot 10^5$. Measurements were taken with a field version of the 3D-acoustic Doppler velocimeter ADV, SonTek Inc., San Diego, [Kraus *et al.*, 1994] at a sampling rate of 25 Hz and with a special measuring system based on micropropeller sensors [Nikora *et al.*, 1994] at a maximum sampling rate of 10 Hz . The data on the three-dimensional flow structure were sampled at five vertical profiles (Figure 1) with a sampling period of about 320 seconds in each point. They were processed on the basis of algorithms described in Grinvald and Nikora [1988] and Nezu and Nakagawa [1993], see Sukhodolov *et al.* [1997].

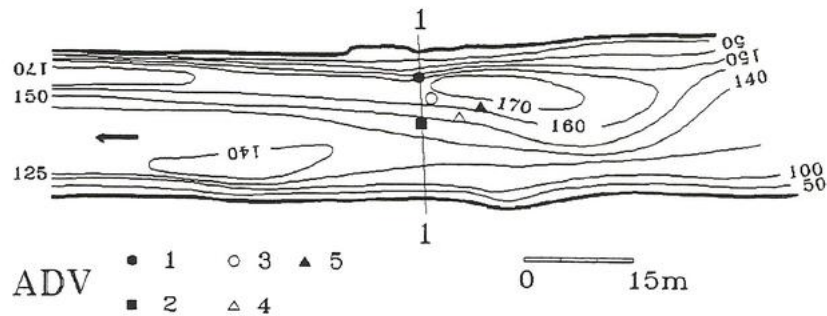


Figure 1. The experimental site at the Spree river with positions of ADV verticals.

Analysis

The streamwise mean velocity field U in the river cross-section 1-1 is presented by isolines in Figure 2 along with the mean transversal and vertical velocity components measured in verticals 1-3. Both the isolines of the longitudinal component and the plane vectors reveal the presence of a secondary current with longitudinal axis. Its driving force $(\overline{w'^2} - \overline{v'^2})$, basing on the anisotropy of the mean square fluctuations of the vertical and transversal velocity components,

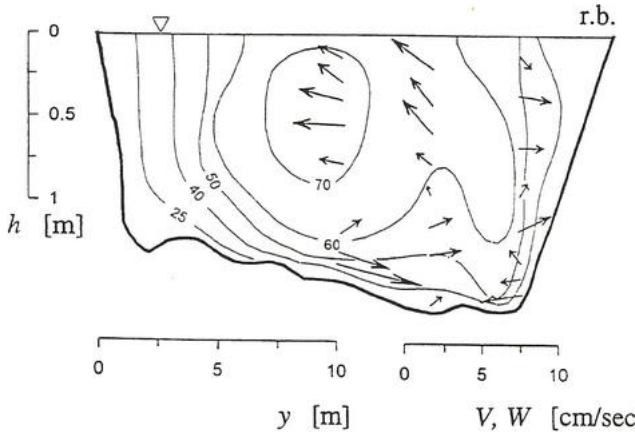


Figure 2. Isovelfs of longitudinal velocity (cm/s) and transversal (V) and vertical (W) velocity components in three ADV verticals of cross section 1-1.

contribution to the turbulent kinetic energy $K = 0.5 (\overline{u'^2} + \overline{v'^2} + \overline{w'^2})$ comprising of their mean square fluctuations, see Figure 4. The streamwise component's one makes up 45 - 55% irrespective of depth. On the contrary, the dependence of the transversal and the vertical velocity shares on relative depth becomes evident. In the central part of the flow their contributions are 30 and 20 %, respectively. Near bed and surface, the share of the transversal component grows

respectively, introduced by boundary influences (free surface, river bed, banks), according to McLean [1981] should, as the longitudinal flow shear stress, decrease linearly from the river bottom to the free surface what seems to be fulfilled in the central part of the flow, see Figure 3.

Measurement of three velocity components at a high temporal resolution allows to assess their individual

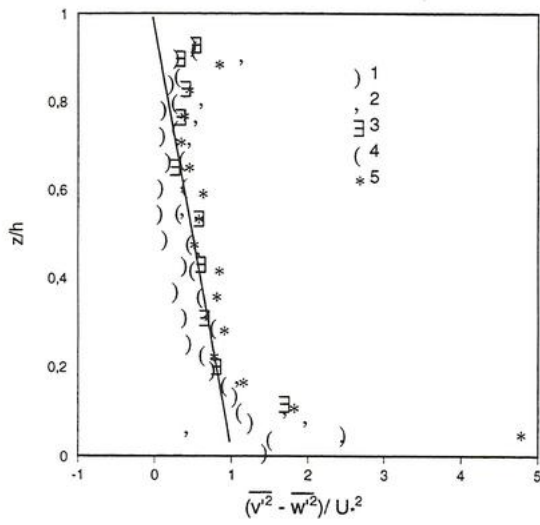


Figure 3. Driving force of secondary currents at the five ADV verticals.

up to 50 % and drops down to 2% - 10% for the vertical component. This observation underlines the necessity of taking into account the marked 3D character of flow near boundaries. Absolute K -distribution over depth is depicted in Figure 5 including a comparison with a semi-theoretical formula [Nezu and Nakagawa, 1993] for predominantly 2D flow (U_* - shear velocity)

$$\frac{K}{U_*^2} = D_k \exp(-2C_k z/h),$$

which seems to be obeyed quite well in the central flow region (compare differences between average laboratory flume and present river data fits).

Spectral analysis of the measured data revealed the occurrence of isotropic turbulence over a wide band of frequencies, and up to 3-4 Rad/s in the intermediate region. However, the isotropic band becomes relatively narrow near the bed and the surface. Temporal spectra of all three components obey Kolmogorov's -5/3 law (not shown).

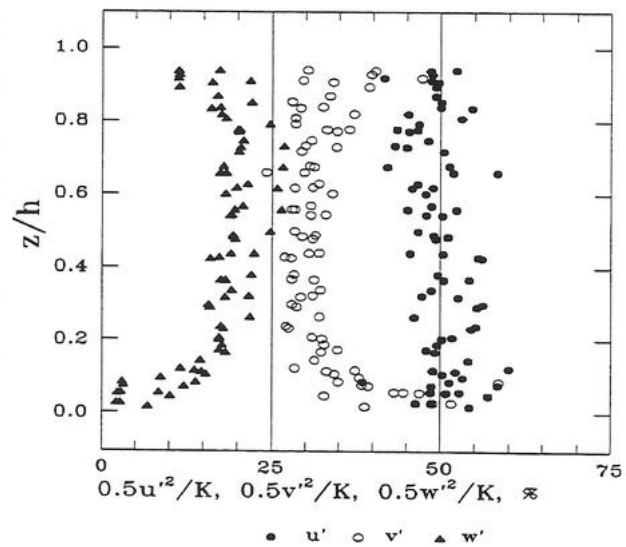


Figure 4. Share of velocity components' fluctuations to turbulent kinetic energy over the vertical.

Conclusions

The study has shown that the river flow is markedly three-dimensional even for simple conditions. However, in its central part it can be considered as quasi-two-dimensional. The universal parameters which were determined to describe turbulent flow characteristics in laboratory flows within the frames of a 2D approach do not fit to the case of river flow. This is explained by the effect of bed roughness on turbulence. Analysis of frequency spectra confirms the existence of Kolmogorov's inertial subrange for river turbulence. Close to the river bed isotropy almost

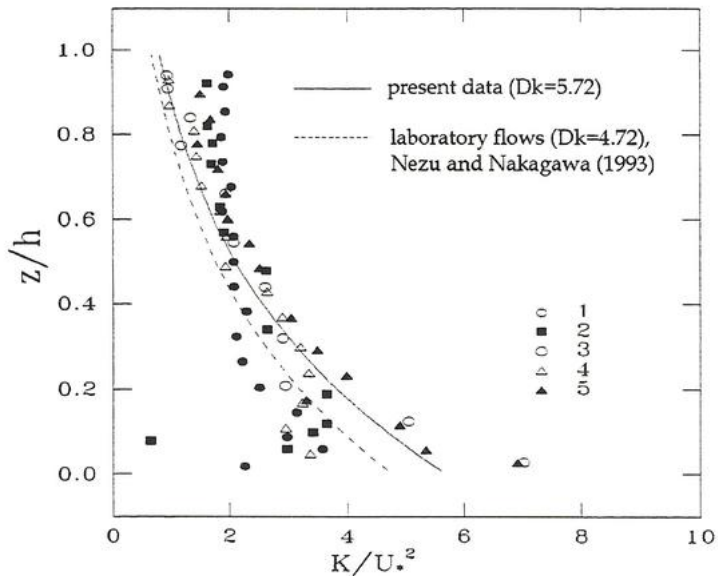


Figure 5. Vertical distribution of turbulent kinetic energy and comparison with model ($C_k=1.0$).

completely disappears. Investigation of 3D properties of the flow allowed to detect turbulence driven secondary currents and to analyse their origin. The performed analysis confirms the applicability of simplified equations to model the driving force inducing these secondary currents due to the anisotropy of turbulence.

References

- Grinvald, D.I., Nikora, V.I., *River turbulence* (in Russian), Hydrometeoizdat, Leningrad, Russia, 1988.
- Kraus, N.C., Lohrmann, A., Cabrera, R., New acoustic meter for measuring 3D laboratory flows, *J. Hydraul. Engng ASCE*, 120(3), 406-412, 1994.
- McLean, S.R., The role of non-uniform roughness in the formation of sand ribbons, *Marine Geology*, 42, 49-74, 1981.
- Nezu, I., Nakagawa, H., *Turbulence in open-channel flows*, Balkema Publ., 1993.
- Nikora, V.I., Rowinski, P., Sukhodolov, A., Krasuski, D., Structure of river turbulence behind warm-water discharge, *J. Hydraul. Engng. ASCE*, 120(2), 191-208, 1994.
- Sukhodolov, A.N., Thiele, M., Bungartz, H., Turbulence structure in a river reach with sand bed. Submitted.

IMPACT OF THE SKIN EFFECT ON THE NEAR-SURFACE TEMPERATURE PROFILE

Christoph Zülicke and Eberhard Hagen (Baltic Sea Research Inst., Warnemünde, Germany)

1. Introduction

The heat flux through the surface layers of the ocean plays a crucial role for climate and weather. Global application of infrared remote sensing devices to oceanic problems require detailed knowledge of the near surface temperature profile (Schluessel, 1990). The skin sea surface temperature (skin-SST) is emitted in the infrared from the uppermost 10 µm depth - it represents a key parameter for the thermal radiation balance and all atmospheric processes above the ocean. The skin layer just below the surface is characterized by molecular transport processes and is usually less than a millimetre thick. It is followed by a region, where turbulent transport processes are realising the transports. We will call this actively mixing surface layer of some meters depth "near surface layer". The fine structure of the skin must be properly parameterized because usual measurements of bulk-SST are done at various depths (using buoys, buckets, cooling water inlets, CTD and XBT soundings). At the one hand, correct calibration of remotely sensed skin-SST needs adjustment for this reference depth of the bulk-SST. At the other hand, the estimation of the skin-SST from oceanic circulation models or routine observations needs correct parameterizations, too.

The approach is as follows: the difference between the skin temperature at the surface (T_0) and the bulk temperature at the depth z ($T(z)$)

$$\Delta T(z) = T(z) - T(0) = \Delta T_{\text{skin}} + \Delta T_{\text{bulk}}(z) \quad (1)$$

is decomposed into a contribution from the skin and the bulk. For both layers, different theories will be used. We consider mean profiles, as they are formed by hourly mean values.

2. Surface Renewal in the Skin Layer

The skin layer is characterized by molecular transport processes. It extends from the surface of the water ($z=0$) into some depth ($z=-\delta^*$). In this section we summarise some mean properties of the heat conduction from the Soloviev and Schluessel (1994) paper.

The mean temperature difference through the skin layer is

$$\Delta T_{\text{skin}} = \Delta T_* = T_* - T_1 \quad (2)$$

where $T_1 = T(z=-\delta_*)$ is the bulk temperature at skin depth δ_* . The bulk temperature is assumed to be constant in depth - this assumption is used for the construction of the skin-bulk-SST difference from observations using a stepwise linear temperature profile (Grassl, 1976), or as a boundary condition for theoretical considerations (Liu et al., 1975). The Soloviev and Schlüssel, 1994, parameterization reads (see Fig. 1)

$$\Delta T_* = \Lambda_0 \Pr^{1/2} \frac{q_0}{u_{*0}} \frac{(1 + Ke / Ke_{cr})^{1/2}}{(1 + Rf_0 / Rf_{cr})^{1/4}} \quad (3-1)$$

The driving forces constitute depth-constant fluxes of momentum and heat - they read surface friction velocity u_{*0} and upwelling surface heat flux Q_0 resp. normalized $q_0 = Q_0/(c_p \rho)$. Further, a number of dimensionless parameters has been used: the surface Richardson number $Rf_0 = \alpha g v q_0 / u_{*0}^4$, the Keulegan number $Ke = u_{*0}^3 / (gv)$ and the Prandtl number $\Pr = v/\kappa$; the remaining constants are $Rf_{cr} = 1.5 \cdot 10^{-4}$, $Ke_{cr} = 0.18$ and $\Lambda_0 = 13.3$. For later use we quote here some check values for pressure $p = 0$ Pa, salinity $S = 35$ PSU and temperature $T = 20$ °C from Landolt and Boernstein (1989): kinematic viscosity $v = 1.05 \cdot 10^{-6}$ m²/s, acceleration due to gravity $g = 9.81$ m/s², specific heat capacity $c_p = 4015$ Ws/(kgK), density $\rho = 1025$ kg/m³, thermal expansion coefficient $\alpha = 2.6 \cdot 10^{-4}$ 1/K. With the kinematic conductivity $\kappa = 1.49 \cdot 10^{-7}$ m²/s we have a Prandtl number of $\Pr = 7$. The depth of the skin layer is estimated from the assumption of a linear temperature profile

$$\delta_* = \kappa \frac{\Delta T_*}{q_0} = \frac{\Lambda_0}{\Pr^{1/2}} \frac{v}{u_{*0}} \frac{(1 + Ke / Ke_{cr})^{1/2}}{(1 + Rf_0 / Rf_{cr})^{1/4}} \quad (3-2)$$

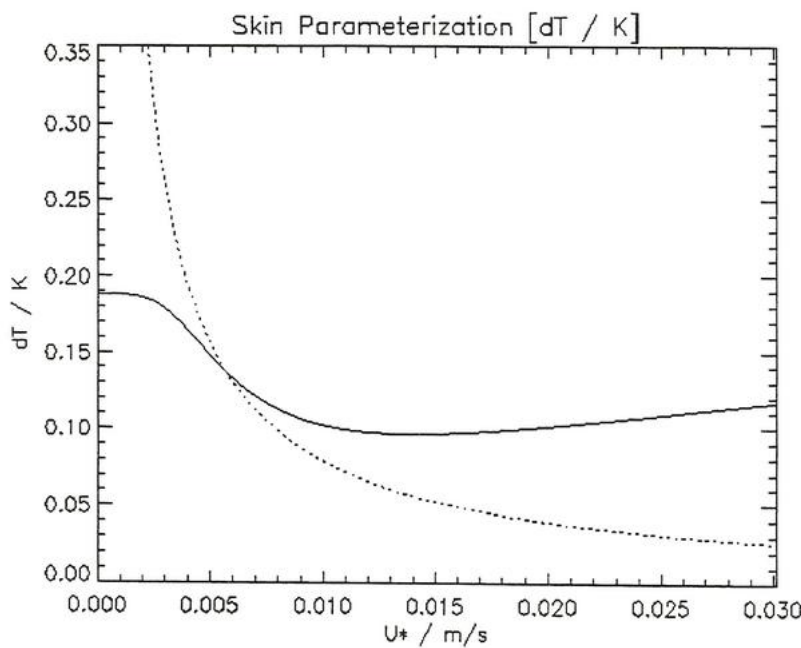


Figure 1: Wind-dependence of the skin-bulk temperature difference ΔT_* for fixed heat flux and varying winds (solid line). The dotted line represents the Saunders, 1967, approximation (set $Rf_{cr} \rightarrow \infty$ and $Ke_{cr} \rightarrow \infty$; Eq. (3-1)).

3. Stationary Turbulence in the Bulk Layer

Using the findings for the skin layer we continue the temperature profile into the bulk of the water. In particular, the bulk temperature T_1 of the calculations above will be identified with the temperature at the boundary of the turbulent layer. For the bulk layer just below, we adopt results from the Monin-Obukhov similarity theory (Monin and Ozturk, 1985).

General Formulation:

For the calculation of the temperature profile we adopt the following formula

$$\Delta T_{bulk}(z) = \int_{z_1}^z dz' q_0 \frac{1}{ku_* z'} \varphi_T \left(\frac{z'}{L} \right) \quad (4-1)$$

We have used here the Monin-Obukhov length $L = u_*^3 / (g \alpha q_0)$ and the van Karman constant $k=0.4$. For a general formulation, we use the following form of the universal function

$$\varphi_T(\zeta) = \begin{cases} 1 + 5\zeta & : 0.0 \leq \zeta \\ (1 - 16\zeta)^{-1/2} & : -1.0 \leq \zeta < 0.0 \\ (-29 - 99\zeta)^{-1/3} & : \zeta \leq -1.0 \end{cases} \quad (4-2)$$

with $\zeta = z/L$ (Large et al., 1994). The integral (4) can be solved numerically. However, we will continue with analytical expressions for some physically interesting limiting cases.

Free convection on strong cooling:

In particular, we find for the case of free convection ($Q_0 = 100 \text{ W/m}^2$, $U_* = 0 \text{ m/s}$, $Rf_0 = +\infty \gg Rf_{cr}$, $Ke = 0 \ll Ke_{cr}$, Fig. 2). For the universal function we use the limit for unstable stratification $\varphi(\zeta \rightarrow -\infty) \rightarrow -99\zeta$ and obtain from Eq.s (3) and (4)

$$\Delta T = \frac{\Lambda_0 Pr^{1/2} Rf_{cr}^{1/4}}{(\alpha g v)^{1/4}} q_0^{3/4} + \frac{3(99)^{-1/3}}{k(k\alpha g)^{1/3}} q_0^{2/3} \left(\frac{1}{z^{1/3}} - \frac{1}{z_1^{1/3}} \right) \quad (5)$$

The skin contribution ΔT_{skin} at 10 cm depth forms 65% of the overall skin-bulk difference ΔT ; at 1 m depth they are still 62%.

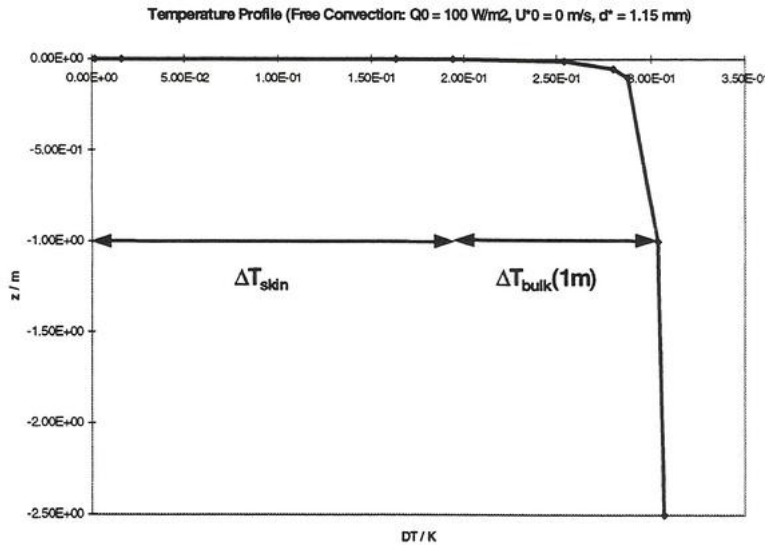


Figure 2: Depth-dependent skin-bulk temperature difference $\Delta T(z)$ for the free convection/strong cooling case according to Eq. (7) with $Q_0 = 100 \text{ W/m}^2$, $U_{*0} = 0.0 \text{ m/s}$, $\delta_* = 1.15 \text{ mm}$, $\Delta T_* = 0.19 \text{ K}$. There are indicated the different skin and bulk contributions at 10 cm and 1m depth.

Forced convection (moderate winds):

For the case of moderate winds ($Q_0 = 100 \text{ W/m}^2$, $U_{*0} = 0.01 \text{ m/s}$ resp. $U_{10} = 8.1 \text{ m/s}$ in neutral atmosphere; $Rf_0 = 6.49 \cdot 10^{-6} \ll Rf_{cr}$, $Ke = 9.72 \cdot 10^{-2} \ll Ke_{cr}$) we find neutral stratification at 1 m depth and use for Eq. (4) $\varphi_T(0.0248 \ll 1.0) \approx 1.0$. It results the logarithmic profile

$$\Delta T(z) = \Lambda_0 \Pr^{1/2} \frac{q_0}{u_{*0}} + \frac{1}{k} \frac{q_0}{u_{*0}} \ln\left(\frac{z}{z_1}\right) \quad (6)$$

The skin contributions to the temperature difference make, in this case, 73 % at a depth of 10 cm and 65 % at 1 m. The temperature profile by Eifler, 1993, predicts an 80% impact of the skin at 1 m depth, quite similar to our findings.

Breaking Waves (strong winds):

For stormy situations ($Q_0 = 100 \text{ W/m}^2$, $U_{*0} = 0.03 \text{ m/s}$ resp. $U_{10} = 25 \text{ m/s}$ in neutral atmosphere, $Rf_0 = 7.16 \cdot 10^{-8} \ll Rf_{cr}$, $Ke = 2.83 \gg Ke_{cr}$) the skin terms are changing, whereas the form of the bulk expression remains logarithmically (for 1 m depth we find $\varphi_T(0.0008) \ll 1.0 \approx 1.0$).

$$\Delta T(z) = \frac{\Lambda_0 \Pr^{1/2}}{Ke_{cr}^{1/2}} \frac{q_0 u_{*0}^{1/2}}{(gv)^{1/2}} + \frac{1}{k} \frac{q_0}{u_{*0}} \ln\left(\frac{z}{z_1}\right) \quad (7)$$

Here, 92% of the temperature difference at 10 cm come from the skin (88% at 1 m).

4. Summary

Based on the surface renewal and similarity theory a consistent picture for the heat flux near the ocean surface was developed. Limiting laws for the cases of neutral and unstable stratification of the water body are presented. It is demonstrated, that below the conductive skin layer (order 1 mm thickness) there are arising significant contributions to the temperature difference.

For operational applications, the knowledge of a bulk-SST at a certain depth and the involved fluxes allows for an estimate of the skin-SST, which is relevant for the thermal radiation emitted into the atmosphere and related climatological problems. The particular choice of the bulk-SST could be the engine water inlet (or another routine observation) or the temperature of the uppermost grid point in numerical models.

We would like to thank Peter Schlüssel (University of Munich, Germany) and Walter Eifler (Space Applications Institute, Ispra, Italy) for a number of encouraging discussions.

References

- Eifler W.: A hypothesis on momentum and heat transfer near the sea-atmosphere interface and a related simple model, 1993. J. Marine Systems 4: 133-153.
- Grassl H., 1976: The dependence of the measured cool skin of the ocean on wind stress and total heat flux. Boundary-Layer Meteorology 10: 465-474;
- Landolt and Boernstein, 1989: Numerical Data and Functional Relationships in Science and Technology (Springer; Berlin) New Series V/3a: 233 ff.;
- Large W.G., J.C.McWilliams, S.C.Doney, 1994: Oceanic vertical mixing: A review and a model with nonlocal boundary layer parameterization. Rev. of Geophysics 32, 4: 363-403.
- Liu W.T., J.A.Businger, 1975: Temperature profile in the molecular sublayer near the interface of a fluid in turbulent motion. Geophys. Res. Lett. 2, 9: 403-404.
- Monin A.S., R.V.Ozmidov, 1985: Turbulence in the Ocean (Reidel, Dordrecht);
- Saunders P.M., 1967: The temperature of the ocean-air-interface. J. Atm. Sci. 24: 269-273.
- Schlüssel P, W.J.Emery, H.Grassl, Th.Mammen, 1990: On the skin-bulk temperature difference and its impact on satellite remote sensing of the sea surface temperature. J. Geophys. Res. 95, C8: 13,341-13,356;
- Soloviev A.V., P.Schlüssel, 1994: Parameterization of the cool skin of the ocean and of the air-ocean gas transfer on the basis of modelling surface renewal. J. Phys. Oceanogr. 24, 6: 1339-1349;
- van Scoy K.A., K.P. Morris, J.E. Robertson, A.J.Watson, 1995: Thermal skin effect and the air-sea flux of carbon dioxide: A seasonal high-resolution estimate. Global Biogeochemical Cycles 9, 2: 253-262;

Fluctuating fields due to wave breaking

Walter Eifler, Joint Research Centre, Ispra, Italy

ABSTRACT:

In a recent paper (Eifler,1997) the influence of wave-breaking, modelled as periodic event, on momentum-, heat-, and mass-transfer has been shown.

The 'once-through' model used for this study observes the air-water interface from a fixed position and sees in this way periodically passing continuous, undisturbed interface parts, and parts disrupted by wave breaking. The time fraction of passing disrupted interface is assumed to be given by the wind depending space fraction of white cap coverage.

The results presented in the above cited paper were obtained for a constant wave breaking period of 12 seconds independent of the wind speed. Here the influence of a variable wave breaking period on the fluctuating field characteristics is investigated.

While the earlier results were characterised by a limited penetration depth in the range of several decimeter of the field fluctuations into the water body, the new results show, the penetration depth is considerably increasing with increasing wave breaking periods.

Eifler,W., 1997, Periodic wave-breaking and its effect on momentum-, heat-, and mass-transfer, submitted to Phys.Chem.Earth (Proceedings of the XXII Gen.Ass.EGS, Vienna, 21-25 April,1997)

Simulating Flow, Turbulence, Waves, Seiches and SPM in Tidal and Inland Waters by 1D Models

Matthias Regener¹

Institut für Meereskunde, Universität Hamburg , Germany

Helmut Baumert²

Institut für Chemie und Biologie des Meeres

Carl von Ossietzky Universität, Oldenburg and HYDROMOD GbR, Wedel/Holstein,
Germany

Introduction

A basic 1-d model has been derived to investigate the role of turbulence in relation to density stratification in space and time. Two adaptations of this model are presented:

- A version for tidal waters applications (Version I) and
- a version for inland waters (*i.e.* relativ small enclosed basins) applications (Version II).

1. Model Version I

Because of its great impact on coastal morphodynamics and biochemical dynamics, SPM dynamics has become an important issue in marine science. Considering SPM dynamics on different time and space scales one has to distinguish cohesive and non-cohesive material, *i.e.*

- small time and space scales are typical for transport of non-cohesive sediments and the dynamics of moveable beds and
- larger scales are dominant in cohesive SPM transport and floc dynamics including autocatalytic production (cell division) of new flocs due to biological processes.

In accordance with this distinction two versions of the tidal waters model were established:

- Model version Ia considers the dynamics of cohesive material (*e.g.* flocs) especially aggregation and disaggregation of particles and particle-particle interaction. Focusing on these processes no interaction of particles with the bottom is included for the time being. In contrast to version Ia
- Model version Ib deals with non-cohesive material (*sand*) regarding a particle flux from (erosion) and to the bottom (sedimentation) but consequently does not consider particle-particle interaction.

¹regener@ifm.uni-hamburg.de

²baumert@dkrz.de

While model version Ib is supposed to be valid in shallower coastal waters with predominately strong tidal currents, model version Ia is intended to be applicable to deeper waters with less strong tidal currents. In both model versions Ia and Ib the sinking velocity is taken to be dependent on the present SPM concentration in order to allow for so called hindered settling. Another observed phenomenon which is included in both model versions is the effect of SPM concentration on the density of seawater. Near bed high floc concentrations can establish sharp concentration gradients and corresponding density gradients suppressing turbulent motion within the boundary layer, especially when turbulence is weak.

To derive model versions Ia and Ib, the $k-\varepsilon$ model has been extended by the inclusion of a transport module for SPM, which includes, exclusively for model version Ib, sinking and diffusion processes (after *Sheng & Villaret* [1989]). In model version Ia, at present, only a single floc size class is considered. However, further development will lead to at least three size classes.

With regard to wave activity, tidal and surface wave action is considered. At present the action of surface waves is described by a suitable surface boundary condition for the TKE equation (*Craig & Banner* [1993]). In order to resolve the strong gradient layer close to the bottom, a non-uniform spatial grid was introduced in both model versions. Since model version Ib has been designed for shallower waters, it takes care of the changing water depth due to tidal action. For that reason in version Ib it is necessary to allow the grid to adapt to the time dependent variation in water depth (moveable bed), thus also changing the model's domain of integration. Compared to measured temperature data the tidal waters version of the model performs well.

2. Model Version II

In order to predict vertical profiles of temperature and water quality parameters in view of distinct dynamic properties of lakes, the reservoir version was elaborated. Developing such a model one has to consider the impact of internal and external oscillations (seiches) forced by barotropic and baroclinic pressure gradients on the hydro-thermodynamics of the lake in a way that the vertical integral of horizontal velocities vanishes. Considering these seiches allows for a compensation current at the bottom of each layer (*e.g.* mixed and stratified layer). This vertical velocity profile is responsible for a corresponding vertical TKE profile, which reduces, compared to the case with no pressure correction, the entrainment and subsequently the mixed layer depth (*Kranenburg* [1984]). To take care of this phenomenon, we included a suitable correction for the pressure terms in the momentum equations. The model performed well compared to measured data.

3. Basic Model Equations

Starting point for development of both the tidal and the inland waters versions was the $k-\varepsilon$ model described by *Baumert & Radach* [1994] and *Burchard & Baumert* [1995]. The kernel of the model, the Reynolds averaged equations, reads as follows:

$$\begin{aligned}
\partial_t \bar{u} + \partial_z \langle \tilde{u} \tilde{w} \rangle &= f \bar{v} - \frac{1}{\rho_0} \partial_x p, \\
\partial_t \bar{v} + \partial_z \langle \tilde{v} \tilde{w} \rangle &= -f \bar{u} - \frac{1}{\rho_0} \partial_y p, \\
\partial_t \bar{T} + \partial_z \langle \tilde{w} \tilde{T} \rangle &= \frac{1}{\rho_0 c_p} \partial_z I, \\
\partial_t \bar{S} + \partial_z \langle \tilde{w} \tilde{S} \rangle &= 0, \\
\partial_t \bar{\phi}_i + \partial_z \langle \tilde{w} \tilde{\phi}_i \rangle + w_{s,i} \partial_z \bar{\phi}_i &= \Omega_i^+ + \Omega_i^-.
\end{aligned}$$

where \bar{u} , \bar{v} , \bar{w} , \bar{T} , \bar{S} and $\bar{\phi}_i$ are the ensemble means of the velocity components, temperature, salinity and suspended matter (SPM, non-cohesive material in model version Ib and cohesive material in model version Ia) concentration, respectively. \tilde{u} , \tilde{v} , \tilde{w} , \tilde{T} , \tilde{S} and $\tilde{\phi}_i$ represent their fluctuations. In both model versions Ia and B ϕ_i denotes the i 'th fraction of SPM under consideration, with $i = 1..N$ and N the total number of fractions which are accounted for. Since at the moment only one floc size class is included in model version Ia and one SPM fraction in model version Ib, $N = 1$ in both models. In the 1-d case the equation of continuity degenerates to $\bar{w} = 0$. $\langle \tilde{u} \tilde{w} \rangle$ and $\langle \tilde{v} \tilde{w} \rangle$ represent turbulent fluxes of momentum, ρ_0 is the mean density and p the hydrostatic pressure at the depth z , for which $p(z, t) = g \int_z^\zeta \rho(\bar{T}(z', t), \bar{S}(z', t), \bar{\phi}(z', t)) dz'$, with ζ the deviation from the mean water level. $\langle \tilde{w} \tilde{T} \rangle$, $\langle \tilde{w} \tilde{S} \rangle$ and $\langle \tilde{w} \tilde{\phi}_i \rangle$ are the turbulent fluxes of heat, salt and SPM, respectively. $w_{s,i}$ denotes the sinking velocity of the i 'th SPM fraction, f is the Coriolis parameter, g the gravitational acceleration and $\frac{1}{\rho_0} \partial_x p$ and $\frac{1}{\rho_0} \partial_y p$ represent the horizontal pressure gradients in x and y directions, respectively. Since model version Ib deals exclusively with non-cohesive material, Ω_i^+ and Ω_i^- are defined with regard to the cohesive material in model version Ia only. They denote sources and sinks regarding the i 'th floc size class included in model version Ia and represent the interaction between different floc size classes due to physical, biological and chemical processes. These processes are responsible for an increase or decrease in floc size class concentration due to coagulation of smaller flocs to bigger ones or to the breakup of bigger flocs into smaller ones.

c_p is the specific heat capacity of seawater. $\partial_z I$ represents the differential absorption of incoming radiation. In model version Ia the water depth is fixed to H and since changes in water depth in model version Ib occur stepwise rather than continuous, water depth can be regarded to be constant in this case at any time step as well.

Molecular viscosity and diffusivity are neglected as they are small compared to their turbulent counterparts.

Whith the exception of the SPM equation all model equations are solved by a fully implicit three-point, two-layer finite-difference scheme (see *Samarskij* [1984]). The numerical solution of the SPM sinking/diffusion problem is carried out utilising the control volume method of *Patankar* [1980]. This method incorporates a power law interpolation scheme, sequential implicit time marching and deals with both smaller and larger grid Peclet numbers. The numerical diffusion inherent in the advective/sinking term is reduced by applying the Hybrid Linear/Parabolic Approximation (HLPA) introduced by *Zhu* [1991].

All model versions were coded using Borland's PASCAL package to run on PCs under DOS (version 3.2 or better) as well as using the IBM-AIX XL

Pascal compiler to run them on IBM-RISC workstations.

Acknowledgments

Funding for this work was provided in the framework of the EU-project PROMISE (MAS3 CT 950025) and by the Landesanstalt für Umweltschutz des Landes Baden-Württemberg through HYDROMOD-Project-No. P811002, Germany. We would like to thank Barnabas Szilagyi and Prof. Gisbert Stoyan for valuable discussions on the theoretical aspects of the used numerical schemes.

References

- Baumert, H. and G. Radach (1992) - Hysteresis of turbulent kinetic energy in nonrotational tidal flows: a model study. *J. Geophys. Res.* Vol. **97**, 3669 - 3677.
- Burchard, H. and H. Baumert (1995) - On the performance of a mixed-layer model based on the k- ϵ turbulence closure. *J. Geophys. Res.* Vol. **100**, C5, 8523 - 8540.
- Craig, P. D. and M. L. Banner (1994) - Modeling wave-enhanced turbulence in the ocean surface layer. *J. Phys. Oceanogr.*, Vol. **24**, No. 12, 2546 - 2557.
- Kranenburg, C. (1984) - Wind-induced entrainment in a stratified fluid. *J. Fluid Mech.*, Vol. **145**, 253 - 273.
- Patankar, S. (1980) - Numerical heat transfer and fluid flow. Hemisphere Publishing Corporation, New York, pp. 197.
- Sheng, Y. P., Villaret, C. (1989) - Modeling the effect of suspended sediment stratification on bottom exchange processes. *J. Geoph. Res.*, Vol. **94**, No. C10, 14.429 - 14.444.
- Zhu, J. (1991) - A low-diffusive and oscillation-free convection scheme. *Comm. in Appl. Num. Meth.*, Vol. **7**, 225 - 232.

Energy transfer efficiency from wind to waves and into the surface layer of natural waters

A. Wüest and A. Simon

Swiss Federal Institute of Environmental Science and Technology (EAWAG) and Swiss Federal Institute of Technology (ETH); CH-8600 Dübendorf, Switzerland; e-mail: alfred.wueest@eawag.ch

More than 800 temperature microstructure profiles were taken during a period of 12 days in Lake Neuchâtel (Switzerland) in order to quantify and parameterize wind-driven surface boundary layer turbulence (Simon, 1997; Simon et al., 1997). Dissipation of turbulent kinetic energy (TKE) was determined by the so-called *Batchelor method* analyzing power spectra ϕ_T of temperature microstructure segments collected from a pair of FP07-probes on a uprising profiler ($w_p \approx 8 \text{ cm s}^{-1}$). Simultaneous measurements of surface waves and wind allowed to balance TKE transferred from wind to waves and into the surface boundary layer. The data were collected under widely differing meteorological conditions.

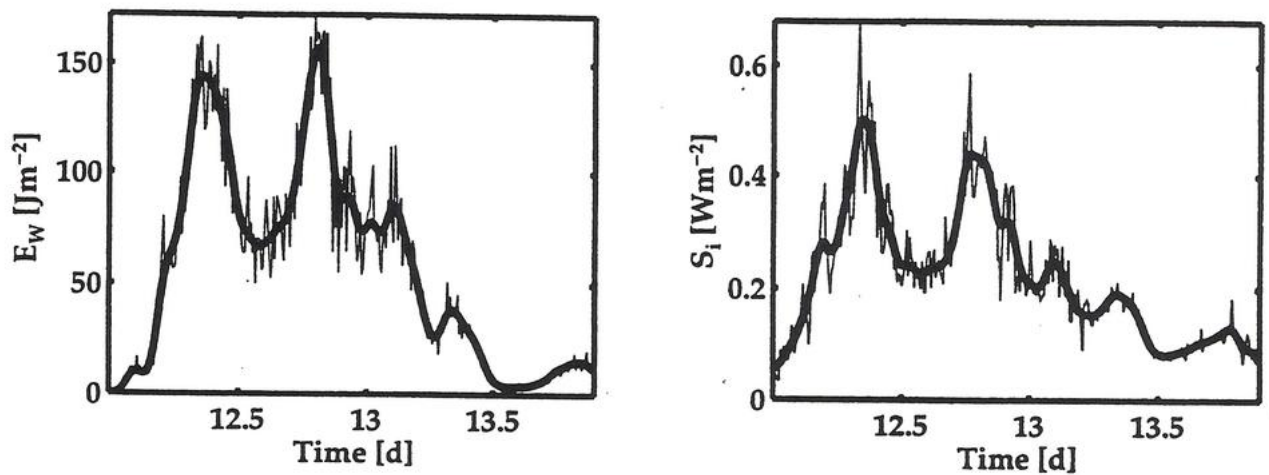
Lake Neuchâtel (length, width and mean depth are $\approx 38 \text{ km}$, $\approx 6 \text{ km}$ and 64 m , respectively) was chosen as the experimental site, since this lake faces the strongest of regularly occurring wind in Swiss lakes. This exposition to relatively strong winds was considered as a guarantee for a large forcing variability. In addition, the lake is large enough to ensure, that the influence of the lake boundaries on the structure of the surface boundary layer is negligible and that the fetch is long enough to allow waves to reach saturation. The location of the moorings (local depth of about 40 m) has been selected due to wind exposition and the steep shoreline, which was profitable to run the profiler from a land station about 300 m away from the shore.

Between 1.5% and 3.5% of the wind energy downward flux from the atmosphere 10 m above water ($:= p_{\text{Air}} C_D W_{10}^3$) has been found to be transferred to surface waves. Comparison to the total rate of dissipation of energy in the surface boundary layer demonstrates that surface waves are a large energy reservoir for the TKE balance in the surface boundary layer. In our study, the wave energy content varied from $1-10^2 \text{ J m}^{-2}$. Since in medium-sized lakes as Lake Neuchâtel a significant amount ($\approx 50\%$) of the wave energy is transported horizontally to the shore (time scale: $t \approx \text{Lake dimensions / group velocity} \approx \text{hours}$), the remaining energy available for mixing in the water column has been found at a lower level than previously observed in the ocean surface layer.

Observed dissipation followed the *Low of the Wall* relationship within the surface boundary layer below 1m depth. Only in the uppermost wave-affected surface

layer (WASL) dissipation was enhanced. Vertical integrated profiles of dissipation have been found to consist with the rate of wave energy loss estimated by Longuet-Higgins (1969) and a linear energy box model. It appears that dissipation due to wave breaking scales with the wave energy content divided by a wave-dependent time scale T_d . Two independent data sets (wave energy data and dissipation data) suggest that the inverse of the dissipation time scale T_d^{-1} is on the order of 10^{-5} s^{-1} .

In this presentation, the most energetic period of 2 days length [12/13 March 1996; see Figure: Wave energy content (left) and energy input from atmosphere (right panel)] will be discussed in detail. The results will be set in context to the overall findings of the 12 day period.



A 1D reduction of a 3D estuarine model for simulating dissipation rate measurements in the Eastern Scheldt.

Hans Burchard and Adolf Stips, Joint Research Centre, Ispra, Italy

In this paper, a one-dimensional numerical model of the water column is presented which has been designed in order to reproduce measurements of the dissipation rate in the Eastern Scheldt.

The main forcing is here the semidiurnal M_2 tide which affects the flow in the water column by variations of sea surface slope and height. It is obvious that the prediction of the sea surface slope is a crucial point. The reason for this is that the bottom friction velocity, an important scale for the dissipation rate, is directly depending on the external pressure gradient which is established by the surface slope.

Here, a method is shown how standard point velocity measurements (Anderaa) can be used for predicting the surface slope such that the bottom friction velocity is approximated with high accuracy. Furthermore, an estimate for the horizontal advection terms is given. The quality of this estimate is tested by comparing 1D and 2D model results.

For the calculation of turbulent quantities, a two-equation k-epsilon turbulence model is used where k is the turbulent kinetic energy (TKE) and epsilon the dissipation rate of the TKE.

The measurements of the dissipation rate have been carried out in the Eastern Scheldt Estuary with a free falling Micro-Structure - Turbulence (MST) Profiler. Although the temporal resolution of the measurements was poor (four casts per hour), the expected temporal and spatial structure (M_4 period, 1/z behaviour towards the bottom) of the dissipation rate could be reproduced. The qualitative and quantitative correspondence between these difficult measurements and the simulation is fairly good.

Comparison of dissipation of turbulent kinetic energy determined by shear and temperature microstructure

Kocsis, O. (1), H. Prandke (2)

(1) Swiss Federal Institute of Environmental Science and Technology (EAWAG)
and Swiss Federal Institute of Technology (ETH);
CH-8600 Dübendorf, Switzerland
kocsis@eawag.ch

(2) ME Meerestechnik-Elektronik GmbH;
Iserstrasse 6, D-24610 Trappenkamp
hprandke@compuserve.com

Key words: Turbulent mixing, lakes, temperature microstructure,
shear microstructure, dissipation

Abstract

Two methods to determine dissipation of turbulent kinetic energy from microstructure temperature and microstructure shear were compared in a 12 days measurement campaign in March 96 in Lake Neuchâtel . Since the two profilers are both optimized for the respective method with such differing requirements, the two profilers were operated separately in a fixed position with a horizontal distance of about 30 m. The time series (measuring interval 15 min.) covered calm weather conditions and periods with wind speed exceeding 10 m/s as well as thermal convection and thermal stratification periods.

The dissipation rates are ranging between 10^{-11} and $10^{-5} \text{ W kg}^{-1}$. To compare the dissipation rates time series was splitted according to the different hydrological and forcing conditions.

The comparison revealed excellent agreement with the bulk of the deviations being smaller than the measurement error of the 2 methods ($s_m=2.8$). Only 2 exceptions were found:

- (1) In the top surface layer (0-2 m) during strong winds the μT -dissipation values tend to be smaller by up to a factor of 10. This deviation is not statistically significant, since only a very limited number of dissipation values could be determined during the windy regime.
- (2) During strong heating conditions an increase of dissipation in the μT -probe has been registered in the depth range from 3-5 m by up to a factor of 10.

Taking into account the wide range of dissipation and the intermittency, the agreement - with the bulk of the data within the measurement error and some exceptions within a factor of 10 - is very good.

From this comparison we can formulate advices for the use of the 2 methods: In the dissipation range $10^{-10} \text{ W kg}^{-1} < \varepsilon < 10^{-6} \text{ W kg}^{-1}$ the 2 methods give identical results, while only the $m\mu T$ -method can be used in systems with low dissipation rate ($\varepsilon < 10^{-10} \text{ W kg}^{-1}$), the shear method is preferable for high dissipation rates above $10^{-6} \text{ W kg}^{-1}$.

2nd Workshop on "Physical Processes in Natural Waters"

3-5/11/1997

CEC Joint Research Centre

Ispra (Varese), Italy

Modelling the salinity profile in the developing lakes of an open-cast mine under consideration of the lakes' dynamics an the groundwater flow

Bertram Boehrer

UFZ-Gewässerforschung

Am Biederitzer Busch 12, D - 39114 Magdeburg, Germany

boehrer@lake.gm.ufz.de

Introduction:

With the declining dependence on brown coal mining, many of the open cast mines in the former GDR are abandoned and two new lake areas are forming within the Central German and Lausatian region. Many of those lakes show a rather uncommon combination of dissolved and suspended materials, which are partly from natural sources and partly from anthropogenous sources. In many cases the slopes of the mine pits are designed rather steep. However under dry underground conditions, they guarantee stability, while they can be of concern in the period when the water level is rising. Therefore it is the intention to bring the water up to its final level as fast as possible. If available, water can be taken from a near-by stream or river, especially, if a eutrophication can be excluded or a certain level is acceptable.

This contribution is concerned about the forming lakes in the abandoned open-cast mine of Merseburg-Ost, where lakes have been forming over a period of three years now. So far, the inflow has mainly come from the groundwater sources. The incoming waters from the deeper layers of the soil, Zechstein, carries a high load of dissolved minerals mainly NaCl from washed-out natural salt deposits in this area (see Fig. 1). Concentrations of up to three times ocean water can be found in the bottom layers of the lakes today, falling to some 8kg/m^3 in the epilimnion. The plan is to start filling the lakes from a near-by stream and the final water level could be reached within three years. In this region precipitation and evaporation

from an open water surface would yield a deficit, but at the chosen levels the lakes would receive enough groundwater inflow to balance this loss and guarantee an overflow from Lake 1b into Lake 1a. The latter will drain into a near-by stream.

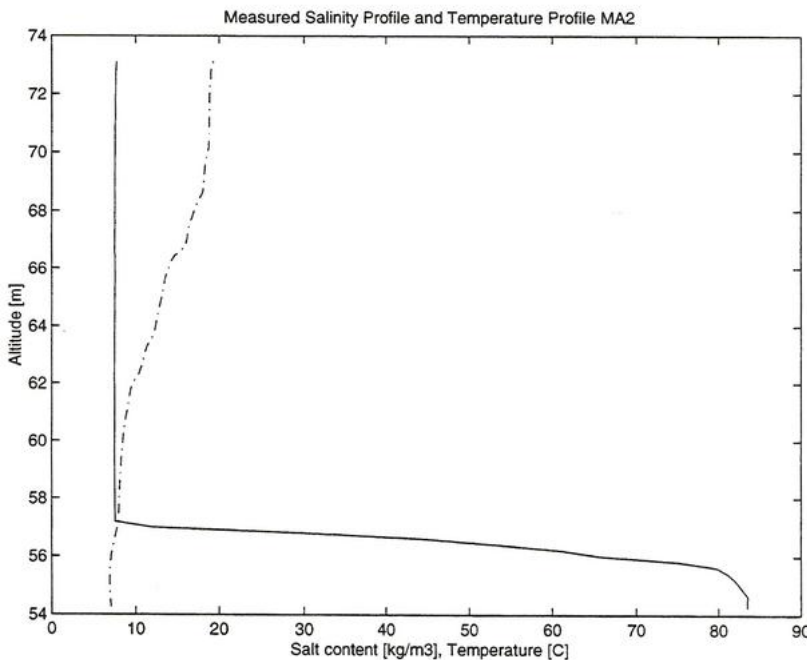


Figure 1: The salinity and temperature structure in Merseburg-Ost Lake 1a, on 19th of June 1997, before flooding with fresh water from a near-by stream

The major concern about the final state of these lakes is the possible vertical salt transport through that window which the water body forms within the stratified ground water. The ascending salt could be feared to enter the groundwater at an elevated level and influence the quality of the near-surface groundwater. Those considerations have indicated to make a prognosis for the future development of the salinity profiles in the developing lakes of the abandoned lignite mine of Merseburg-Ost.

A limnological transport model able to incorporate the groundwater inflows and outflows into the lakes' dynamics had to be used. As the groundwater flows proved to be sensitive to the density stratification in the lake a close coupling was necessary. Our partner HPC developed a three-dimensional groundwater model capable of including the varying density stratification, while we, UFZ, included the groundwater flows into a limnological transport model to predict the future stratification in the lakes.

Model:

The model was required to supply information about the transport of salt through the water column. It had to allow strong and variable groundwater inflows and outflows. As it was designed for a long-term prognosis (in the range

of 50 to 100 years), it was required to run very robustly. The input information about weather and the number of parameters that need calibration should be kept small, as the lakes to model do not exist as such yet. The computation time should be around 10 to 30 minutes for a year. The numerical diffusion had to be smaller than the molecular diffusion of salt.

The seasonal dynamics was only interesting as far as it could be involved in the longterm changes of the salinity profile. We therefore decided not to model the processes happening on the water air interface. From measurements in the years 1996 and 1997, we extracted the surface temperature and the wind speed (cubic average) over the months. The sum of precipitation and evaporation was set to a value of $-5.1 \cdot 10^{-9} m/s$ all year round. Exactness was required only below the depth of the semi-annual deep convection.

The model used 1000 boxes in the vertical and resolved the lakes in steps of $3.5 cm$ to $4 cm$. The boxes were fixed in size and location. The model proceeded in time steps of 2 months, first implying the outflows, evaporation, and inflows. They were introduced in the model at the depth they entered the water column. The kinetic energy put in by the wind was calculated. In the case of enough kinetic energy to overcome the potential energy to mix the second box from the top into the most upper box, the waters were mixed and both boxes were set to the surface temperature. The remaining wind energy for mixing was reduced by the required amount for the vertical mixing. In the case of an unstable stratification (e.g. surface cooling) the recycled energy was included at a certain portion in the available mixing energy. Proceeding down through the water column, the model formed an isothermal epilimnion (or mixolimnion in late autumn and spring). The last box to be mixed was mixed in part, according to the portion of the remaining energy to the necessary energy to mix the entire box.

The diffusion of salt and heat was calculated in separate steps. In both cases, the diffusion length would have exceeded the box dimensions by far. We used the standard deviation of the diffusion: $\sigma = \sqrt{2\kappa t}$ and distributed the salt (or temperature, respectively) over a number of neighbouring boxes, yielding the same standard deviation as above. Thereafter occurring unstable configurations were mixing until a stable stratification was achieved again.

The data exchange with the ground water model was performed after a number of complete years starting from one year intervals which increased to 10 years in the final. In total a time interval of 100 years has been modeled.

Upper Water Column Dissipation and Stability in View of External Forcing.

Bjarke Rasmussen, Department for Microbiology and Marine Ecology, National Environmental Research Institute, Denmark. Email: br@dmu.dk.

Adolf Stips, Space Applications Institute, CEC Joint Research Centre, Italy. Email: adolf.stips@jrc.it.

Abstract: Temperature and dissipation micro-structure observations in lake Maggiore, Italy, are evaluated by profiles, potential energy anomaly (Fig.1), depth integrated dissipation (Fig.2), and bulk modelling. The daily heat-flux cycle and night-time wind shear stress are the dominant external forcing (Fig. 2). The contribution of breaking waves on the TKE budget can be neglected due to minimal winds and corresponding small wave steepness. A stable stratified water column (Fig 2, Fig 3) is established from the lake surface and downwards during the day-time net-heat gain of the water column. During day time periods of net-heat loss, first the water column just at the lake surface becomes unstable (Fig 2, Fig 3), hereafter in the metres below. The time scale to reduce the kinetic energy of the water column by a factor of 3 is 4-6 hours. To increase it by a factor of 3 the needed time scale is 1-3 hours. A good qualitative agreement is found between bulk modelling and the observation set in terms of depth integrated dissipation and potential energy anomaly.

Keywords: Dissipation, Potential Energy Anomaly, Near-surface Stratification, Unstable Layering, Micro Structure.

Acknowledgements: Thanks to the labour contributions of unnamed staff at the JRC to perform the campaign. The campaign has been made during a post doc study financed by the Danish Research Foundation.

Introduction: Observations of the undisturbed micro-structures yield the possibility to improve the evaluation of processes dominating water column mixing and stabilisation also in terms of modelling originally based on observations from standard hydrographic equipment. The aim of the present paper is therefor to document the formation of near-surface stable and unstable layers, to estimate time scales for changes in the dissipation, as well as to quantify changes in depth integrated dissipation and potential energy anomaly as being functions of the external forcing.

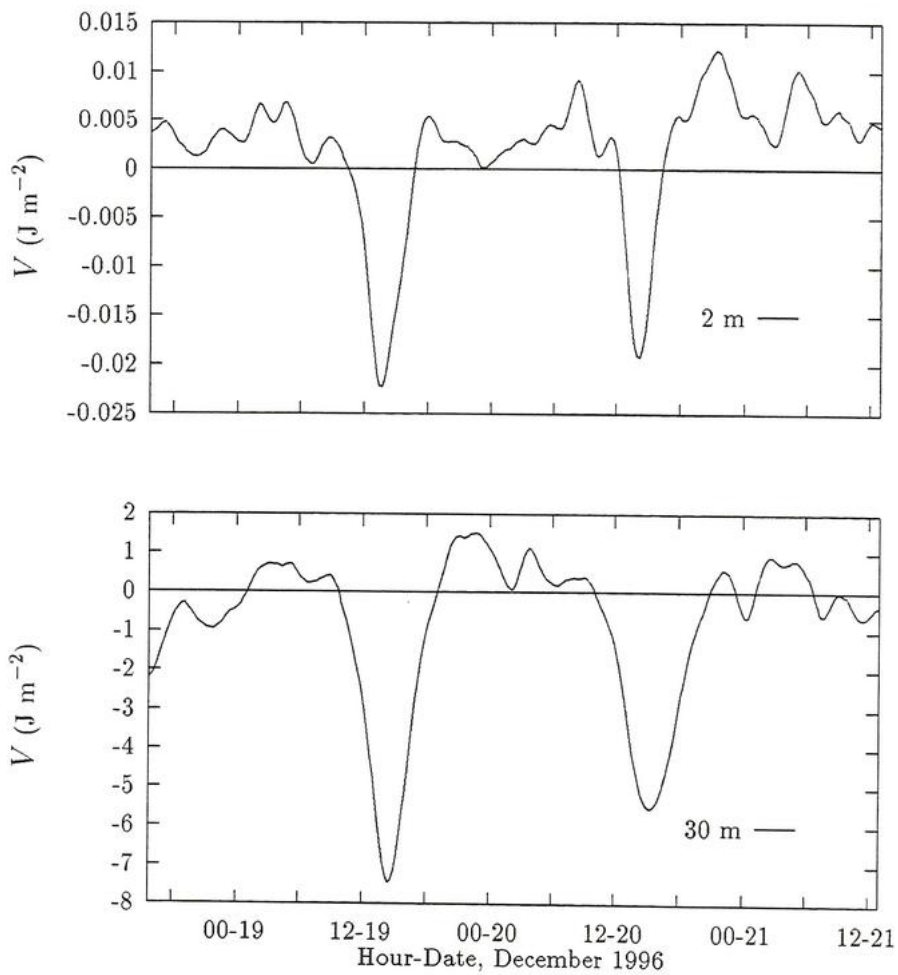


Figure 1: Potential energy anomaly (V) from the surface down to depths 2 and 30 m. A Parzen-filter excluding events of a time scale less than 3 hours has been used.

Methods: Microscale profiles of pressure, temperature, conductivity, and dissipation have been conducted using the ME microstructure profiler every 15 min from December 18th 14.00 to the 21th at 14.00. Measurements were made from depths about 30 m to the surface. Single measurements (29 of 291) did not penetrate through the surface. Erroneous or missing near-surface data have been replaced by interpolation over time. The mean dissipation and temperature in depth 2-30 m are taken to equal the values in the water column below. Calculations of the potential energy anomaly and of depth integrated dissipation are made by summation over the observation set. The potential energy anomaly over the depth range h is calculated with reference to the averaged density over the depth range h .

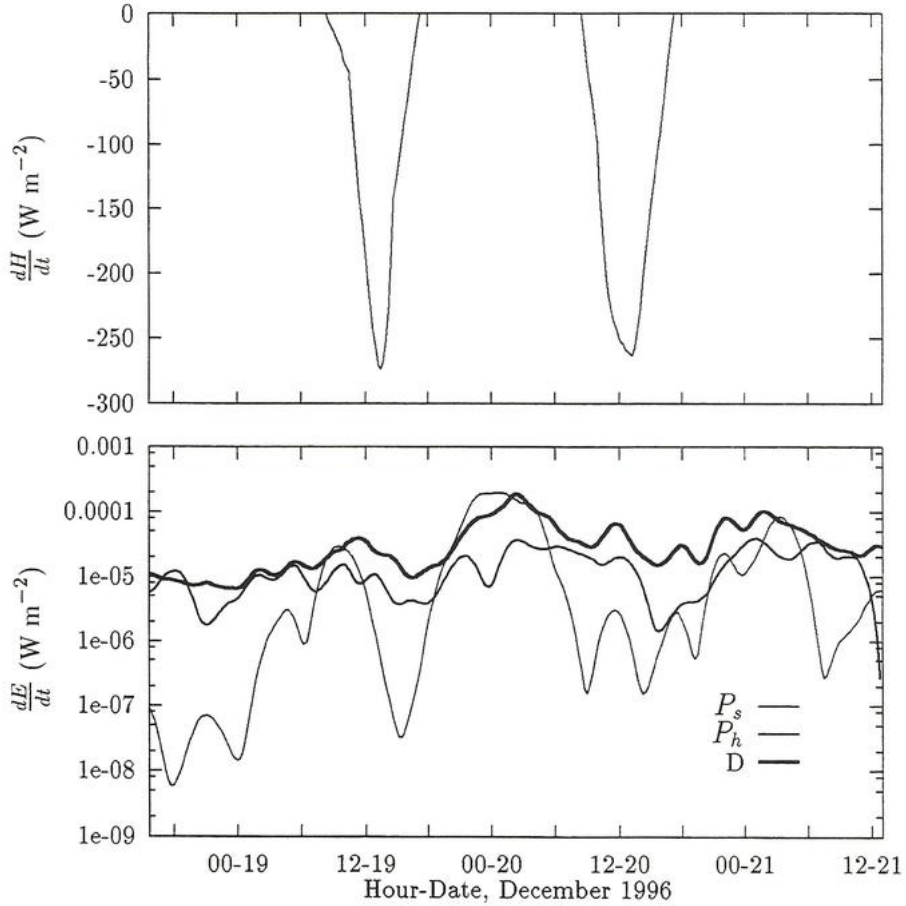


Figure 2: Top: Heat gain of the water column ($\frac{dH}{dt}$) Bottom: Change in kinetic energy due to wind shear stress (P_s), heat efflux (P_h) and observed dissipation (D). A Parzen-filter excluding events of a time scale less than 3 hours has been used.

External Forcing Estimates: The external forcing from the wind shear stress is estimated from wind velocity observations on the study site, approximately 20 m from the ME microstructure profiler. The wind velocity remains less than 5 m s^{-1} . Hence, the drag coefficient formulation for a smooth flow over the lake surface is used to estimate the friction velocity (u_*). A ME-Anemometer at height 0.85 m is used. The heat flux is estimated from changes in the water column heat content using a Parzen-filter excluding events of a time scale less than 3 hours. Advection transport terms are only of importance during the night to December 20th.

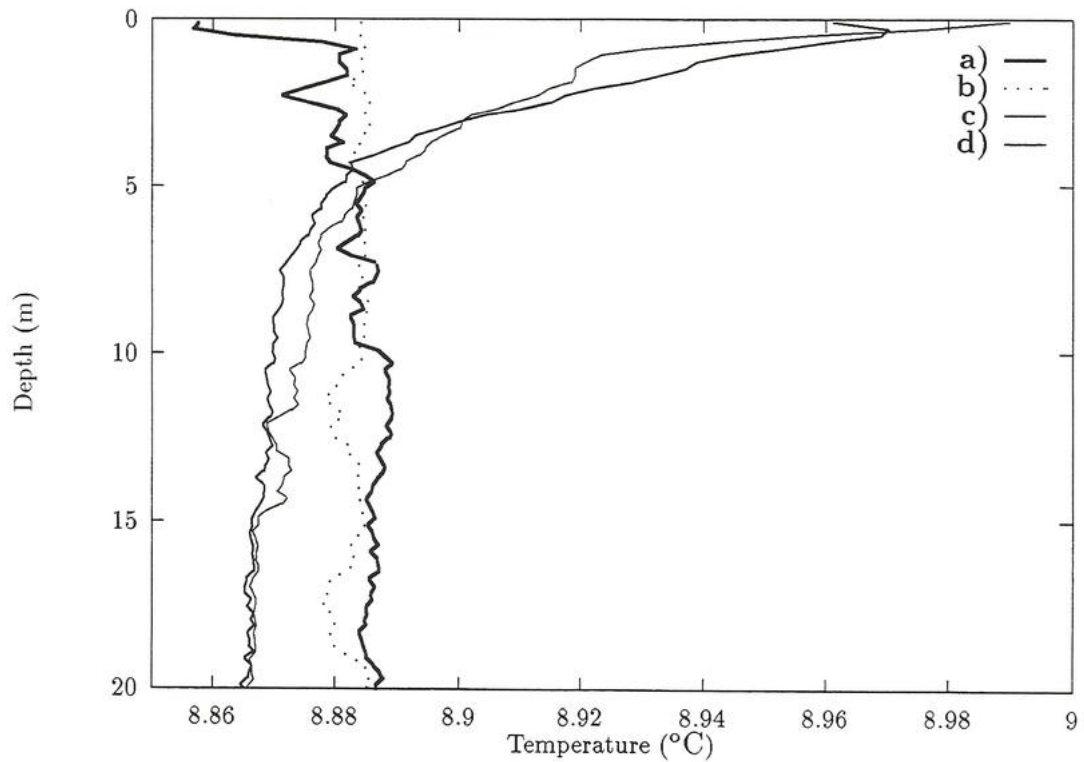


Figure 3: Temperature profiles during night (a and b) and day time with net-heat gain (c) and net-heat loss (d).

Discussion: A weak but persistent stable stratification develops just below the water surface (Fig. 1.top) during minimal winds and a net heat gain of the water column (Fig. 2). The stratification is found next to the lake surface (Fig. 3.c) At decreasing irradiance the water column becomes unstable at the lake surface, while stably stratified below (Fig. 3.d) During night-time, near-surface stratification is alternating between homogeneity and unstable conditions (Fig 2. Bottom, Fig 3. a and b). Patches of denser water are found temporally in at larger depths (10 to 20 m, Fig 3. b) The time scale for changes in the dissipation suggest that the dissipation is reduced by a factor of 3 within 4-6 hours after an mixing event. After calm periods the dissipation increase by a factor of 3 within 1-2 hours. The changes in dissipation and potential energy anomaly are in good qualitative agreement with the external forcing (Fig. 1 and 2). However, the quantitative agreement between model and observations demonstrate discrepancies (not shown).

On progressive internal waves in the Lake of Geneva

R. Jiang(1), S.A. Thorpe(2) and U. Lemmin(1)

(1): LRH; EPFL; 1015-Lausanne; Switzerland

(2): Southampton Oceanographic Centre; Southampton, SO14 3ZH, UK

Abstract:

Measurements were made to study dynamics of progressive internal waves in the stratified Lake of Geneva. Observations from different years document the omnipresence of these waves. In order to elucidate the relationship between progressive internal waves and turbulence in the thermocline in the near shore zone, a detailed experimental study was carried out in the summer of 1996 using data from moored current meters, thermistor chains and CTD profiles. The characteristics of these waves will be discussed.

For the data analysis, a methodology is developed to analyze and interpret the temporal variation of temperatures and currents based on a solution procedure for the Taylor-Goldstein equation and subsequent fitting. The analysis provides estimates of the propagation characteristics, energy density, and directional fluxes of internal waves, and the temporal and vertical distribution of the Richardson number, R_i , on scales which may be smaller than that separating the measuring instruments. More than 70% of the observed temperature variance can be explained by the results of the analysis.

The method also provides for quantitative estimates of the rate of dissipation and vertical turbulent mixing coefficients K_z . The results are consistent with those obtained by other methods indicating that instability resulting from a superposition of progressive internal waves contributes to mixing.

The horizontal distribution of stratification and mixing in a shallow lake

Andreas Lorke, Institute of Freshwater Ecology and Inland Fisheries, 12563 Berlin, Germany

The vertical distribution temperature, temperature microstructure and turbulent kinetic energy dissipation rate was measured in Müggelsee along a transect in the main wind direction (E-W). Müggelsee is a shallow polymictic lake. The overall length of the lake along the transect is 4 km, the maximum depth 7 m and the mean depth 4.9 m. Measurements were carried out at 8 stations with a spacing of 500 m by means of a CTD and a microstructure profiler. In addition to the profiler measurements a thermistor chain was employed at station no. 3 (see Fig. 1 or 2).

Preliminary results of these measurements at August 26, 1997 are presented in this contribution.

Wind conditions during this time were typically characterized by an easterly wind pulse during noon and calm conditions from the late afternoon till the next morning. At August 26, 1997 the maximum wind speed was 4.5 ms^{-1} . Calculating the fundamental period of the uninodal internal seiche using a simple two layer model results in a period of $T=22 \dots 26 \text{ h}$. This is approximately the period of the wind forcing. The near resonant forcing results in a large isotherm displacement with values up to the half of the mean depth of the lake. Fig. 1 shows the isotherms from three tracks measured on August 26, 1997. The vertical temperature distribution along the transect as well as the data from the thermistor chain indicate the presence of vertical modes of the seiching also (see track 1 in Fig. 1), which cannot be explained by the two layer model.

Turbulent kinetic energy dissipation as well as temperature microstructure activity show also a distinct horizontal distribution, which can partially relate to the varying wind fetch in the near surface zone or also to varying stratification in deeper regions of the lake (Fig. 2).

Fig. 1: Isotherms obtained from CTD profiles at stations 1 to 8
(black area: lake morphometry, gray area: no data available)

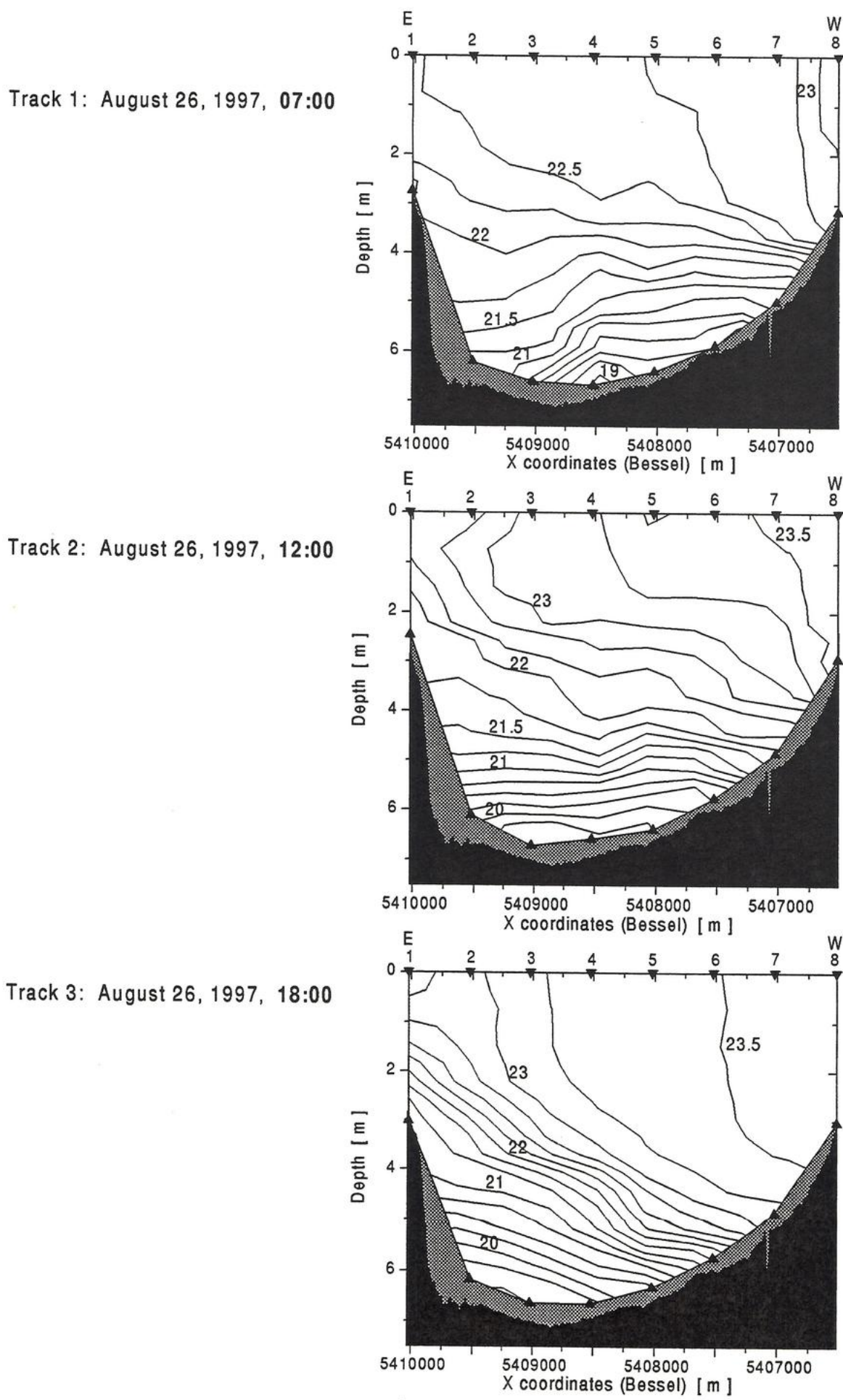
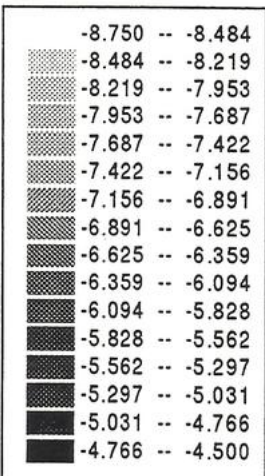
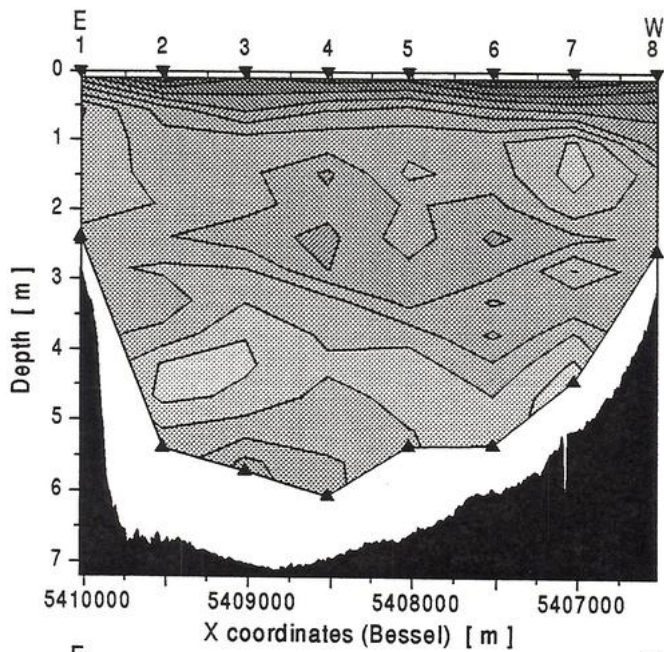


Fig. 2: Contour plots of turbulent kinetic energy dissipation rates at stations 1 to 8
 (black area: lake morphometry, white area: no data available)

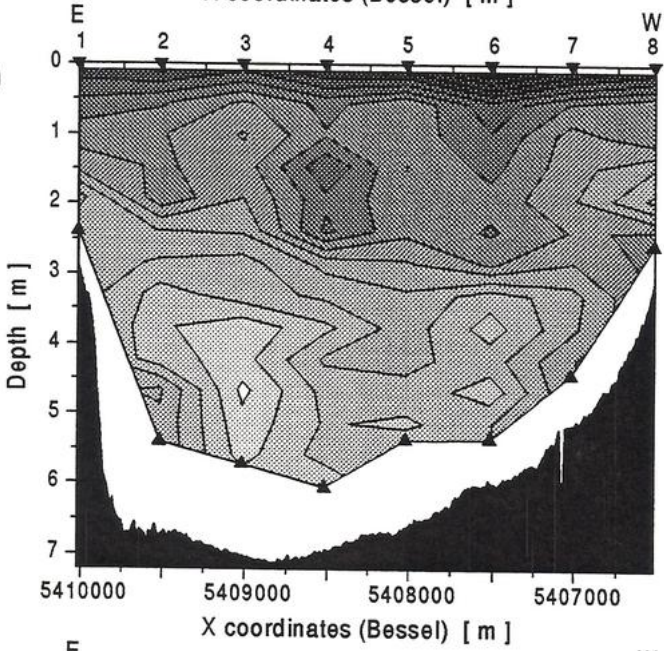
Turbulent kinetic energy dissipation
 in log. (m² s⁻³):



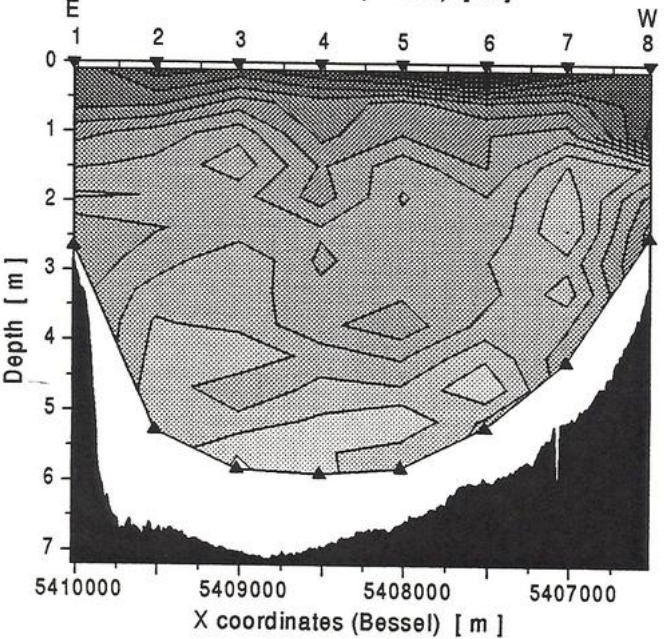
(scale is the same for all graphs)



Track 2: August 26, 1997, 12:00



Track 3: August 26, 1997, 18:00



NATURAL WATERS DYNAMICAL-STOCHASTIC MODELLING

I.E.TIMCHENKO

Marine Hydrophysical Institute, 2 Kapitanskaya str. Sebastopol,
335000 Ukraine. e-mail: aoi @ mhi 2. sebastopol. ua.

Objectives of the natural waters study and management are to much different. It seems natural, that systems analysis should be implemented for effective solving most of them. Systems analysis is goal-seeking method, using all accessible information to reproduce the natural waters dynamics. Main conceptions of the systems analysis are formulated. From the research study view point, the natural waters are distributed parameters systems, which state vector-functions consist of the physical, chemical, biological and others space/time fields. The main problem is the reconstruction of smoothed (averaged) components of this fields, based on dynamical operators, initial and boundary conditions and real-time data, assimilated in the model.

To solve this problem general, a dynamical-stochastic model (DS-model) was suggested [1]. This model operates with 3 components of real natural waters fields (the conditional on input information dynamical operator, conditional on assimilated data mean value and -random "forecast error" component. Applying Kalman/Tzafestas results, the main problems have been solved elsewhere [2].

To meet practical applications requirements this problem should be simplified. It was suggested, that error covariance could be presented in Kolmogorov/Prandtl form . That results in a great simplification of the equations and that permits also to evaluate turbulent exchange coefficients in data assimilation procedure.

Many experiments have been made to validate suggested hypothesis. Main results of them are supplied:

- simulated 4D density field analysis (North Atlantics);
- 4D archive and real-time density surway data assimilation (Central Tropical Atlantics and off-shore polygons);

- SST profiles and scanned satellite data assimilation in differential model of upper mix-layer (Atlantic ocean, Mediterranean sea).

Further development of main DS-model are discussed, focusing on the ecological and economical aspects of water resources consumption. Examples of DS-model for "water basine-land" natural-economic systems are presented [3].

References:

- 1.Timchenko I.E. Stochastic modelling of ocean dynamics.Harwood Acad. Publ. Chur-London-Paris-New-York. 320 p. 1984.
- 2.Timchenko I.E. Systems methods in ocean hydrophysics.Naukova Dumka. Kiev. 280 p. 1986.
- 3.Timchenko I.E. et al. Marine environment systems analysis.MHI publ. Sebastopol. 240 p. 1996.

WATER RENEVAL OF POJO BAY DEEP WATERS

Malve, O. (1 & M. Virtanen (2

(1 Finnish Environment Institute, P.O.Box 140, FIN-00251 Helsinki, Finland

(2 EIA

The Pohja Bay is a coastal semi-enclosed basin at Hanko peninsula, south crest of Finland. The bay is a narrow, SW-NE-oriented branch of the Gulf of Finland. Its width is 1-2 km and length 14 km. The entrance to the bay is shallow (4.5 m), irregular network of narrow passages between small islands. The maximum depth of Pohja Bay is 40 m and the average depth 15 m. The salt content of the epilimnion is very low (0-2 psu) due to fresh water inflow from the drainage basin. On the other hand the salt content of the hypolimnion is higher (3-5 psu). During winter and more occasionally during summer inflow from the Gulf of Finland renews the oxygen storage of the hypolimnion.

However in recent years, the oxygen concentration of the hypolimnion has been approaching zero. Resulting dissolution of phosphorus, eutrophication and the death of fish populations has been tried to hold back with artificial aeration of deep waters.

The aim of this study was to define the deep water renewal and esturiane circulation in the Pohja Bay, and to quantify water, salt and oxygen budgets of the bay. Currents and water level as well as chemical variables and hydrography (CTD) were measured continuosly or during field excursions with 1 to 3 week intervals. Water, oxygen and salt balances of the epi- and the hypolimnion were calculated and modelled. 3D-hydrodynamic water quality model was constructed to study the impact of artificial aeration on water quality of the hypolimnion as well as to dimension needed aeration rate and other potential water protection measures.

Periodic flow components in the Irbe Strait and their contribution to the water exchange.

Madis - Jaak Lilover, Urmas Lips and Janek Laanearu

Department of Marine Physics, Estonian Marine Institute, Tallinn,
Estonia

Introduction

The water quality of a semi-enclosed basin depends crucially on the water (nutrients, pollutants) exchange through the straits connecting the basin with the open sea.

Although the water exchange properties between the Gulf of Riga and the Baltic Proper through the Irbe Strait have been investigated in a few studies the periodic flow components have not been described satisfactorily. The present paper is a continuation of the study on dynamics and circulation in the Irbe Strait presented at the 1-st Workshop in Kastanienbaum, 16-18 September 1996 (Lilover and Lips, 1996). Here we shortly characterise the forcing components in the Irbe Strait area, then draw a regular strait flow scheme and finally the current variability and the role of periodic flow components in the water exchange are discussed.

Study area

The Irbe Strait (sill depth $H_S \approx 25$ m, cross-section area $F_{IS} \approx 0.45 \text{ km}^2$, width $W_{IS} \approx 30$ km, length $L_{IS} \approx 40\text{km}$) connects the Gulf of Riga (total volume of 410 km^3 , area $F_{GoR} \approx 19000 \text{ km}^2$, maximum depth $H_M \approx 60\text{m}$) and the Baltic Proper. The second connection of the gulf with the open Baltic is through the Suur Strait and the Moonsund area. The cross-section of this area is 10 times smaller than that of the Irbe Strait. The annual river discharge into the Gulf of Riga is about 30 km^3 , which makes the freshwater input per an area unit higher than into the whole Baltic Sea. Due to the latter and the restricted water exchange through the straits the mean salinity in the Gulf is 5.5 psu which is by 1.6 psu lower than in the adjacent region of the Baltic Sea.

Forcing components and mean flow scheme

Due to the relatively high freshwater supply into the Gulf of Riga the barotropic forcing by the sea level difference between the gulf and the Baltic Proper and the

baroclinic forcing by the density differences between these basins can be regarded as the main steady forcing components driving the water flow through the strait. The wind forcing playing an important role for the time scales of several days and less can be regarded as the main short-term forcing component.

The comparison of the mean baroclinic and barotropic forcing showed that they have the same magnitude. According to this balance the surface water is forced to flow out by the surface pressure gradient and the bottom water is forced to flow in by the opposite pressure gradient due to the density difference between the basins. As an internal deformation radius being 3-4 km is much less than the width of the strait, the strait appears to be wide for the meso-scale features, like rotationally dominant fronts, to occur in the strait area.

In full agreement with the listed water exchange and forcing factors a quasi-permanent salinity front separating the Gulf of Riga and the Baltic Proper waters occurs in the Irbe Strait. Relaying on the geostrophically balanced water flow this observed S-shaped frontal boundary indicates that the Gulf of Riga water should flow out in the northern part of the strait and the Baltic Proper water should flow in along the southern slope of the strait. The vertical structure of the measured density field at the cross-section corresponds well to the latter flow scheme. The inclination of the boundary between the open sea water and the gulf water indicates that the flows in the layers under discussion must be contra-directional. The direct ADCP measurements of the current reflected also well the expected mean current structure in the frontal area.

Current variability

The intermittent wind forcing causes the short-term flow oscillations of different periods, which are added to the described mean flow. In the result the actual flow field is much more complicated than the mean flow scheme. The spectral analysis of time series of currents revealed the most pronounced energy peaks in semi-diurnal, diurnal and synoptic frequency bands.

The decomposition of the current record, measured during 10-days intensive measurement campaign in June 6-15, 1995, into the above- mentioned three frequency

bands showed that the diurnal and low-frequency ($30\text{h} < T < 4\text{days}$) oscillations are the most energetic explaining 36% and 37% respectively of the total variance of currents (Fig. 1). Only about 8% of the energy belongs to the semi-diurnal band with inertial oscillations (≈ 14 h) and semi-diurnal tides which are supposed to be non-energetic in the Baltic Sea. Probably inertial oscillations give the most of energy of this band. The hypothesis (Petrov, 1979) of the diurnal period having the tidal origin (K_1 tide respectively) was rejected by Raudsepp and Elken (1995) who simulated daily oscillations by the GFDL circulation model where the tidal forces were not included. Considering the system the Irbe Strait - the Gulf of Riga as a Helmholtz resonator, one can get self-oscillation period of about 24 hours ($T=2\pi/\omega$, $\omega=(gF_{IS}/L_{IS}F_{GoR})^{1/2}$). The system resonance to the atmospheric forcing and to the Baltic Sea barotropic seiches with periods close to the diurnal is probably beyond the observed current diurnal oscillations.

The low-frequency oscillations of currents revealed periods (from 43.2 to 48.6 hours) close to the wind forcing oscillation period (48 h) during our measurement campaign. These wind oscillations resulted in the sea-level oscillations and the related current oscillations with nearly the same period. The sea-level difference had a time lag of about 6 h and worked against the wind stress. In the middle of the strait the current appeared to be well correlated and responded quickly without time lag to the sea-level difference changes in the upper layer. In the bottom layer the current responded with time lag of about 10 hours. At the entrance of the strait the time lag to the sea-level difference changes was 7.7 and 4.7 hours respectively.

Consequently, the low-frequency current correlating well with the sea level elevations appeared to be preferably contra-directional to the wind stress.

Despite of the large amplitudes of the wind forced current fluctuations the fluctuating components of the current do not contribute much to the water exchange in the case of frequently observed central position of the salinity front. The estimated distance which a water parcel can cover in a half of the two-day oscillation period is less than 10 km. Because of the 40 km length of the strait these shifts are too short to produce large inflows into the gulf.

Therefore, the quasi-permanent flows - the inflow of the Baltic Sea water in the lower layer of the southern part and the outflow of the gulf water in the northern part of the strait - seem to contribute the most to the water, salt and nutrient exchange through the Irbe Strait.

References

- Petrov, B.S., 1979. Water balance and water exchange between the Gulf of Riga and the Baltic Proper. In: Sbornik rabot rizhskoj gidrometeorologicheskoy observatorii, 18, Riga, pp. 20-40 (in Russian).
- Raudsepp, U., and J. Elken, 1995. Application of the GFDL circulation model for the Gulf of Riga. In: A. Toompuu and J. Elken (eds.), EMI Report Series, 1, Tallinn, pp. 143-176.
- Lilover, M.-J., and U. Lips, 1996. Horizontal and vertical structure of currents in the Irbe Strait. In: Extended abstracts of the workshop on “Physical Processes in Natural Waters”, 16-18 Sep. 1996, Kastanienbaum, Switzerland.

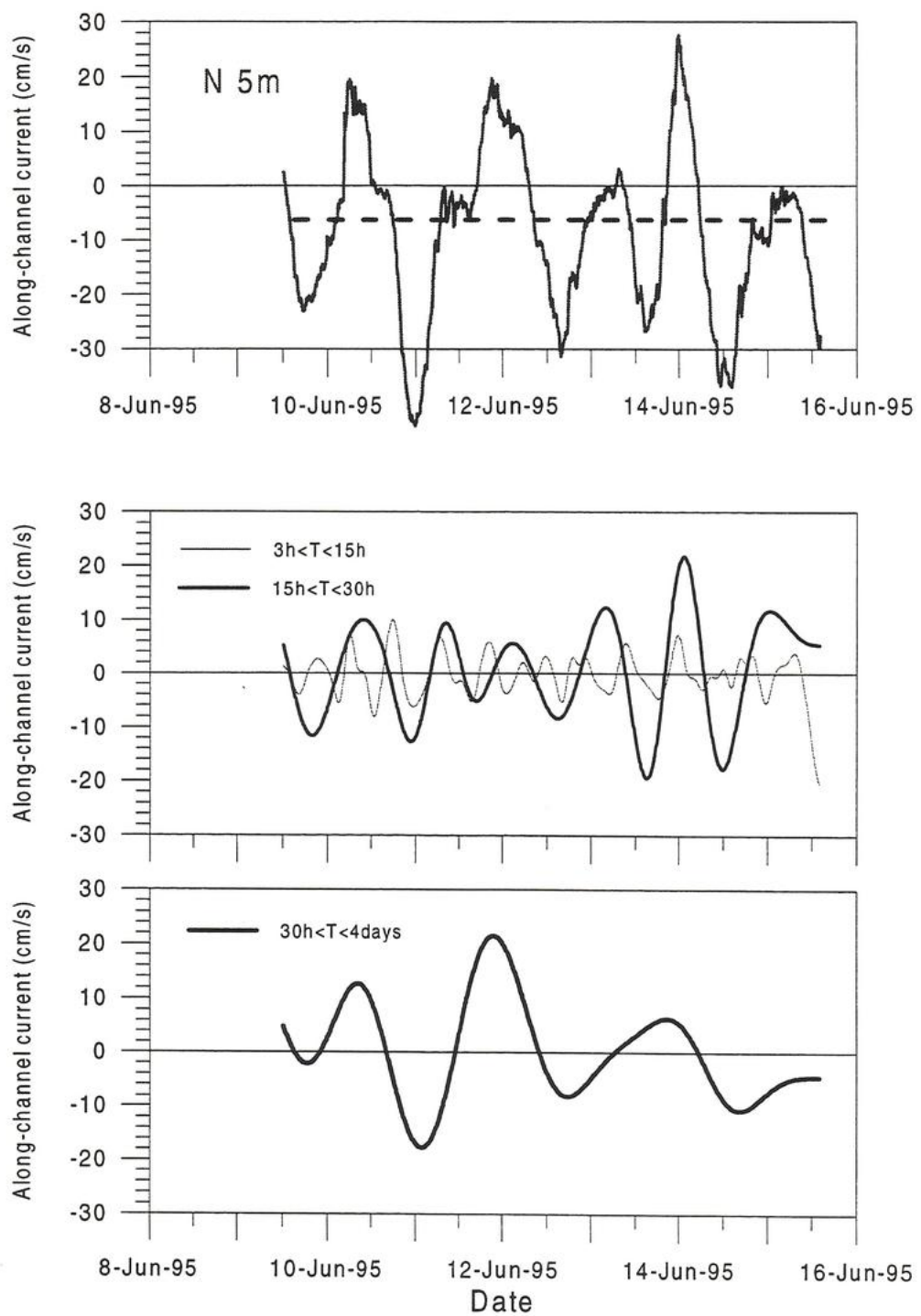


Figure 1. Along-channel current measured at 5 m depth in the northern side of the Irbe Strait (upper panel) and the same current record decomposed into three frequency band (lower panels).

Circulation patterns in Lake Constance induced by local windfields
(extended abstract)

Contribution at the 2nd Workshop on „Physical Processes in Natural Waters“ from 3 to 5 November 1997 at Ispra

Erich Bäuerle and Georg Hertkorn

Limnological Institute at the University of Constance

ABSTRACT

The paths of drifting fishnets and images of remote sensing give strong hints at an eddy-like circulation pattern in the Bay of Friedrichshafen (Upper Lake Constance) during land/lake breeze regimes. With a numerical 2-dimensional two-layer model an episode during autumn 1994 is simulated. The results are promising, although clearly exposing our insufficient knowledge of the wind field on the lake.

INTRODUCTION

Conventionally, in numerical modeling of lake circulation wind-driven currents are attached to large-scale wind fields which are assumed to be uniform over the lake. This assumption, which is crucial, is completed by rather coarse specifications regarding the temporal course of the wind. Changing directions and speeds over the lake are hardly describable based on observations taken at shore-bounded or even inland stations. Time history of wind fetch is not deducible from such measurements and - honestly spoken - the parametrization of the wind stress acting at the water surface often turns out to be an arbitrary act. This study stands to this tradition.

OBSERVATIONS

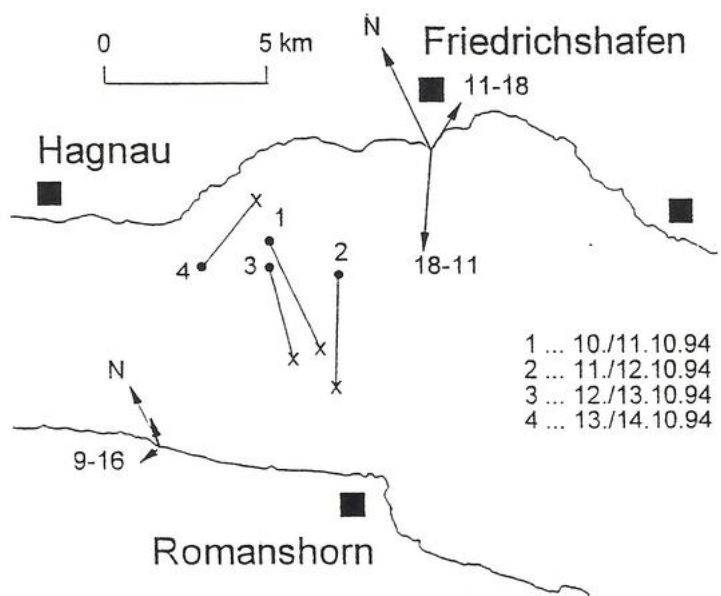


Fig.1: Positions of bring out (o) and haul home (x) of drifting fishernets at 4 consecutive days in October 1994.

Due to lucky observations (see Fig.1) we got notice of considerable epilimnic currents (≈ 10 cm/s). The distance between the positions where a native fisherman casted his more than 400 m long and 8 m deep drifting nets at evening and hauled them home early at the following morning was striking as generally the actual winds were faint. Only the northern part of central Upper Lake Constance (Bay of Friedrichshafen) experienced winds worth mentioning. At this part of the lake a land/lake breeze with nightly wind speeds up to 5 m/s has developed.

The question arises whether this local wind field was able to accelerate the epilimnic water masses of the stratified lake.

THE MODEL

With a two-dimensional two-layer model of wind-driven circulation we tried to reproduce the observed currents. According to observations from 5 sites around the lake the wind is assumed to blow only during the night as landbreeze concentrated at Friedrichshafen. Due to the autumnly stratification with a well-mixed deep epilimnion and because of the inherent depth averaging facilities of the fishernets we hoped to meet the situation with such a simple model. A two-dimensional theory on wind-driven currents in the x,z-plane surely would fail as it predicts recirculation in the lower part of the epilimnion - in contradiction to the directions of the drifting fishernets during the first 3 nights. The observations of the fourth night suggest a recirculation in the horizontal plane due to a horizontal gyre. Variability in both horizontal directions is an indispensable demand. It remains an open question whether the two-layer model meets the vertical structure of the wind driven currents in the lower parts of the epilimnion.

RESULTS

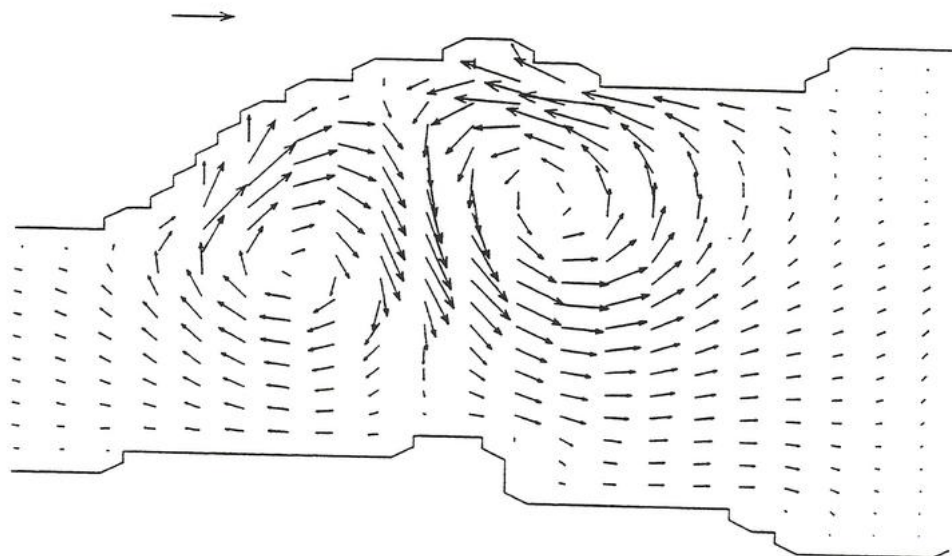


Fig.2: *The calculated vector field of currents in the epilimnion of the central Upper Lake Constance at the end of the third night ($t = 72$ h).*

First results of the numerical model reproduced some principles of the observations (drifting with wind in the center of a double-celled gyre, recirculation outside the region of direct wind forcing) but showed significant discrepancies with respect to the absolute values of the horizontal velocities and the position of the gyre.

Further improvements would be possible if appropriate wind fields were constructed. But, due to the deficiencies in the observations of both the currents and the wind field it is not possible to formulate an inverse problem.

Apart from that, it became clear that consideration of the Coriolis force is essential in order to get reasonable agreement with the observations. In Fig.3 we oppose the vertical displacements in the Bay of Friedrichshafen at some moments of the first night calculated with (left) and without (right) taking into account the effects of Earth's rotation. At $t = 4$ h (Fig.3a) the interface indicates upwelling in the inner part of the bay. The snapshot at $t = 8$ h (Fig.3b) shows how a quasi-geostrophic balance is build up in the case of Coriolis effects (left), contrary to the non-rotating case (right) with upwelling at the northern and downwelling at the southern coast. At $t = 12$ h (Fig.3c, left) two well organized gyres have developed if Coriolis effects are taken into account. It is interesting to notice that at the northern shore an internal Kelvin wave has been created and is travelling with the shoreline to the right towards Lake Überlingen (the western part of Upper Lake Constance), whereas with $f = 0$ the disturbance of the interface seems to travel away in both directions at the southern coast .

It will be worthwhile to study the implications for the regions of the lake not directly influenced by the wind.

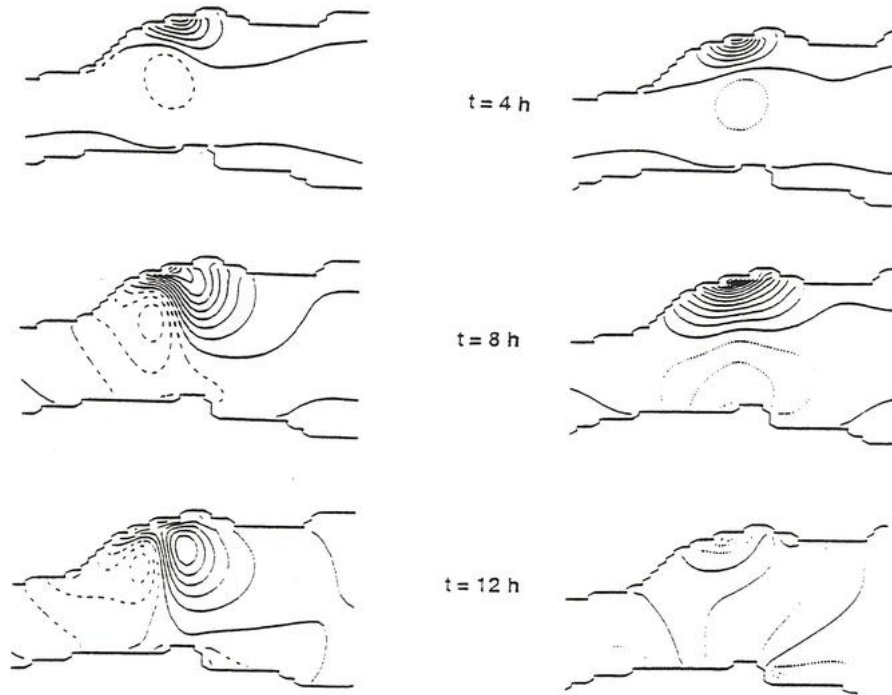


Fig.3: The vertical displacements of the interface at $t = 4$, 8 and 12 h after onset of the wind. Left: with, right: without Coriolis effects.

Lateral renewal of deep water in Lake Constance by convective cooling in winter over ascending bottom

Eckard Hollan
Institut für Seenforschung, Langenargen, Germany

Extended abstract

Synoptic surveys by CTD-measurements since 1992 indicate large transient density currents, which originate from the marginal region of the lake, when it has been subdue to strong cooling at the surface. Such bottom currents advance into the deepest region and provide a partial renewal of the stagnant deep hypolimnetic waters, before vertical local convection over the deepest region has penetrated so far, if at all during a generally mild winter.

Three selected recent examples of such currents from late winter 1996 are displayed in Fig. 2. Two of them from 7 March and 14 March have been detected on the same transect in the Bay of Friedrichshafen (see Fig. 1, stations 18 through 27 on the right in italic numbers) and the third one on 13 March in the Bay of Konstanz (stations 1 through 8 on the left). The uneven counting of the depth lines results from altitude lines in the original chart of the most recent depth survey from 1990.

The horizontal coordinate of the group profile diagrams in Fig. 2 is the distance in km along the transect. The vertical coordinate gives the depth, which is represented in two scales: deep stations below 100 m refer to 0 - 250 m or 0 - 200 m, while the depth scale of shallow stations is enlarged by the factor of 2.5 in order to emphasize the supposed origin of cold water. Temperature profiles are shown by heavy full lines and those of specific conductivity referring to 20°C by light full lines. The accuracy of the temperature and conductivity measurements is 0,01 K and 1 μ S/cm, resp.

The scales of temperature and conductivity are drawn separately in each diagram. The tick marks on them labelled by the italic station numbers (e.g. 18 - 27 in the upper diagram of Fig. 2) mean the origin at which the scale has to be put horizontally against the vertical hatched line of the corresponding profile on the transect. In the central diagram some origins are shifted to keep the graphical representation clear. A guide to read the absolute values of conductivity is the roughly constant vertical distribution in the convective upper layer throughout the whole transect.

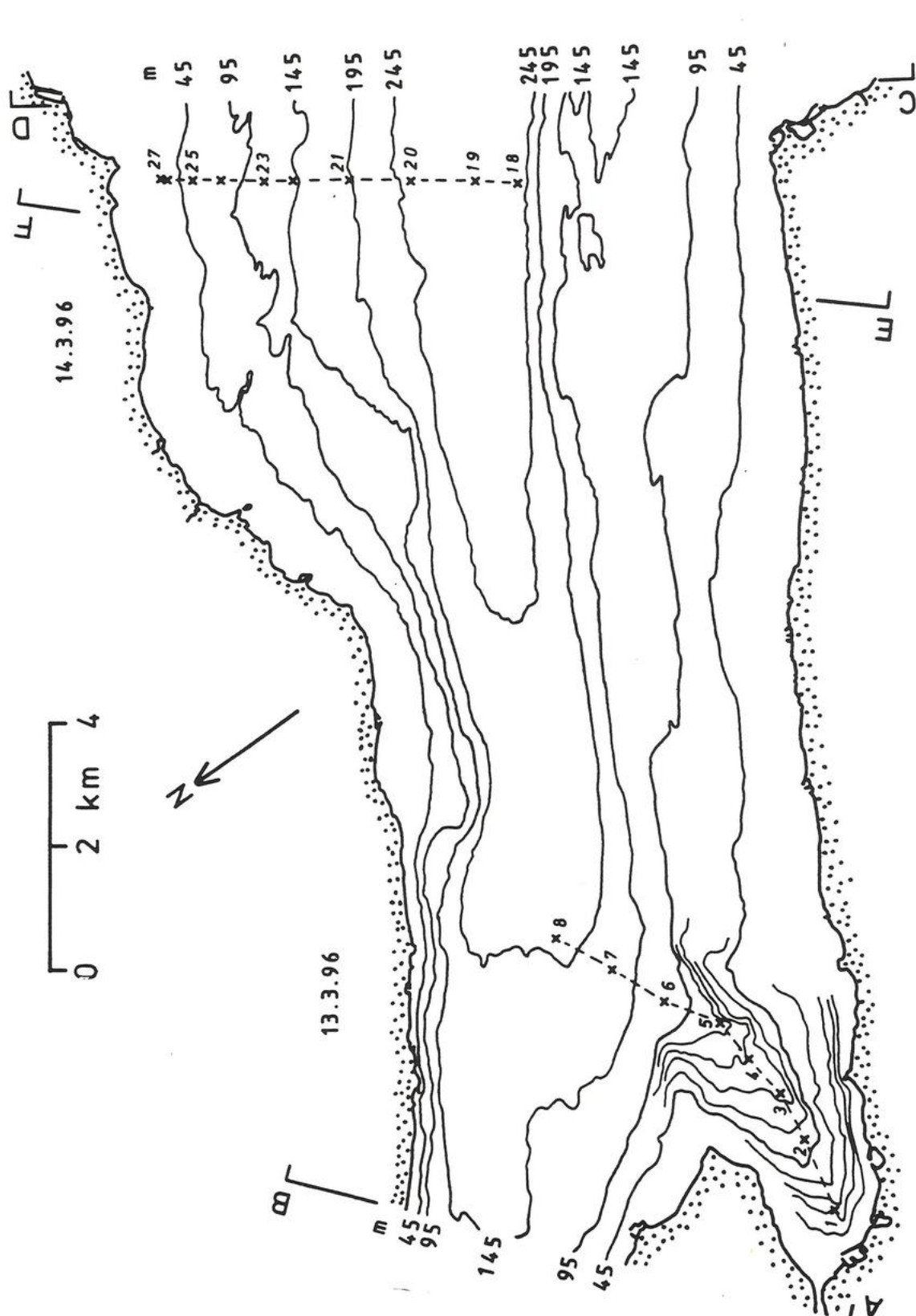


Fig. 1 Map of the transects of Fig. 2 in the western part of the main basin of Upper Lake Constance. The depth lines are drawn in steps of 50 m and designated on the right and left margin. They are completed in steps of 10 m in the Bay of Konstanz (lower left corner).

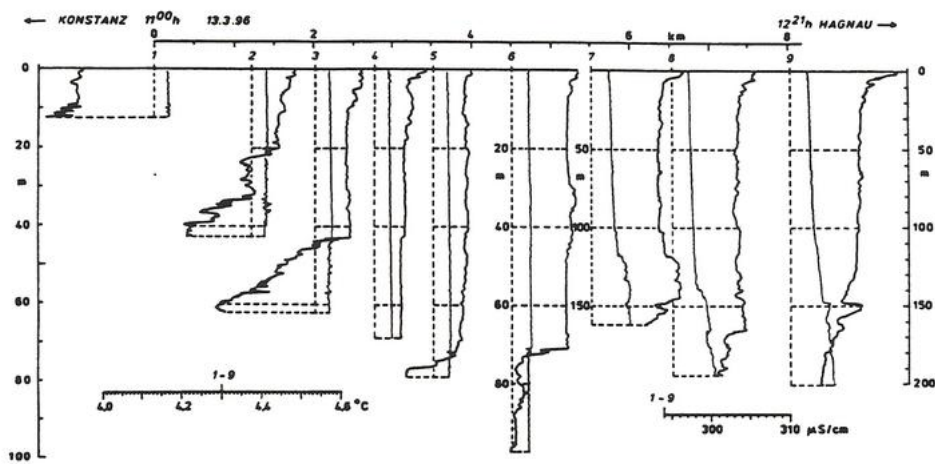
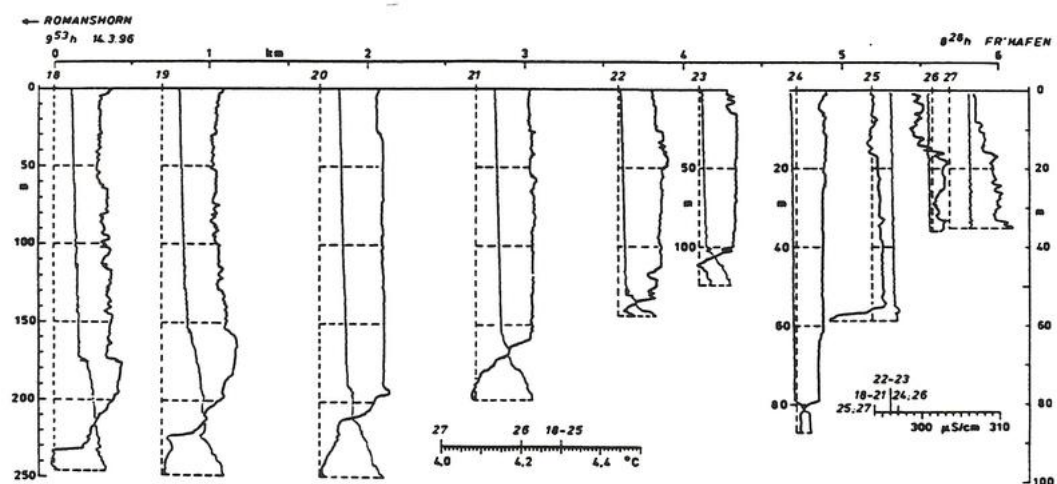
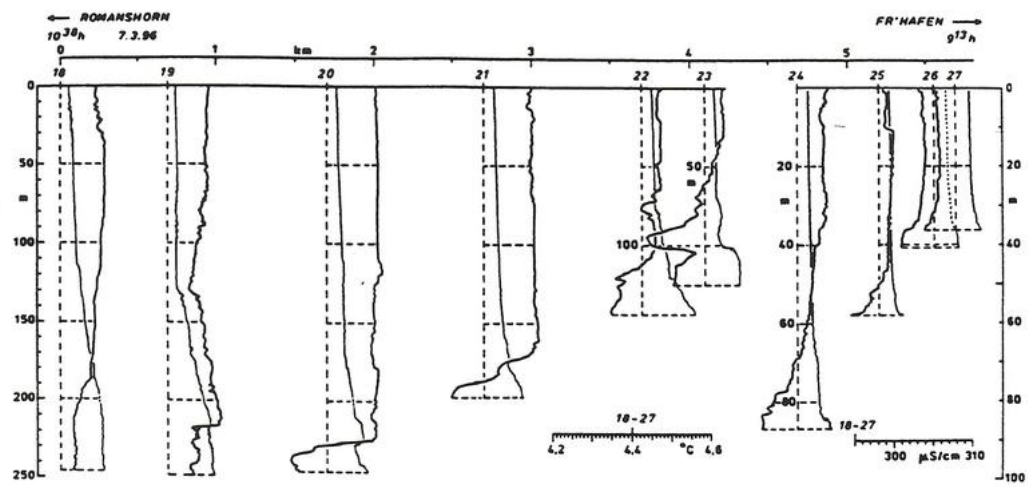


Fig. 2 CTD-profiles along the transects in the Bays of Friedrichshafen and Konstanz on 7 and 14 March 1997, upper two diagrams, and on 13 March 1997, lower diagram, resp. Heavy full line: temperature, light full line: conductivity (further explanation in the text).

The observed events are related to cold weather conditions over the lake during or just before the measurements. In the transect from Friedrichshafen (upper and central diagram in Fig. 2) the cold water appears to stem from the medial deep and shallow regions in this Bay. A far distant contribution in this region from the eastern less deep part of Lake Constance cannot be excluded, as measurements show obtained on a transect a few km eastward. Similar results are observed on a transect in the Bay of Rorschach during the same month.

Distinct events are documented by the grouped profiles from the transect in the Bay of Konstanz from 13 March shown in the lower diagram of Fig. 2. The cold water had been formed during two days of negative air temperature over the lake. Its way along the talweg can be detected till station 3 and toward the deep mouth of the Bay at station 6. The lacking event at station 4 may be related to a short interruption of the flow which is indicated by the flat extent at station 5. The positioning of station 4 is more to the southern side of the talweg and may thus have avoided the shallow bottom flow there. The event in the Bay of Konstanz proves the cause by surface cooling, since no cold river inflow occurs in this region of the lake, instead there is the strong single outflow at the inner end of the Bay at Konstanz.

As first results from the intensive measurements from February through June 1996 it is evident that the process of formation and penetration is strongly transient and related to topographical structures: ascending bottom at the margin of the lake, in particular focussing by bay-like depth configurations. The depth of the intrusions depends also from the remnant weak density stratification in the hypolimnion from the previous winter and warm season. Density currents by river inflows attain more influence in the course of spring time, when their discharges increase. Such contributions are mostly detectable by a clear signal of the conductivity parameter.

From these observational findings a considerable lake-own renewal mechanism of deep waters during winter time is inferred in terms of convectively driven density currents. They depend on the size, general shape and the marginal mesoscale depth configuration of the lake basin. The preceding thermal development of the deep stratification and the history of the actual winter prescribe dynamically occurrence, intensity and depth of penetration of these catabatic currents. A detailed explanation of their formation is still pending and requires more observations of higher resolution in space and time.

Modelling the Adriatic Sea under consideration of the orographic peculiarities

Srdan Dobricic and Walter Eifler

Space Applications Institute, JRC, Ispra

The specific position of the Adriatic Sea between high mountains on the west, on the east, and on the north, and with the orographic openings through the Po valley and Otranto strait makes the problem of the modelling of physical processes in it closely connected with the requirement to have the meteorological forcing data on the high temporal and spatial resolution. This requirement is further requested by the fact that the local meteorological phenomena are governed both by the land-sea interaction and orographic influence along the coastline, and by the influence from larger midlatitude meteorological systems that pass the Adriatic Sea.

For this reason a coupled, two way interacting, system consisting of high resolution ocean and a high resolution atmospheric limited area models is used in order to realistically simulate both ocean dynamics in the Adriatic Sea and in the atmosphere in its surroundings. The limited atmospheric model is initialised and forced through lateral boundaries by a global circulation model data available on the coarser resolution.

The ocean model is the ISPRAMIX model, developed at Space Applications Institute at JRC (Eifler and Schrimpf 1992). The model is a 3-d primitive equations model used for climatological simulations in Atlantic. The atmospheric model is the ETA model from NCEP Washington, already for a number of years used for the twice daily operational forecasts for North America.

The ocean model has the height vertical coordinate and a step-like bottom representation. The atmospheric model uses the so called eta coordinate in vertical. It is a generalised sigma coordinate able to make a step like representation of mountains, still keeping some of advantages of the sigma system.

The step like representation of mountains, free of errors in the pressure gradient force at large mountain slopes may significantly contribute the quality of the simulations for the atmospheric phenomena influenced by topography. It was shown by Mesinger et al. (1988) that the step-like representation of mountains helped to produce superior forecasts compared to those by the sigma system, both in the case of the cyclogenesis in the lee of Alps and for the redevelopment of a cyclone in Appalachians. Furthermore, the step-like representations in areas of steep topography gives the possibility to simply improve the accuracy in the representation of the model orography, by increasing the resolution in both horizontal and vertical direction.

The ocean model uses the C-grid staggering of horizontal points in Arakawa's notation, while the atmospheric model uses the E-grid staggering. The difference in the horizontal points arrangement creates the problem of the matching of the coastlines in two models. Two coastlines can not be matched without relatively large changes in one of two model's dynamics. At this stage of the development of the coupled system this problem is overcome by the horizontal interpolation.

A possible inconvenience for the high resolution simulations in the atmosphere is the use of the non-staggered position of u and v velocity components on the E grid in the atmospheric model. In the area with high mountains, like the Adriatic Sea, at high resolution simulations, it is necessary to use a relatively large artificial diffusion in order to prevent the numerical noise. This requirement is contradicting the requirement that the subgrid scale influence on horizontal mixing diminishes with the increasing of the horizontal resolution.

Both models are hydrostatic, meaning that it is assumed that horizontal scales of the motion are much larger than vertical. The resolution currently used for simulations is at the boundary between the hydrostatic assumption at the atmospheric model and the use of the nonhydrostatic model must be further investigated.

The interaction between two models is achieved by the specification of surface fluxes from the atmospheric model as the upper boundary condition for the ocean model and by the specification of the SST from the ocean model as the lower boundary condition for the atmospheric model. Fields are averaged for each hour of the integration of each model and then that value is used as the boundary condition for the next hour of the integration of models.

After setting up the system, for the purpose of the physical modelling in the Adriatic Sea, especially concerning the problem of storm surges simulations and flow simulations in the ocean in the cases of major pollution events in the North Adriatic, a several numerical experiments were performed in order to estimate the sensitivity of ocean simulations on the horizontal resolution of the wind forcing field.

The case study was from the beginning of November 1994, during the disastrous flood in the north-western part of the Po valley, caused by extremely large precipitation. The synoptic situation was characterised by large scale southerly flow towards Alps. During the event the strong wind over the Adriatic Sea was channelled by the surrounding mountains and was flowing from south-east causing the sea level raise in its northern part.

In order to test the sensitivity on the resolution of the forcing, the ocean model was run at the resolution of 4km in horizontal and was forced by two limited area 96 hours forecasts. One was performed at the 10km resolution and the other at the 70 km resolution. The second experiment used the resolution which is comparable to the highest resolutions used operationally by global models.

The main simulated dynamics of the event are reproduced similarly by both simulations, due to the influence of the bottom topography on the ocean model simulation and due to a relatively simple wind flow pattern over the Adriatic for this period. The main differences in the flow below the surface are along coastlines. In Fig. 1. the flow at the depth of 6 meters is shown for both simulations. In the figure 2 the corresponding forcing fields at the ocean model resolution are displayed.

In the northern Adriatic the typical clockwise circulation is disturbed by the strong wind forcing from the south-east at the surface. Still the circulation at the high resolution forcing experiment maintains the cyclonic shape of the flow due to the narrow forcing by the local north-east wind along the coast between Trieste and Venice. This feature is completely absent at the coarse forcing experiment and consequently the clockwise circulation is completely disturbed.

The sea level height predictions displayed in Fig. 3 show large quantitative differences in the period of the peak surge, and less pronounced differences for the rest of the simulation period.

Unfortunately, still there was no possibility to compare observations in the ocean with simulations, and in the future it is necessary to make these comparisons in order to better quantify the influence of the horizontal resolution of both models on the quality and accuracy of the ocean simulations in the Adriatic Sea.

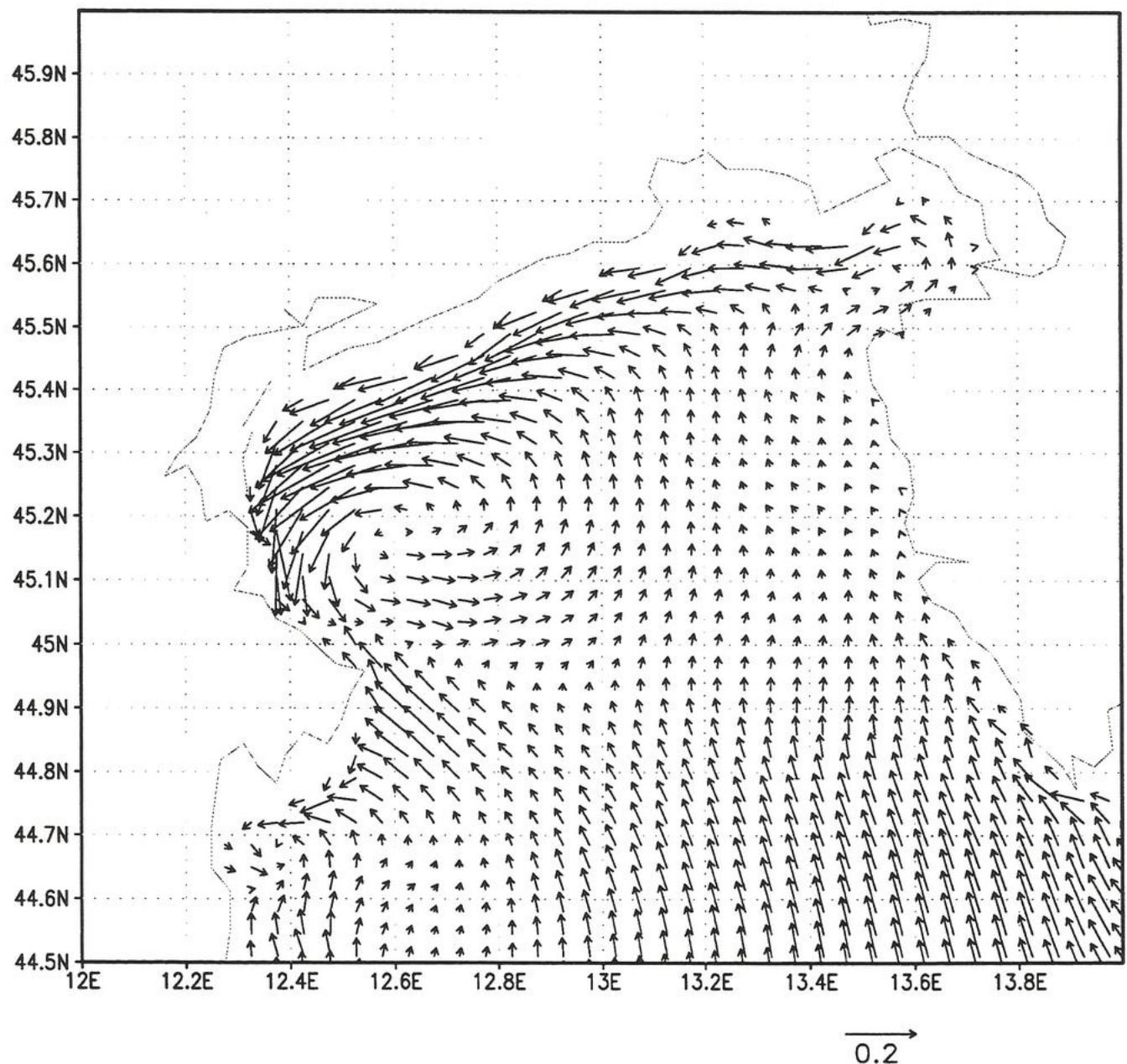
References:

Eifler W. and Schrimpf W., 1992: ISPRAMIX, a Hydrodynamic Program for Computing Regional Sea Circulation Patterns and Transfer processes. *Report EUR 14856 EN*

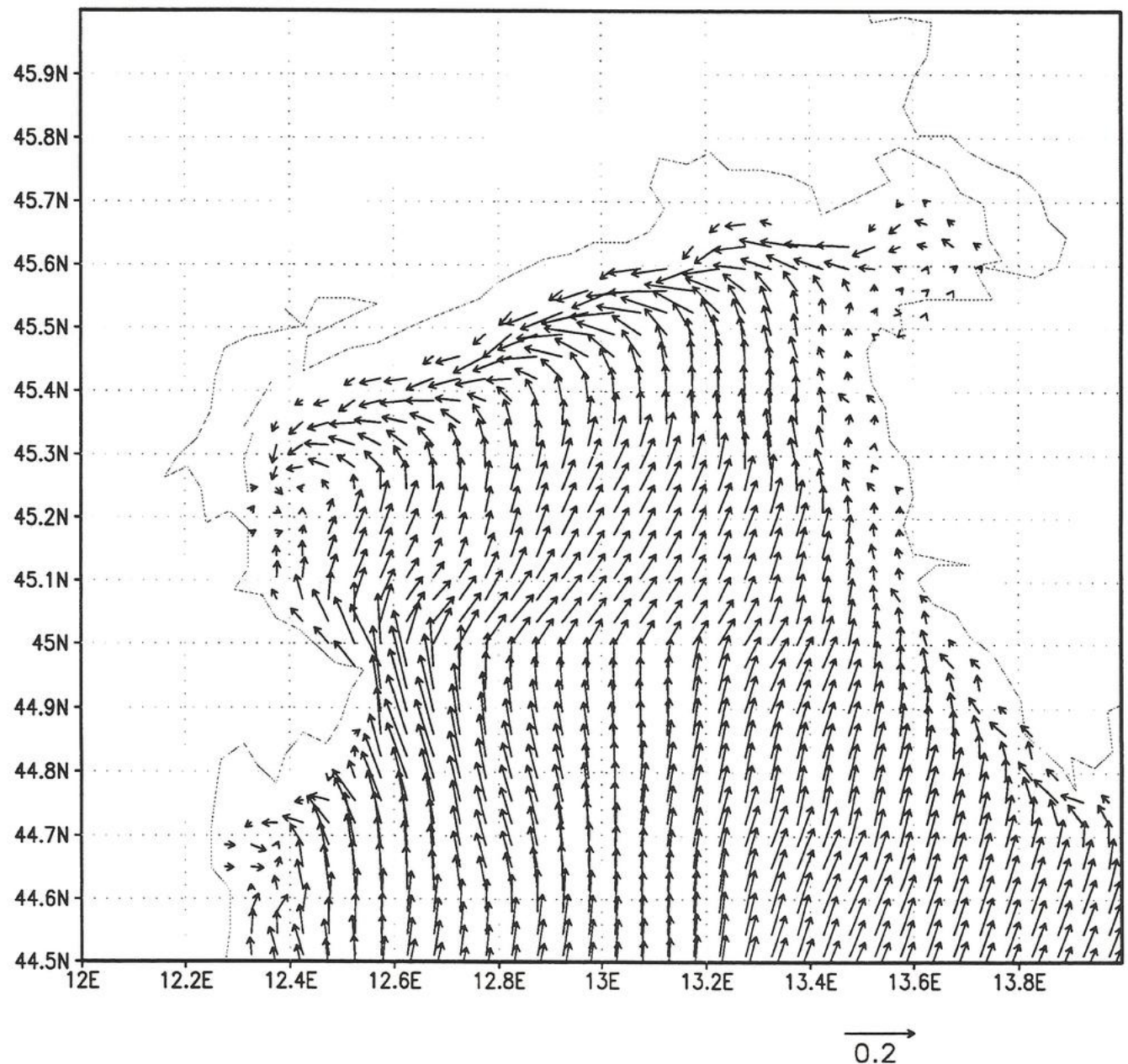
Mesinger, F., Janjic I. Z., Nickovic S., Gavrilov D., and Deaven D.G., 1988: The Step Mountain Coordinate: Model Description and Performance for cases of Alpine Lee cyclogenesis and for a case of an Appalachian Redevelopment. *Mon. Wea. Rev.*, **116**, 1493-1518

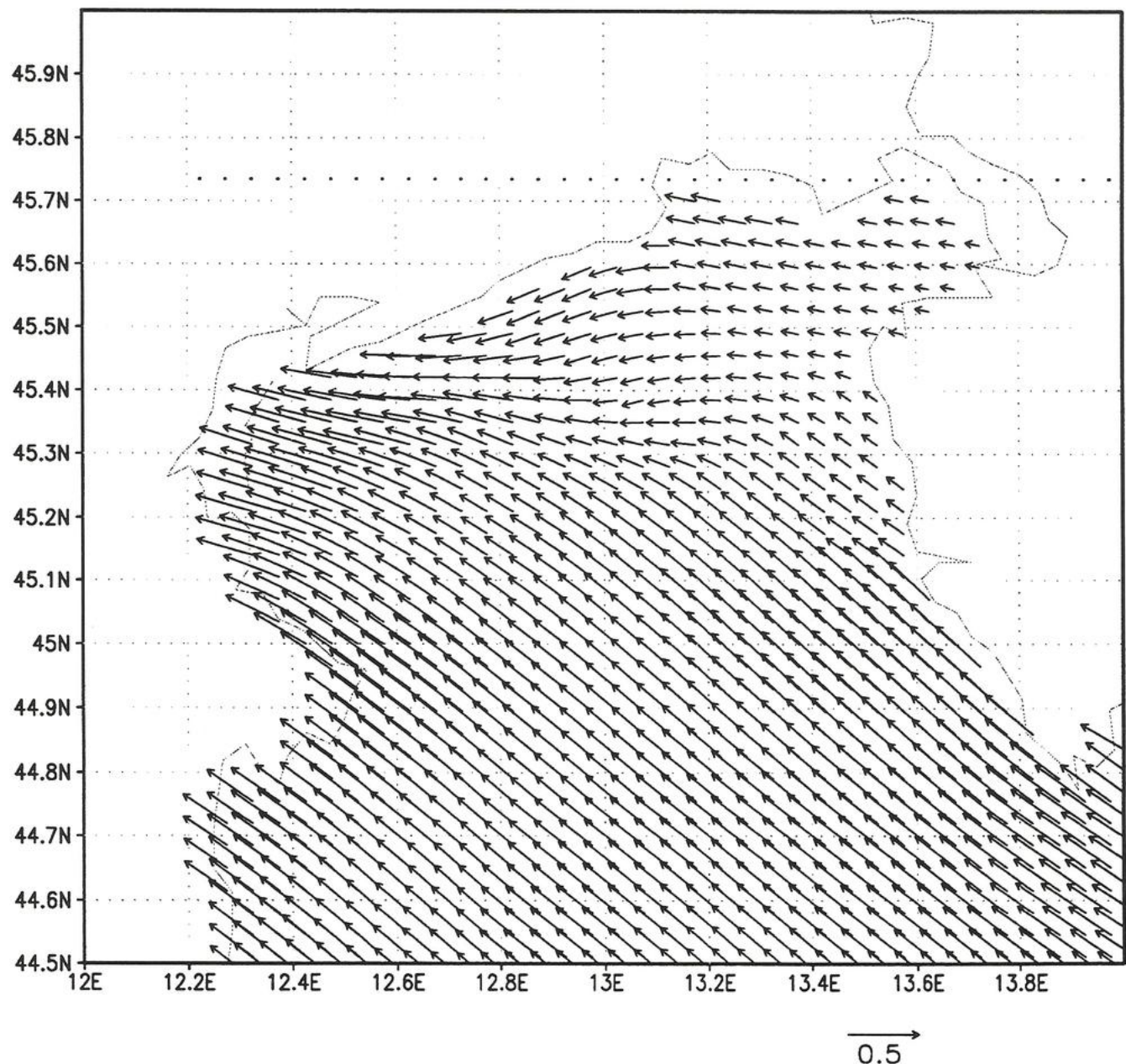
Figure captures:

1. Currents in the Northern Adriatic in m/s at the depth of 6m on 05.11.94. at 12UTC. a) forcing by the high resolution atmospheric model; b) forcing by the low resolution atmospheric model.
2. Friction velocity in Northern Adriatic in m/s on 05.11.94. at 12UTC a) simulated by the high resolution atmospheric model, b)simulated by the low resolution atmospheric model.
3. Sea level height simulated by the ocean model in meters at the ocean model point located at 45.4°N and 12.4°W. Dashed line is for the forcing by the low resolution and full line for the forcing by the high resolution atmospheric model.

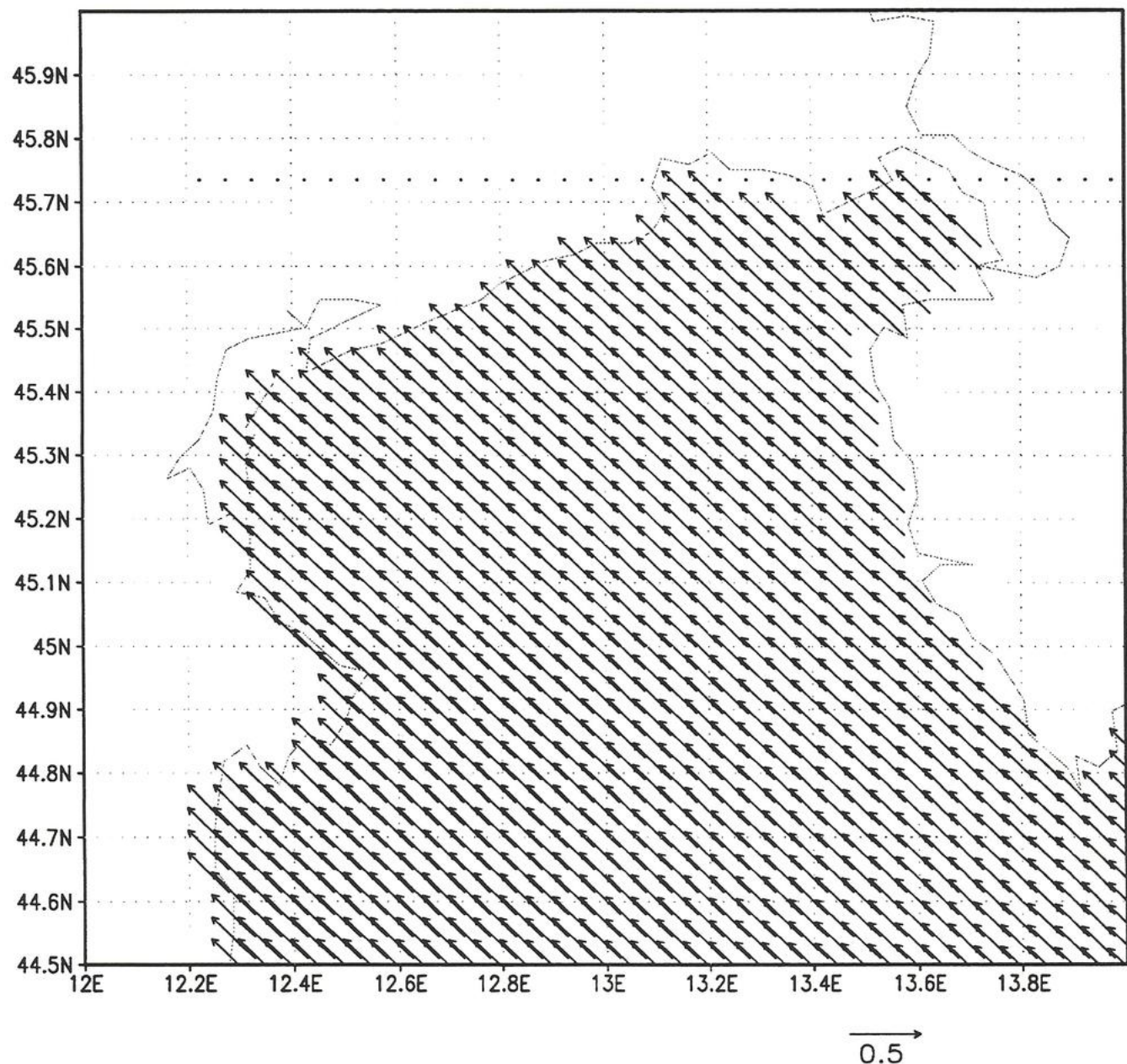


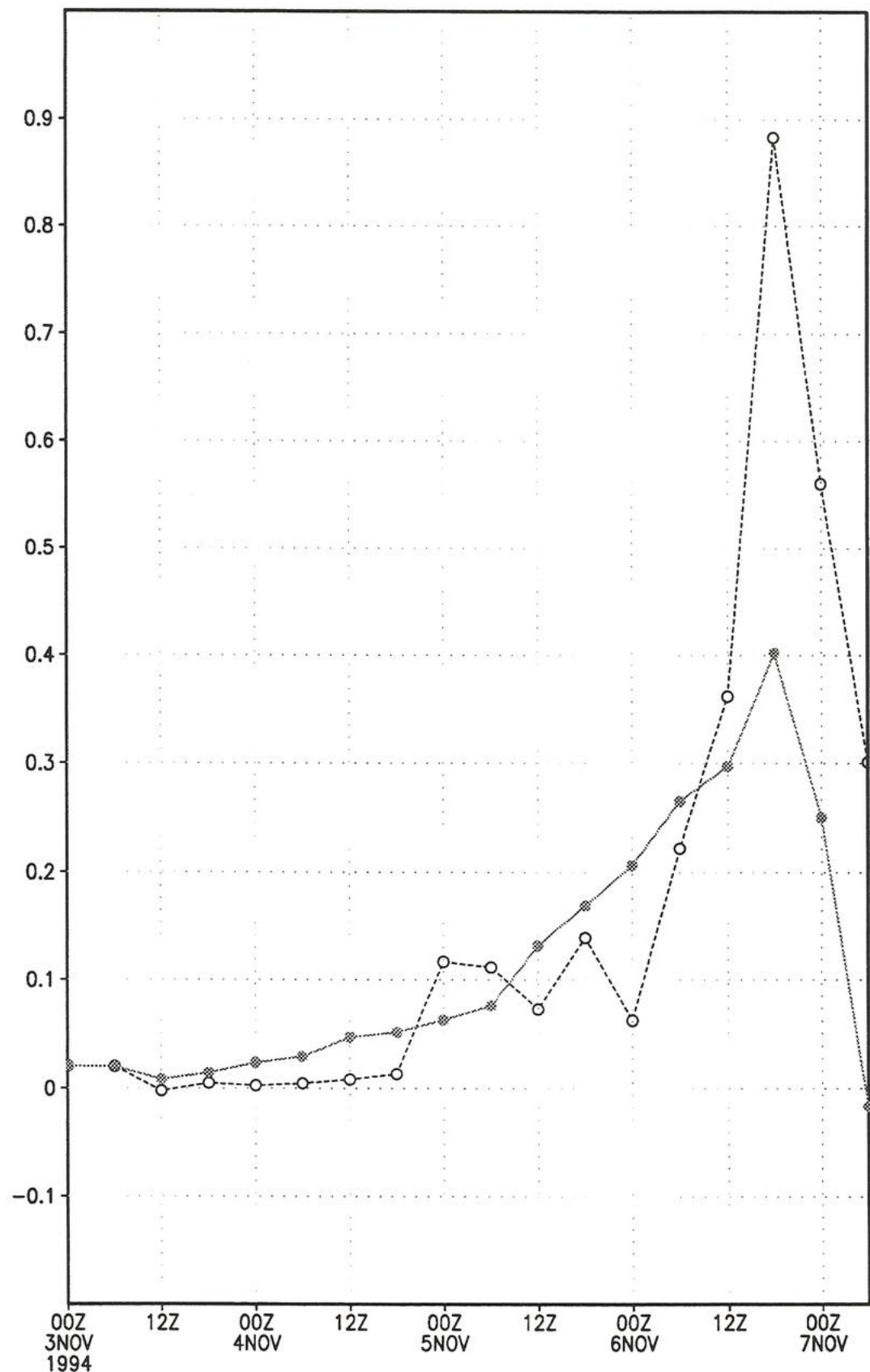
1a





2a





Second-step inhomogeneities in a lake due to the differential cooling

Mean flow characteristics of a thermal gravity current

E. Roget^(*), J. Colomer^(*) and R. Juanola^().**

*** Física Ambiental**

**** Física Aplicada**

Universitat de Girona. Campus de Montilivi. Girona, Catalunya. E-17071

A review (Roget et al., 1993, Roget and Colomer, 1996) of the mean flow characteristics of a thermal gravity current is presented emphasising the existence of horizontal gradients in small lakes. The current, which is generated by the gravitational instability due to the differential cooling rates between different areas of the lake, generates second-step horizontal inhomogeneities, both, longitudinal (the vertical structure of the water column varies along the path of the current) and transversal (the current flows confined to the western shore of the lake).

Characteristics of the studied lake

Lake Banyoles (42°7'N, 2°46'E) is composed by two main basins (lobes) with areas of 0.49 and 0.62 km² and mean depths of 10.0 and 18.0 m, respectively. The inflow to the lake is mainly from underground sources (in the southern lobe, up to the 90% of the total inflow). The streams which flow into the lake are placed on both, the northern and the southern lobe, but the streams which flow out are only located in the southern lobe. From a global hydric balance, a residence time in the northern lobe of about one and a half year is expected. However, due to the gravity current, during autumn, the residence time can be of only 5 days.

Spatial distribution of the heat input to the lake

The inflow of the underground sources of the lake has a relatively stable temperature of about 18° all over the year, being an important source of heat to the lake and, specially, to the southern lobe. As an example, at the beginning of autumn, when the cooling rate of the northern lobe due to the surface heat fluxes is 7 W m⁻³, and that of the southern 4W m⁻³, the underground heat inflow in the southern lobe is 2 W m⁻³; in the northern lobe is one order of magnitude lower. Accordingly, after one month a difference between

the temperature of both lobes of more than 7° should be expected which, of course, is not the case, the differences being of half a degree.

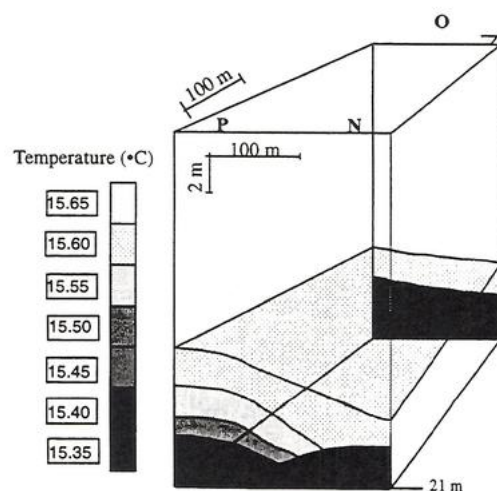
The thermal gravity current

The baroclinic forcing due to the temperature differences between the two lobes generates a gravity current with velocities up to 12 cm s^{-1} at the area connecting the two lobes. This maximum velocity correspond to a total volume exchange between the two lobes of 10^4 l s^{-1} and so the water in the northern lobe is renovated every 5 days, that is, about 100 times the time deduced from a global hydric balance. This gravity current, affects the whole lake and, when no extreme wind conditions are presented, dominates the global circulation.

Second-step horizontal inhomogeneities

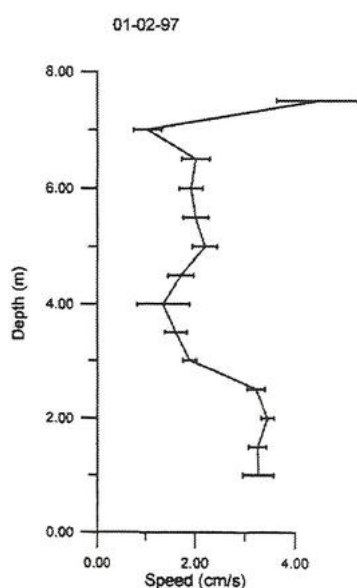
Although the main effect of the gravity current (generated by spatial differences in the energy inputs) is to homogenise the lake as a whole, it also establishes the more subtle spatial inhomogeneities here summarised:

a.- The current flows confined to the western shoreline of the lake establishing transversal gradients. This fact can be observed from the following figure where the thermal structure of two sections transversal to the flow, in the region connecting the two lobes is presented.



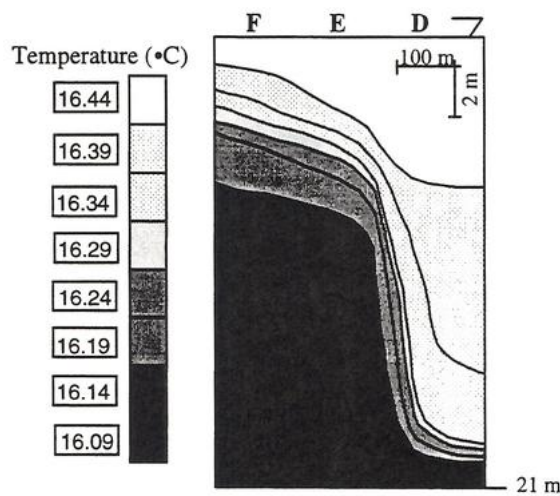
Because the temperature is a natural tracer of the flow, from this figure can be concluded that the current is deflected towards the right. This deflection can be due to the bottom morphometry as is found in many other studied flows in the northern hemisphere (i.e. Hamnblin and Carmarck, 1978). However, in these cases it is concluded that, in addition to the influence of the bottom, the effect of the earth's rotation also accounts for the deflection. In the case of Lake Banyoles, a characteristic transversal pressure gradient ($1/\rho_0)(dp/dx)$ can be evaluated from the mean cross temperature gradient in the figure ($g'H/W$; W and H , being the transversal and vertical lengths) and is found to be $8 \times 10^{-6} \text{ m s}^{-2}$. That is, of the same order than the Coriolis term, fV , which is of $5 \times 10^{-6} \text{ m s}^{-2}$, suggesting that the Coriolis force could account for the deflection of the current. In fact, the Rossby number for the current ranges between 0.1 and 1, and the Rossby radius of deformation between 100m and 1000m (the mean width of the lake is 520 m) corroborating the importance of the rotation effect.

On the other hand, the inertia of the current compared to the frictional force of the bottom could also be evaluated with the non-dimensional number $E_b = V C_b / h f$, where f is the Coriolis parameter, h the thickness of the current and C_b the bottom drag coefficient (2×10^{-3} , Laska, 1981). This number is analogous to the Ekman number, but the acceleration due to internal friction has been replaced by the acceleration of the current due to the bottom friction. The obtained values of E_b ranged between 0.1 and 1 so, the effect of the bottom friction should also be relevant.



From another point of view, the bottom friction is also a source of turbulence, even when the current velocity is low, as can be observed from the presented velocity profile taken at half of the winter, when the current is very smooth. The error bars in the velocity profile account for the *rms* values (from 240 data sampled at 0.5 Hz at each sampling depth) and next to the bottom they are always observed to be significantly larger (although not much larger when the lake is slowly cooling), suggesting that bottom generated turbulence must effect the dynamics of the gravity current (at least their mixing). Shear generated turbulence at the upper interface of the current (4 m above the bottom) is also found to be important.

b.- The entrainment of the bulk water into the current and also its gradient change along the path of the current. A rapidly changing vertical structure of the current can be observed from the following scheme where the isotherms along the path of the current in the central area of the lake are presented. From a heat balance, the non-dimensional entrainment coefficient between stations F-E (5×10^{-2}) is found to be smaller than that between stations E-D (2×10^{-1}), as should be expected due to the different slope of the bottom. Accordingly the vertical structure of the water column (velocity, mixing and temperature) changes along the lake due to local effects.



REFERENCES

- Roget, E., Colomer, J., Casamitjana, X. and Llebot, J.E., 1993. Aquatic Sciences, 55/3, 1015-1621.
- Roget, E. and Colomer, J., 1996. Aquatic Sciences, 58/4, 1015-1621.
- Laska, M., 1981. Mitt. der Versuchsanstalt für Wasserbau Hydrologie und Glaziologie. Nr. 54, Zürich.
- Hamblin, P.F. and Carmack, E.C., 1978. J. Geophys. Res. 63 (C2):885-899.

Shimaraev M.N., Domisheva V.M., Gorbunova L.A.
Limnological Institute (RAS, Siberian Branch)

Limnic role of exchange processes in Lake Baikal

Results of complex studies in the frame of INTAS Project "Deep Water Formation in Lake Baikal" during 1993-1996 discovered an influence of exchange mechanisms to some features of vertical transportation of substances and a structure of deep waters which can be traced by limnic indicators.

One of the indicators of spatial differences in intensity of renewal is an information about oxygen flux directed towards the deep water layers during May - June. During spring renewal oxygen flux directed down over the depth 100 m is estimated equal on average 70-100 g O₂/m². Increased fluxes (up to 170-230 g O₂/m²) are typical for near shore regions, whereas anomalously high ones (up to 300-600 g O₂/m²) are registered in the area affected by thermal bar in Central Baikal (Shimaraev et al., 1996). These results reflect substantial spatial unevenness of the renewal intensity as well as transportation of substances connected with the renewal. A heterogeneity in the oxygen input produces conditions for different intensity of biochemical processes with oxygen's participation in deep zone. An influence of exchange mechanisms to the structure of deep waters traced by physico-chemical and biological indicators is especially clear at the parts of spring thermal bar. Due to deep water depths in Lake Baikal, thermal bar itself does not prevent (as it happens in other lakes) an exchange of near shore and lake waters occurring deeper than 200-250 m. Near slope circulation on the spring thermal bar provides a penetration of the waters enriched in diatomic plankton (Likhoshway et al., 1996), chlorophyll, suspended particles, and microorganisms mineralizing organic matter from the upper layers to the deep depths in pelagic zone (Shimaraev et al., 1995). This process results in increased horizontal gradients of some limnic characteristics, and also in appearance of local intrusions in the deep zone which can be transported as lenses of water whose physico-chemical characteristics differ from surrounded environments.

Data on vertical distribution of nutrients obtained simultaneously with CTD-measurements during different months in 1993-1996 discover substantial heterogeneity of the waters also in open lake. For example, it can be shown using the data on silica in

Southern Baikal. Differences in Si concentrations are observed not only in the upper water layers due to peculiarities of silica consumption by diatomic plankton, but also within the entire water column.

One of the possible reasons for this phenomena may be different activity of deep-water renewal caused by vertical movements of water masses in the field of currents. Zones of sinking should be characterized by decreased, whereas zones of upwelling - by increased Si concentration. A peculiarity of waters circulation in Southern Baikal is an existence of two big macro-whirlwinds separated by the zone of convergence (Shimaraev et al., 1994). Data show that the area characterized by low Si concentrations is more often located near Listvenichnoe Bay (in May, June 1995, September 1996) and that coincides with the location of convergence (sinking) zone on the schemes of currents published by different authors. The area with high Si concentrations coincides with the center of macro-circulation located to the north of Listvenichnoe Bay on the scheme of currents.

General peculiarity of averaged for 1993-1996 vertical profiles of nutrients is an increase of their concentrations from Southern and Central towards Northern Baikal. Such type of changes is not connected with the differences in local input of nutrients with the riverine waters and is probably caused by differences in nutrient consumption by phytoplankton, as well as with different intensity of deep-water renewal in different parts of the lake.

Using a silicon as example, it was shown that taking intensity of deep-water renewal into account, it is possible to estimate the elements of internal Si cycle within the different parts of Lake Baikal. Data on deep-water renewal were taken from the results of water age determination using helium/tritium ratio (Hohmann et al., 1997). Averaged data on Si concentrations measured during 1993-1996 at 240 deep-water stations located in different parts of the lake were used to construct the pattern of Si vertical profile. The mean for the lake Si flux through 250 m depth directed upwards is equal 14 g/m² yr. Si flux in southern, middle and northern basins is 15.4; 15.1, and 11.8, the riverine input - 13.9; 9.5, and 2.2 g/m² correspondingly. Using the data on total for the lake biological Si uptake from (Callender, Granina 1995), as well as mentioned above data on Si input from the rivers and deep water layers to the trophogenic layer, one can calculate annual Si (remineralised in 0-250 m layer) consumption by diatoms. It equals 26.4 g/m², and that is 1.88 times higher compared

to the flux from deeper layer. Taking this ratio for every part of the lake, we obtain that annual diatoms production in southern, middle and northern basins is 58.4, 53.1, and 36.3 gSi/m² correspondingly.

Data on seasonal dynamics and vertical distribution of the temperature, dissolved oxygen, and nutrients collected both during 1993-1996 and earlier allow us to calculate the first estimates of the vertical heat and substances fluxes through the boundary between the upper and deep waters in Lake Baikal.

In May-June a change of mean (calculated taking into account a morphometry of the basins) oxygen stocks within the layers below 250 m approximately on 4-5% corresponds to the deep water renewal by surficial waters. Taking into account that annual renewal is close to 12.5% (Weiss et al., 1991), one can calculate that spring to late autumn renewal ratio is close to 1:2 (Shimaraev et al., 1996).

Using the coefficients of vertical exchange calculated from the data on temperature (Shimaraev et al., 1994) and vertical gradients of some lake characteristics, the first estimates of annual vertical fluxes through the upper boundary of deep zone in Southern Baikal have been obtained (Shimaraev, 1996):

1) heat flux directed down which compensates cooling of the deep zone during spring and end of the year is equal to 170-210 MJ/m²;

2) oxygen input equal to 70 g O₂/m² is close to the annual oxygen losses for biochemical processes in the deep zone calculated by (Weiss et al., 1991);

3) exchange processes cause transportation of 0.3 phosphorus, 1.4 nitrate nitrogen, 22-27 g/m² carbon from the deep water to upper zone; that is 12-18% from their annual consumption needed for primary production of organic matter.

Verifying of these estimates and discovery of individual peculiarities of the vertical heat- and masstransportation in other basins demand a continuation of the studies of deep water renewal in Lake Baikal.

References

Scimaraev M.N., Grachev M.A., Imboden D.M., Okuda S., Granin N.G., Kipfer R., Levin L.A., Endoh S. International hydrophysical experiment on Lake Baikal: processes of spring deep water renewal. Dokl. RAN, 1995, Vol. 343, Issue 6, 824-827.

Ye.V.Likhoshway, T.G.Potyomkina, A.Ye.Kuzmina, V.L.Potyomkin,
M.N.Shimaraev. The distribution of diatom algae near a thermal bar in Lake Baikal. J.
of Great Lakes Res., 1996, Vol.22, 55-65.

Shimaraev M.N., Domysheva V.M., Gorbunova L.A. Oxigen dynamix in Lake
Baikal during spring mixing. Dokl. RAN, 1996, Vol. 347, Issue 6, 814-817.

M.N.Shimaraev, V.I.Verbolov, N.G.Granin, P.P.Sherstyankin. Physical
limnology of Lake Baikal: a review. Irkutsk-Okayama. 1994. 80 pp.

Hohmann R., M.Hofer, R.Kipfer, F.Peeters, H.Baur, M.N.Shimaraev, and
D.M.Imboden. 1997. Distribution of helium and tritium in Lake Baikal.
J.Geophys.Res. 1997 (accepted).

E. Callender, L.Granina. Geochemical mass balances of major elements in Lake
Baikal. Limnol. Oceanogr., 1997, 42(1), 148-155.

Weiss R.F., E.C.Carmack, V.M.Koropalov. Deep-water renewal and biological
production in Lake Baikal. Nature, 1991. Vol. 349, No. 6311, 665-669.

Nonlinear effects of buoyancy near the temperature of maximum density

and examples of thermobaric instability.

N. Granin, A. Kay.

The thermobaric instability for the case where cold water overlies slightly warmer water is well known [Carmack & Weiss, 1991; Weiss *et al.*, 1991; Shimaraev & Granin, 1991]. The reverse case (where a layer of warm water overlies a layer of cooler water) is not documented. Suppose the interface between the layers is situated below the T_{md} profile, but with both layers colder than 3.98°C (the value of T_{md} at the surface). This configuration is stable. However, if the interface is moved upwards through the local compensation depth (defined by Carmack & Weiss [1991] as the depth at which the two layers have equal density), it will become unstable, and convection will ensue.

Consider also the “profile of maximum density”, in which the temperature is equal to T_{md} throughout the water column. Any vertical displacement of a water parcel will then generate a buoyancy force directed upwards (because the surrounding water is denser than the displaced parcel). Although this appears to be a restoring force in the case of a water parcel initially displaced downwards, such a parcel would “bounce” back above the equilibrium, and then accelerate upwards. Thus the water column is unstable (in the sense that any small disturbance of the equilibrium will lead to large-scale motion): even though the Brunt-Vaisala frequency is zero, the profile of maximum density is not neutrally stable. The Brunt-Vaisala frequency describes local stability, but the concept of local becomes inoperative in the special case of the profile of maximum density. This is because calculations of Brunt-Vaisala frequency for a given temperature profile usually use only the coefficient of thermal expansion $d\rho/dT$, neglecting the second derivative $d^2\rho/dT^2$ [Millard *et al.*, 1990]. That approximation is not valid when the coefficient of thermal expansion is zero, as is the case at T_{md} .

Both the above instabilities will lead to upward mixing and are possible mechanisms for transport of nutrients up to the photic zone in Summer, provided that the convection penetrates into the zone where there are significant nutrient concentration gradients. In this paper we will use a simple “particle dynamics” formalism to describe the instability of the profile of maximum density and other phenomena that occur in fresh water bodies near T_{md} . We emphasise the importance of the second derivative in the density–temperature relationship for these phenomena. The phenomena require only that the density should have a maximum with respect to temperature, and that the temperature of maximum density should decrease monotonically with depth; these conditions will normally be satisfied in freshwater lakes.

The quadratic approximation to the equation of state,

$$\rho = \rho_m - \lambda(T - T_{md})^2, \quad (1)$$

in which $\lambda = 8.25 \times 10^{-3} \text{ kg.m}^{-3}.\text{°C}^{-2}$, is sufficiently accurate to illustrate the essential features of water parcel motion near the temperature of maximum density. The variation of T_{md} with depth is linear,

$$T_{md} = T_{m0} + Mz \quad (2)$$

where $T_{m0} = 3.98^\circ\text{C}$ and $M = 0.002^\circ\text{C.m}^{-1}$; the vertical coordinate z is measured upwards from the water surface (so is negative throughout the depth). The maximum density ρ_m is also a function of depth (through compressibility effects), but this does not concern us since we shall only need to compare the density of a water parcel with that of its immediate environment. Consider a water parcel whose temperature and density differ by T' and ρ' , respectively, from the values in the surrounding water. The buoyancy force on the water parcel is

$$F = -g \frac{\rho'}{\rho_p} \quad (3)$$

per unit mass, and the equation of state (1) then yields

$$F = -\frac{g\lambda}{\rho_p} \{2(T_{md} - T_e)T' - T'^2\}; \quad (4)$$

here, the subscripts p and e refer to the parcel and to the surrounding water, respectively. Equation (4) constitutes the linear and quadratic terms in a Taylor series in T' , in contrast to Millard *et al.*'s [1990] formalism which neglects the quadratic term. While the linear approximation is acceptable in the oceans or in lakes far above the temperature of maximum density, it is clear from (4) that it is not valid in a freshwater body close to T_{md} .

Figure 1 shows the buoyancy force (4) as a function of the temperature difference T' for three cases, $T_e < T_{md}$, $T_e = T_{md}$ and $T_e > T_{md}$. In general, the buoyancy force is downwards when T' lies between zero and $2(T_{md} - T_e)$, but upwards when T' is outside this range. Consider, for example, a water column in which the lapse rate dT_e/dz is equal to dT_{md}/dz , so that a single curve represents the entire water column. Upward motion of a water parcel with constant temperature is then represented by leftward motion along the curve. In the case $T_e > T_{md}$ a small displacement up or down from equilibrium ($T' = 0$) will induce a restoring force on the water parcel, leading to oscillatory motion (internal waves) provided that the parcel never moves above the point where $T' = 2(T_{md} - T_e)$: the water column is *locally* stable. On the other hand, if $T_e < T_{md}$ the buoyancy force will be in the same direction as the displacement, and the water parcel will accelerate away: the water column is unstable and convection will occur. Finally, if $T_e = T_{md}$ the buoyancy force is upwards for any non-zero T' , so that any displacement of a water parcel will result in it eventually accelerating upward. This instability was identified as an explanation for observations of convective mixing around the temperature of maximum density in Lake Baikal (Fig. 2).

References

Carmack E.C. and R.F. Weiss, Convection in Lake Baikal: An example of thermobaric instability, in *Deep convection and deep*

water formation in the ocean., edited by P.C.Chu and J.C. Gascard, pp. 215–228, Elsevier, 1991.

Eklund, H., Fresh water: temperature of maximum density calculated from compressibility, *Science*, 142, 1457–1458, 1963.

Granin, N.G., Thermobaric instability in temperate lakes during summer temperature stratification, paper presented at the ASLO Annual meeting, Milwaukee, 1996.

Millard, R.C., W.B. Owens and N.P. Fofonoff, On the calculation of the Brunt-Vaisala frequency, *Deep Sea Research*, 37, 167–181, 1990.

Shimaraev, M.N. and N.G.Granin, Temperature stratification and mechanism of convection in Lake Baikal, *Doklady Akademii Nauk SSSR*, 321, 831–835, 1991.

Weiss, R.F., E.C. Carmack and V.M. Koropalov, Deep-water renewal and biological production in Lake Baikal, *Nature*, 349, 665–669, 1991.

surrounding water, for cases when the water temperature $T > T_{md}$, $T < T_{md}$, $T = T_{md}$.

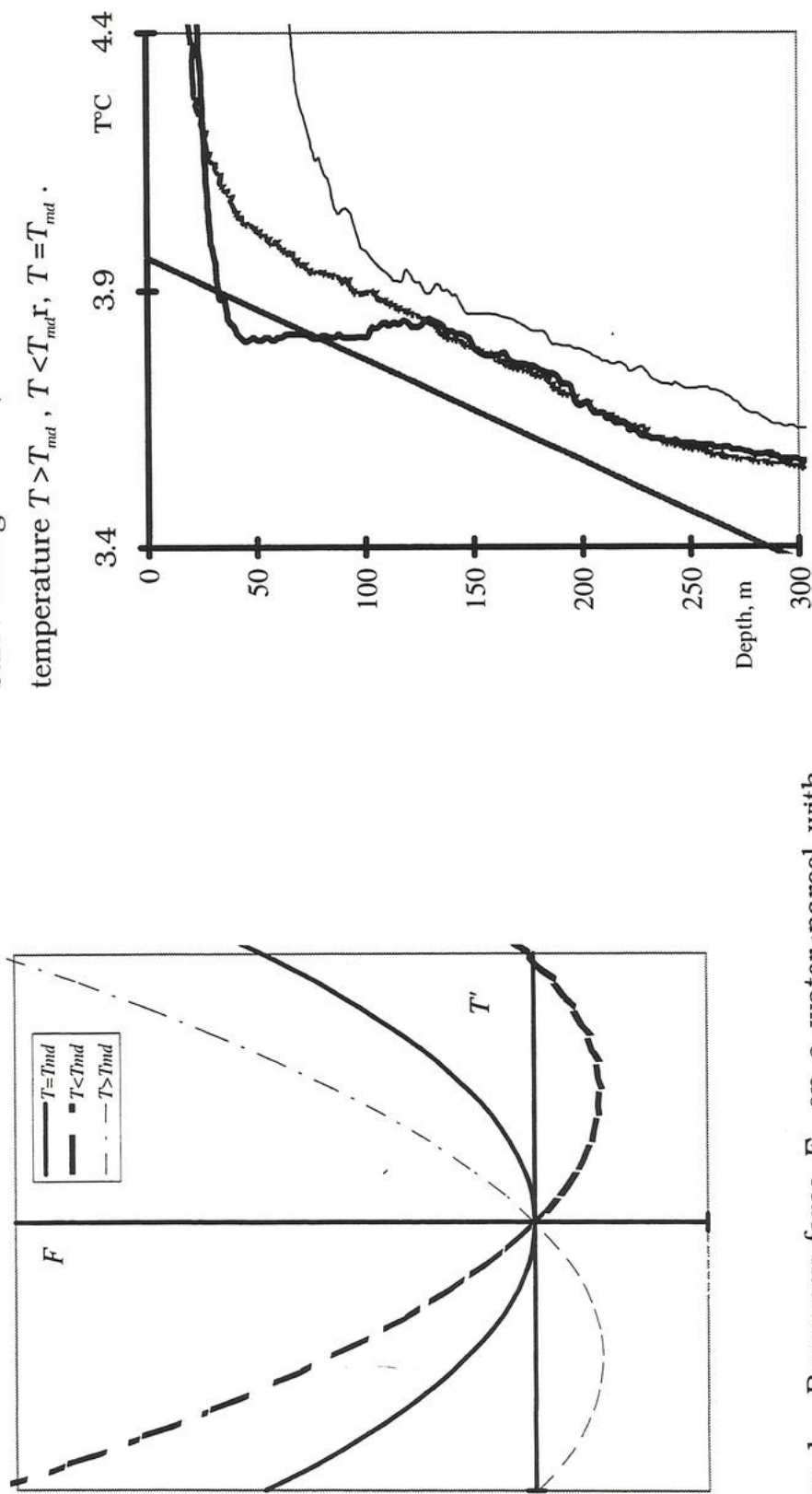


Figure 1. Buoyancy force F on a water parcel with temperature differing by T' from that of the

Figure 2. Temperature profiles at three locations on the
Listvyanka-Tankhoi cross-section in Lake Baikal, 19
August 1995

MAIN FEATURES IN THE T/S REGIME OF DEEP WATER ZONE IN LAKE BAIKAL

P.P.Sherstyankin, L.N.Kuimova, V.L.Potemkin

Limnological Institute SB RAS, Irkutsk 664033, Russia.. E-mail:
sherstyankin@lin.irkutsk.su

Abstract. The complete method of definition of potential temperature θ and density ρ^* according to Kamenkovich (1973) and Sherstyankin et al. (1997) is described. It is shown that the unfull method used before (Gill 1982; Sherstyankin, Kuimova 1995; Peeters,F. et al. 1996 and otherd) gives uncorrect results of calculation of θ and ρ^* .

Introduction. The θ and ρ^* are the most important characteristics for natural waters. It may occur greater difficulty and mistakes if the water temperature T is close to the temperarute of maximum density T_{md} especially in deep water. We have come to the conclusion that the formulae for the calculation of the potential temperature θ (Gill 1982 and otherd) is not complete. Therefore, it gives incorrect results.

The aim of the present report is to study regularities of Lake Baikal deep water zone termohaline regime using T,S-analysis (S is salinity). A method of theoretical and experimental modelling is used.

Results: The Brief Theorie. Let's consider T as one of the most unusual properties of water the temperature of maximal density T_{md} . At normal atmospheric pressure P_a it is about 4°C , and decreases with the increase of pressure P (or Z). This peculiarity dues to the molecular structures of the water (Horne 1969). This function may be expressed as follows:

$$(1) \quad T(S,P) = T_{md}(S,P) + T'(S,P), \quad \text{or} \quad T'(S,P) = T(S,P) - T_{md}(S,P).$$

Absolute value of $T'(S,P)$ increases when $T(S,P)$ becomes increasingly distant from $T_{md}(S,P)$ while water density $\rho(T,S,P)$ decreases (at $P=\text{Const}$). Let us consider three main characteristics of the equation (1): 1. Mathematically it involves any changes of T_{md} with P or Z ; 2. Its physical sense it allows one to take into account the water molecular structures of water determined by any particular equation of the water state (e.g., in the Chen-Millero form (1986), as $T_{md}(z)$ is determined only by the properties of molecular structures of water (Horne 1969); 3. It is easy to obtain the

potential temperature θ and θ' for any P (or Z) using the equation (1) providing that it is necessary to perform an adiabatic transition to the surface, to the atmospheric pressure P_a ($P, Z=0$), i.e., the adiabatic correction $\Delta T_{ad}(P)$ should be taken into account:

(2) $\theta'(T,S,P) = \theta(T,S,P) - \theta_{md}(T_{md},S,0)$ or $\theta(T,S,P) = \theta_{md}(T_{md},S,0) + \theta'(T_{md},S,P)$, where $\theta'(T,S,P) = T'(T,S,P) + \Delta T_{ad}(T,S,P)$; $\theta(T,S,P)$ - potential temperature; $\theta_{md}(T_{md},S,0)$ - potential temperature of maximal density (ca 4°C) for $P=0$ (at surface).

Let us come by for ρ^*

$$(3) \rho^*(T,S, P \rightarrow P_*) = \rho^{*o}(\theta, S) = \rho(T_{md}, S, 0) - \Delta \rho^{\theta(S,0)}.$$

Let us consider the main feature of stability of ρ or frequency Vaisala-Brenta N $N^2 = g^2(d\rho^*/dP)$, where g is a acceleration of gravity. We take into that $\Delta \rho^* = (\rho_t)_{P=P_a} \Delta \theta + (\rho_s)_{P=P_a} \Delta S$, and write

$$(4) N^2 = g^2 [(\rho_t)_{P=P_a} (d\theta/dP) + (\rho_s)_{P=P_a} (dS/dP)].$$

The lower index in ρ means differentiation Let's consider a signs analysis of (4) show in Table.

	$d\theta/dP$	$(\rho_t)_{P=P_a}$	dS/dP	$(\rho_s)_{P=P_a}$	$(\rho_t)_{P_a} (d\theta/dP) -$	$d\rho^*/dp$	N^2
		$(d\theta/dP)$		(dS/dP)	$(\rho_s)_{P_a} (dS/dP)$		
1	2	3	4	5	6	7	8
							9
					a. >0	>0	>0
1				>0	>0	b. 0	0
						c. <0	<0
I	2	>0	<0	0	0	<0	<0
3				<0	<0	<0	<0
1				>0	>0	>0	>0

II	2	0	0	0	0	0	0	0
3		<0	<0	<0	<0	<0	<0	
1		>0	>0	>0	>0	>0	>0	
III	2	<0	>0	0	0	>0	>0	>0
				a.	>0	>0	>0	
3		<0	<0	b.	0	0	0	
				c.	<0	<0	<0	

Brief Discussion. We suppose that formulae for calculation θ on natural waters of type

$$(5) \theta(T, S, P) = T(S, P) + \Delta T_{ad}(T, S, P)$$

(Gill 1982 and otherd) are not complete and give false effect θ_f because takes into account only ΔT_{ad} and not takes into the equilibrium transition in accordance with the equation of water state, i.e. with regard to the properties of molecular structures of water. We obtain a series principled new conclusions. The analysis of (2) and Table shows: any points on the line $T_{md}(P)$ are transformed only into a single point θ_{md} with $\Delta T_{ad}=0$. The points lying in situ to the right (to the left) of $T_{md}(P)$ curve after the transformation into potential temperature θ are situated to the right (to the left) of θ_{md} . As a result, the transformation of (2) has thermodynamic properties from the T vicinity in situ to the θ vicinity taking into account density features of corresponding water densities $\rho(T, P)$ and potential densities ρ^* . It is evidently clear that maximal errors of qualitative and quantitative character in θ calculation are within the range of $T(P) < 4^\circ\text{C}$; e.g., for deep zone of Lake Baikal. We are going to show only one example from Weiss et al. (1991): $T(P = 160 \text{ bars}) = 3.08^\circ\text{C}$. According to (5),

$\theta_f = 3.05^\circ\text{C}$; the sign ρ . changes. According to (2), $\theta = 6.37^\circ\text{C}$ retaining the character of thermodynamic features of surrounding point in situ and on the surface. We obtain next main features in the T/S regime of Baikalian waters (Sherstyankin et al. 1997):

1. In deep zone θ , θ' and T' during all the year increase with P or Z increase, and T decrease weekly. During winter period θ increases from the surface, while T is in mesothermic maximum. During summer period θ is in mesothermic minimum in upper layers.
2. Temperature distribution in deep zone destabilizes density distribution. Indeed, with the increase of pression P (depth) the temperature points deviate from T_{md} towards increase, i.e., θ increases, and ρ^* decreases, and ρ conformly increases. Thus, if supposed (or real) $S=\text{Const}$ density stratification in deep zone owing to temperature is unstable. It is confirmed by theoretical analysis, Table, line 1-2 (N^2 - a imaginary quantity, if isohalinity is available, and θ increases together with P). The deficity of ρ^* in all water column of deep zone is 45, 33 and $9 \cdot 10^{-6} \text{ g/cm}^3$ for Middle, Southern and Northern Baikal, i.e, the instability must appear everywhere (like a cold "boiling"), increasing together with P , but it is not observed.
3. Values of ΔS_{neutr} are calculated for all water column of deep zone, which give a real stability for real $T_{\text{mean/year}}$ for Middle, Southern and Northern Baikal. Due to signs analysis (4) and experimental data of T and calculated by us T' , θ and θ' we see, that on Lake Baikal only unique options of neutral and stable density distribution and $N^2 >= 0$ in deep zone, shown in Table, lines I.1.b&a are inevitable. The calculated values of ΔS_{neutr} which correspond to isopicnic exchange, coincide well with graphical relative isopicns positions, since absolute S or ρ values are unknown. Theoretical indices to higher S values at great depths in Middle Baikal correlate with the availability of large tributaries with a high salinity - Selenga River and Barguzin River (Votintsev et al. 1965).
4. Equidistancy during $T(T,S,P)$ and $T_{md}(S,P)$ observed on Lake Baikal before and after spring homothermy in the depths range approximately from 100 to 300 m (Shimaraev, Granin 1991; Weiss et al. 1991) is a direct index of neutral density stratification, constance of θ (in the range ΔT_{ad}) and constance of S (Table, line II.2).

5. The analysis of a sharp T decrease in the deep zone observed by Weiss et al. (1991) shows that approximately double decrease of θ increase rate which followed it was a reason of approximately double decrease of ΔS_{neutr} decrease. These data and ones in the line I.1.b of Table, corresponding to this case show that in deep zone not only colder waters break-through, as it is correctly mentioned from Weiss et al. (1991) and by Rossolimo (1957), but also less saulty waters can behave so, and it increase the role of surfacial (maybe river) waters in such breaks-through.

On the base θ, S -analysis the main features of deep zone thermohaline structure of Lake Baikal are defined.

Acknowledgements

Research was supported by grants Russian Found. of Basic Res. (96-05-65850 and 96-05-65997).

References

- Chen,C.T., Millero,F.J. Limnol.Oceanogr. 31(3), 657-662 (1986).
- Gill A.E. Atmosphere-Ocean Dynamics (Acadc Press, New York, London, 1982).
- Horne R.A. Marine Chemistry (Wiley, New York-London, 1969).
- Kamenkovich V.M. Osnovy Dinamiki Okeana (Gidrometeoizdat, Leningrad, 1973, in Russian).
- Peeters,F., Piepke, R., Kipfer, R et al. Limnol.Oceanogr. (in press, 1996).
- Rossolimo L.L. 1957. Temperature regime of Lake Baikal. Izd. AN SSSR, Moscow, 552. (R.).
- Shestynkin,P.P., Kuimova L.N. Rep.RAS Vol. 344, 247-251 (1995, in Russian).
- Shestynkin,P.P., Kuimova L.N. Potemkin V.L. Rep.RAS Vol. 355, in press (1997, in Russ).
- Shimaraev M.N., Granin N.G. 1991. Dokl. AN SSSR, Vol. 321, No. 2: 381-385. (Russ.).
- Weiss R.F., E.C.Carmack & V.M.Koropalov. Nature, Vol.349, 1991, p.665-669.
- Votintsev K.K., Glazunov I.V., Tolmacheva A.P. 1965. Hydrochemistry of rivers of Lake Baikal basin. Izd. AN SSSR, Moscow, 496. (Russ.).

Encl. 2.

FRONTOGENESIS IN DEEP RESERVOIRS OF LAKE BAIKAL

Pavel P.Sherstyankin, Lyubov N.Kuimova

Limnological Institute SB RAS, Irkutsk 664033, Russia. E-mail:
sherstyankin@lin.irkutsk.su

Introduction. The processes of mixing in a deep water like the Lake Baikal are under consideration. The thermodynamic characteristics of a deep water depend on depth, and we should take them into account. Under initial conditions, we suppose that waters with equal density and different temperature and salinity take part in the mixing which becomes more dense at cabbeling of parents waters (Garrett & Horn 1978, Fedorov 1983).

We use T, S-analysis bases according to Shtokman (1944), a fine structure of temperature fields T and salinity S according to Stommel and Fedorov (1967). In Ontario Lake (Chen, Millero 1977) and in Lake Baikal (Lee, Sherstyankin 1969) there is given S for fresh waters with low salinity. The main peculiarities of distribution of conductivity in Baikal which are closely connected with salinity including its thin structure are given by Sherstyankin and Khromeshkin (1987).

The main aim of this paper is to work out T,S-analysis for study of processes of mixing and front genesis of fresh waters. We employ the experimentally theoretical approach.

Results: The Brief Theory. We use an equation of state of fresh waters according to Chen, Millero (1986). The equation will be in the form of: $\rho = \rho(T, S, P) = \rho^0(1 - P/K)$, where $\rho(T, S, P)$, $\rho^0(T, S)$ and $K(T, S, P)$ are known functions of T, S .

Let us consider the differential of densities of mixed waters and cabbeling for the analysis of mixing processes. Assuming that ρ is a complex function of T, S and P, we shall write:

$$(1) \quad \Delta\rho = \rho_t \Delta T + \rho_s \Delta S + \rho_p \Delta P, \text{ where}$$

$$(2-5) \quad \rho_t = (\rho/\rho^0) \rho_t^0 - (\rho^2 K_t / \rho^0 K^2) P, \quad \rho_s = (\rho/\rho^0) \rho_s^0 - (\rho^2 K_s / \rho^0 K^2) P, \quad \rho_p = (\rho^2 / \rho^0 K) (1 - K_p P / K).$$

The expressions for thermodynamic functions (2-5) are given by Kuimova, Sherstyankin (1992, 1995a) and show in report on Fig.1. The lower index in ρ means differentiation. The changes of T, S and ρ are easily examined on T,S-diagrams in the

field of lines of equal density - isopycns (Shtokman 1943) shown in report on Fig.2. It is seen on T,S-diagram that isopicns in the area of 4°C pass through the maximum - the temperature of maximal density T_{md} .

The expression for the change of ρ at mixing $\Delta\rho_{cab}$ is given as follows (Kilmatov , Kuznmin. 1991):

$$(5) \quad \Delta\rho_{cab} = -(\rho_{tt}\Delta T^2 + 2\rho_{ts}\Delta T\Delta S + \rho_{ss}\Delta S^2)/8, \text{ where}$$

$$(6-8) \quad \rho_{tt} = (\rho/\rho^o)\rho^o_{tt} - (\rho/\rho^oK)^2(\rho^oK_{tt} + 2\rho K^2/K - 2\rho^o_t K_t)P, \quad \rho_{ts} = (\rho/\rho^o)\rho^o_{ts} - (\rho/\rho^oK)^2(\rho^o_s K_t + \rho^o K_{ts} + \rho^o_t K_s - 2K_t K_s/K)P, \quad \rho_{ss} = -2K_s(\rho/\rho^oK)^2(\rho^o_s - \rho K_s/K)P;$$

where ρ_{tt} , $\rho_{ts}=\rho_{st}$ and ρ_{ss} (in report Fig.3) are the second and mixed derivatives ρ of T and S; $\Delta T=T_2-T_1$, $\Delta S=S_2-S_1$. The indices 1and 2 belong to different mixed waters. The expression (6-8) was obtained and analyzed by Sherstyankin, Kuimova (1992, 1995a).

The mixing of fresh waters may be accompanied both by contraction and decontraction, i.e. both by intensification of the effect of vertical mixing and its reduction. The vertical mixing becomes more effective during the appearance of contraction at mixing for which it is necessary to fulfill the following conditions for mixing waters (Fedorov 1983):

$$(9) \quad a. \Delta\rho = 0 \quad \text{and} \quad b. \Delta\rho_{cab} > 0,$$

taken from the forms (1) and (5), respectively. The condition (9) is steadily followed, the front genesis begins, i.e. on the one hand, the constant flux of waters with different T and/or S is brought into the zone of mixing (frontal zone); on the other hand, the constant descending of mixed waters occurs. The formation of convergent zone takes place. In other words, the mechanism of transfrontal transfer is formed. Not going into details of the analysis of dynamic phenomena typical to frontogenesis (Fedorov 1983, Sherstyankin 1993), we shall think that conditions (9) are necessary and sufficient for the analysis of front genesis.

Theoretically four types of water mixing are possible: at constant S or T, or ρ , and, finally, different mixed variants are possible. Let us consider them in detail.

At $S=Const$. This is an isohaline mixing. The condition of front genesis (9) is written in the form of :

$$(10) \quad a. \Delta\rho = \rho_t \Delta T = 0 \quad \text{and} \quad b. \Delta\rho_{cab} = -\rho_{tt}(\Delta T)^2/8.$$

Note that the condition (10b) as it follows from the analysis of the first summand (5), is fulfilled at any T and S. The condition (10a) is fulfilled only when ρ_t , expression (2), vanishes. It occurs at $T = T_{md}(S, P)$. The front which appears under such conditions is called a thermal barrier or thermal bar.

At $T = \text{Const}$. This is isothermic mixing. The conditions of front genesis (9) are written in the following way:

$$(11) \quad \text{a. } \Delta\rho = \rho_s \Delta S = 0 \quad \text{and} \quad \text{b. } \Delta\rho_{cab} = \rho_{ss} \Delta S / 8.$$

From the analysis of the expression (3) it appears that $\rho_s > 0$ and never vanishes. $\Delta\rho_{cab}$ in the form of the third summand (5) is everywhere < 0 , i.e. the conditions of front genesis are now here realized at any T, S and P. Physically, it is a consequence of strict monotony ρ from S. In practice, ρ_{ss} can be neglected besides the analysis of some sufficient effects.

At $\rho = \text{Const}$. This is isopycnic mixing. The front genesis condition (9) is written as follows:

$$(12) \quad \text{a. } \Delta\rho = \rho_{tt} \Delta T + \rho_s \Delta S = 0 \quad \text{and} \quad \text{b. Expression (5).}$$

It is seen that the fulfilment of conditions (12) is possible within the whole range of T,S-diagram at any P, and can lead to an unlimited number of appearance of front genesis. At unrestricted changes of T, S and P. This is the most common case which is clearly identified on T,S-diagrams. The thermal bar is seen on the surface and at any depth under the necessary condition T for front T_{fab} :

$$(13) \quad T_{fab} = T_{md}(T, S, P).$$

The condition (13) is realized in any possible cases of thermobaric fronts.

In this report there are given necessary (9) and sufficient (10-13) conditions for the appearance of fronts. It means the creation of dynamic conditions for the flow of waters into the zone of front beginning with different T,S-characteristics and for the removal of contracted waters. If this mechanism does not work for any reason, the local increasing of the intensity of vertical exchange will take place. Fronts create an indivisible mechanism of horizontal and vertical exchange - the mechanism of structure formation of waters.

Discussion. The scales of Baikal fronts are closely combined: Longitudinal scales with near shore circulations which occur both in depression and in the whole Lake Baikal; transversal - with the lake width: convergent zone has a thickness not more than 1 km

and its height almost equals to the depth, i.e. it can be more than 1 km (Sherstyankin 1993).

Let us consider T,S-characteristics of Baikal waters and other large lakes. Firstly, the data on the salinity of lakes are very poor (Votintsev 1961). Secondly, the indirect information on fine and step structure of optical data (Sherstyankin 1993) indicates that similar T-structures exist. Thirdly, there should be a seasonal course of salinity, especially in lakes covered by ice, as well as spatial changes both in open parts of lakes and near entering of large rivers which has been proved by conductivity measurements (Sherstyankin & Khromeshkin 1987).

Let us briefly analyze the thermohaline structure of deep waters of Lake Baikal. It is known that the waters are in the state similar to neutral equilibrium (Rossolimo 1957), i.e. and the exchange is close to isopycnic. If ΔS higher values of the dense ratio $R_p > 1$, there is a stable distribution of density in Baikal depressions. At $R_p < 1$, there can be a convective instability of avalanche or plume or other type (Sherstyankin, Kuimova 1995b). The most important structure formation process in Lake Baikal is front genesis (Sherstyankin 1993). If the isopycnic exchange in the convergent zone was observed on Lake Baikal according to indirect hydrooptical observations (Sherstyankin 1993), this exchange was proved in Mediterenian Sea by direct observations (Ovchinnikov et al. 1993).

The peculiarities of frontogenesis on Lake Baikal are discussed in the present report. The correct measurements of T and mainly S are necessary. It is additionaly caused by the fact that Baikal waters are situated in the thermodynamic active zone induced by nonlinearity of thermodynamic parameters.

Acknowledgements

Research was supported by grants Russian Foundation of Basic Researches (96-05-65850 and 96-05-65997). The authors of the paper are very thank ful to the engineer M.A.Martynov.

References

- Garrett C. and Horne E. 1992. J.Geoph.Res., Vol. 83, No.9: 4651- 4656.
Chen C.T., Millero F.J. 1977. Nature, Vol. 266: 707-708.
Chen C.T., Millero F.J. 1986. Limn. & Oceanogr., Vol. 31(3): 657-662.

- Fedorov K.N. 1983. Physical nature and structure of oceanic fronts. Gidromet., Leningrad, (Russ.).
- Kilmatov T.R., Kuzmin V.L. 1991. Izv. AN SSSR, FAO, Vol. 27, No. 8: 883-887. (Russ.).
- Kuimova L.N., Sherstyankin P.P. 1992. Dokl. Russ. Ak. Nauk (Rep. RAS). Vol.325: 159, (R.).
- Lee M.E, Sherstyankin P.P. 1969. Proc. of Mar. Hydophys. Inst. AN UkrSSR, Vol.42: 136, (R.).
- Ovchinnikov I.M. et al. 1993. Oceanology. Vol.33, No.6: 801-807. (Russ.).
- Rossolimo L.L. 1957. Temperature regime of Lake Baikal. Izd. AN SSSR, Moscow, 552. (R.).
- Sherstyankin P.P. 1993. Optical structures and fronts of oceanic type in Lake Baikal. Doct. Diss. Phys&Math Sci., Institute Oceanology RAS, Moscow, 37 p. Suppl., 6 p. (Russ.).
- Sherstyankin P.P., Khromeshkin V.M. 1987. In: The Way of Understanding of Baikal, Nauka, Novosibirsk, 114-123. (Russ.).
- Sherstyankin P.P., Kuimova L.N. 1995a. Dokl.RAS (Reports RAS), Vol.344: 247-251. (R.).
- Sherstyankin P.P., Kuimova L.N. 1995b. The Second Vereshchagin Baikal Conf., Oct. 5-10, 1995. Abstracts. Limnological Institute of SB of the RAS, Irkutsk, pp.228-229.
- Sherstyankin P.P., Kuimova L.N. 1997. Dokl. RAS (Rep. RAS), Vol.355, No.5: in press. (R.).
- Shtockman V.B. 1944. Problems of the Arctics 1943. No.1: 32-71. (Russ.).
- Stommel H., Fedorov K.N. 1967. Tellus, Vol. 19, No. 1: 88-97.
- Votintsev K.K. 1961. Hydrochemistry of Lake Baikal. Izd. AN SSSR, Moscow, 312. (Russ.).

Finestucture, Microstructure, and Thin Layers

Thomas Osborn

Department of Earth and Planetary Sciences

The Johns Hopkins University

Baltimore, MD 21218-2681

Abstract

Microstructure is the signature of turbulence at scales where molecular viscosity and diffusion are important. Quantitative measurements at these scales provide estimates of the cross-isopycnal diffusion rates. Finestucture describes features where buoyancy effects produce horizontal scales substantially greater than the vertical scales. Eckart (1948) created a paradigm of stirring and mixing which shows the role of the flow field and the boundary conditions in producing these irregular spatial distributions and layers.

Biological and chemical 'thin layers' are forced by biochemical processes as well as physical processes. The biochemical processes interact and couple with the physical processes. Thin layers are like some finestucture features in thickness and extent. This similarity is a result of the basic stratification which forces most of the motion to be horizontal and makes layers out of small parcels. While the coupling of processes may bind the biochemical layers to physical layers, it is the vertical shear of the horizontal currents that has the major role in forming both thin layers and finestucture. A crucial physical measurement is the velocity profile with resolution of the variations on the scale of the thin layers and finestucture.

- Extended Abstract -

Photoadaptation of Phytoplankton in Turbulent Water Bodies: Modelling the Coupling of Hydrophysics And Biology

Helmut Baumert¹

Institut für Chemie und Biologie des Meeres
Carl von Ossietzky Universität, Oldenburg, Germany

Introduction. In the pelagic of natural water bodies hydrophysical and hydrobiological processes are often closely coupled. Prominent examples are:

- (a) Phytoplankton cells with inert internal variables like the *Chlorophyll*-carbon ratio, γ ; it is controlled both by the slow photoadaptation of the cell (integrating the experienced light over a longer time) and by irregular vertical movements in the underwater light field due to turbulence.
- (b) SPM flocs (marine or lake snow) which represent relatively autonomous micro-ecosystems; the stickiness of their constituents is mainly governed by biology whereas their formation and breakup are controlled by the hydrophysical microstructure of the ambient water body.

Further examples are multiple-layer formation and convection due to light absorption by phytoplankton in deep levels, modulation of encounter and performance probabilities for zoo- and phytoplankton by turbulence and the formation of lutoclines or fluff layers near the bottom.

In numerical models the above aspects are often strongly simplified: (a) If phytoplankton photoadaptation is discussed at all, it is done in a heuristic, semi-empirical way. (b) If flocs are considered at all, they are mostly treated as static entities.

Based on the stochastic calculus of Langevin and Fokker-Planck equations in this paper a new solution for (a) is presented². The chosen approach can be generalized to other biophysical coupling problems in natural waters.

As to the dynamic effects of changing light intensity for phytoplankton cells, there are two main processes to be distinguished: (i) A short-term internal energy storage in the primary photosynthetic pathway; it has a time scale of (maximum) 100 seconds. (ii) The slow photoadaptation process with a time scale of at least 4 hours.

The role of the two effects in the upper mixed layer (UML) of a lake or in the ocean with UML depth H [m] and vertical turbulent diffusivity D [$m^2 s^{-1}$] can easily be evaluated by the following similarity number,

¹baumert@dkrz.de

²Problem (b) is tackled by Regener & Baumert in this workshop.

$$p = \sqrt{\tau D}/H, \quad (1)$$

where τ [s] is the time scale of the biological process considered. With $H = 25\text{m}$, $D = 10^{-4}\text{m}^2\text{s}^{-1}$, the values of p for (i) and (ii) differ by about one order of magnitude. I.e., effect (ii) has more relevance than (i) and will be discussed here in detail³.

The biological submodel. As biochemical basis for the coupling problem I used a model of phytoplankton photosynthesis and photoadaptation derived earlier⁴:

$$\left. \begin{aligned} P(\gamma, I) &= \frac{\mu_m^o}{\gamma} \left(1 - e^{-\alpha\gamma I/\mu_m^o} \right) e^{-\varepsilon\alpha\gamma I/\mu_m^o} \\ \dot{\gamma} &= \gamma\mu_m^o \left(e^{-\alpha\gamma I/\mu_m^o} - \frac{\gamma_+ - \gamma_-}{\gamma_+ - \gamma_-} \right) e^{-\varepsilon\alpha\gamma I/\mu_m^o}. \end{aligned} \right\} \quad (2)$$

Here the dot denotes the time derivative, P [$\text{gC}(\text{gChl})^{-1}\text{h}^{-1}$] is the instantaneous photosynthetic rate, I [Wm^{-2}] the instantaneous light intensity (PAR) experienced by the cell, γ_- and γ_+ the minimum and maximum *Chl* equipments of a cell, respectively, ε the parameter of reversible photoinhibition, α the initial slope of the P - I curve and μ_m^o [h^{-1}] a parameter closely related to the maximum physiologically admissible growth rate⁴. Whereas α , ε , γ_- , γ_+ and μ_m^o are constant model parameters for constant temperature, $P = P(t)$ and $\gamma = \gamma(t)$ are variables which vary according to (2) with $I = I(t)$ where t [h] is time. While $P = P[\gamma(t), I(t)]$ reacts instantaneously on changes in I , γ follows the course of $I(t)$ with non-linear relaxation. Denoting steady-state variables by a starlet, for constant light $\gamma_* = \gamma_*(I_*)$ is the solution of a transcendental equation and decreases monotonously with increasing I_* :

$$\gamma_* = \gamma_- + (\gamma_+ - \gamma_-)e^{-\alpha\gamma_* I_*/\mu_m^o}. \quad (3)$$

The hydrophysical submodel. Here I use standard model components. The light field is prescribed by the Lambert-Beer law with constant light attenuation coefficient k [m^{-1}]:

$$\frac{dI}{dz} = -kI, \quad I(0) = I_0, \quad I(z) = I_0 e^{-kz}. \quad (4)$$

I_0 is the light intensity just below the surface. The cell depth z [m] depends on time due to turbulence,

$$\dot{z} = v(t), \quad (5)$$

where $v = v(t)$ [m^{-1}] is the fluctuating cell velocity, for simplicity approximated here by a zero-mean, white-noise stochastic process (in the Stratonovich sense):

$$\left. \begin{aligned} \langle v(t) \rangle &= 0, \\ \phi(t) &= \langle v(t')v(t' + t) \rangle = D \lim_{\tau_v \rightarrow 0} \frac{e^{-|t|/\tau_v}}{\tau_v} = 2D\delta(t), \\ D &= \tau_v \sigma_v^2 = \text{const.} = \int_0^\infty \phi(t) dt. \end{aligned} \right\} \quad (6)$$

³(i) is significant for very shallow UMLs (Baumert, H. - Dr.sc. thesis, TU Dresden 1988).

⁴c.f. Baumert, H. - *Int. Revue ges. Hydrobiol.* **81** (1996), 1, 109-139

Here $\delta(t)$ [s^{-1}] is Dirac's delta function, τ_v [s] the autocorrelation time of the Lagrangian velocity fluctuations (vanishing in the white-noise limit), σ_v [$m \cdot s^{-1}$] the r.m.s intensity of those fluctuations (diverging in the white-noise limit), ϕ [$m^2 s^{-2}$] their autocorrelation function (degenerating to a delta function in the white-noise limit) and D [$m^2 s^{-1}$] the turbulent diffusivity⁵.

The coupled model. The interaction between the biological and the physical submodels is obvious: The light intensity I in (2) for a cell at position z is given by the last relation in (4) and the position z itself is given by the solution of (5). Therefore the dynamics of the *Chl*-carbon ratio γ in a cell moving turbulently on the vertical axis in a Lambert-Beer light field can be summarized as follows,

$$\left. \begin{array}{l} \dot{\gamma} = \varphi(\gamma, z), \\ \dot{z} = v(t), \end{array} \right\} \quad (7)$$

where

$$\varphi(\gamma, z) = \gamma \mu_m^o \left(e^{-q\gamma e^{-kz}} - \frac{\gamma - \gamma_-}{\gamma_+ - \gamma_-} \right) e^{-q\gamma e^{-kz}}, \quad q = \frac{\alpha I_0}{\mu_m^o}. \quad (8)$$

Systems like (7) with the statistics of the stochastic forcing function $v(t)$ given by (6) are called Langevin equations. For those systems the corresponding joint probability density function $W = W(\gamma, z, t)$ [m^{-1}] is given by the solution of the corresponding Fokker-Planck equation (FPE). For (7) the FPE reads

$$\frac{\partial W}{\partial t} + \frac{\partial}{\partial \gamma} (\varphi W) - \frac{\partial}{\partial z} D \frac{\partial W}{\partial z} = 0. \quad (9)$$

Results. The construction of the coupled model (7), (8) and (9) did not show up problems. Difficult is the solution of (9): It is a highly non-linear (double exponentials in φ !) and time dependend partial differential equation in the two-dimensional state space (γ, z) . Fortunately one is most interested in the conditional expectation value $\bar{\gamma} = \bar{\gamma}(z, t)$,

$$\bar{\gamma}(z, t) = \int_0^\infty \gamma W(\gamma, z, t) d\gamma, \quad (10)$$

rather than in the full probability density $W = W(\gamma, z, t)$. This allows for substantial simplifications. The evolution equation for $\bar{\gamma}$ is obtained by multiplying (9) by γ and subsequent integration:

$$\frac{\partial \bar{\gamma}}{\partial t} - \frac{\partial}{\partial z} D \frac{\partial \bar{\gamma}}{\partial z} = \int_0^\infty \varphi W d\gamma - [\gamma \varphi W]_0^\infty. \quad (11)$$

The inspection of (2) shows that the states $\gamma = 0$ and $\gamma = \infty$ cannot be occupied by the system. I.e. the last term in (11) is zero. In analogy to this derivation a similar equation can be derived for the second conditional moment, $\sigma_\gamma^2 = \bar{\gamma^2} - \bar{\gamma}^2$, as a function of z and t , as well as for higher moments. For the evaluation of integrals like that in (11) the function φ can be expanded into a Taylor series

⁵Note that D remains constant and finite in the white-noise limit: the vanishing τ_v and the diverging σ_v 'compensate' each other.

around $\gamma = \bar{\gamma}$ such that, with the abbreviations $\varphi' = \partial\varphi/\partial\gamma$ and $\varphi'' = \partial^2\varphi/\partial\gamma^2$, I finally found the following approximate description for $\bar{\gamma} = \bar{\gamma}(z, t)$ ⁶:

$$\left. \begin{aligned} \frac{\partial\bar{\gamma}}{\partial t} - D\frac{\partial^2\bar{\gamma}}{\partial z^2} &= \varphi(\bar{\gamma}, z) + \frac{1}{2}\sigma_\gamma^2\varphi''(\bar{\gamma}, z), \\ \frac{\partial\sigma_\gamma^2}{\partial t} - D\frac{\partial^2\sigma_\gamma^2}{\partial z^2} &= 2D\left(\frac{\partial\bar{\gamma}}{\partial z}\right)^2 + [2\varphi'(\bar{\gamma}, z) - \bar{\gamma}\varphi''(\bar{\gamma}, z)]\sigma_\gamma^2. \end{aligned} \right\} \quad (12)$$

This system is closed and can be integrated numerically. If the surface light intensity is stationary, the solution of (12) becomes stationary too and provides finally the diffusive-stationary⁷ *Chl*-carbon ratio, $\bar{\gamma} = \bar{\gamma}(z)$, as a function of depth alone. Given this function, by means of the first equation in (2) the total production, Π [$\text{g C m}^{-2}\text{h}^{-1}$], of a water column reads

$$\Pi = C_a \int_0^H P[\bar{\gamma}(z), I(z)] dz, \quad 0 \leq D \leq \infty, \quad (13)$$

where $I(z)$ is given by the last equation of (4) and C_a [g Chl m^{-3}] is the *Chlorophyll* concentration assumed to be constant on the vertical, corresponding to the constant coefficient of light attenuation, k .

Discussion. In cases with $0 < D < \infty$ the integral (13) needs the knowledge of $\bar{\gamma}(z)$ as solution of (12). In the special cases of very low or high diffusivity ($D = 0$ or $D = \infty$, respectively) the solution of (12) is not needed.

The special case of zero diffusivity, $D = 0$, corresponds to the idea⁸ of vertically fixed algae which fluctuate only in horizontal directions. In that case a single cell does not experience fluctuating light. Its *Chl*-carbon ratio then is given by γ_* according to (3) with $I_* = I_0 e^{-kz}$ so that the special non-diffusive production integral becomes

$$\Pi_{D=0} = C_a \int_0^H P\{\gamma_*, [I_*(z)], I_*(z)\} dz. \quad (14)$$

The special case of very high diffusivity, $D = \infty$, corresponds to the idea⁹ of algae which move so fast that their *Chl*-carbon ratio fully adjusts to the vertically averaged light intensity, \bar{I} :

$$\Pi_{D=\infty} = \frac{C_a}{H} P\left[\gamma_*(\bar{I}), \bar{I}\right], \quad \bar{I} = \frac{1}{H} \int_0^H I(z) dz = \frac{I_0}{kH} (1 - e^{-kh}). \quad (15)$$

In the full paper the formulae (12) - (15) are evaluated for different UMLs containing populations of *Chlorella vulgaris* for which the coefficients of the biological submodel (2) are known in detail. The results are presented, compared and discussed by Figures and Tables.

⁶For simplicity I present only the expansion terms of first and second for the case $D = \text{const}$.

⁷In contrast to the simple stationary case (3).

⁸This idea is often attributed to Talling (1957).

⁹This idea is sometimes attributed to Riley (1957).

SCOBI - THE SWEDISH COASTAL/OCEAN BIOGEOCHEMICAL MODEL

Eleonor Marmefelt

Swedish Meteorological and Hydrological Institute, S-601 76 Norrköping

email: Eleonor.Marmefelt@smhi.se,

phone: +46 (11) 15 82 16, fax: +46 (11) 17 02 07

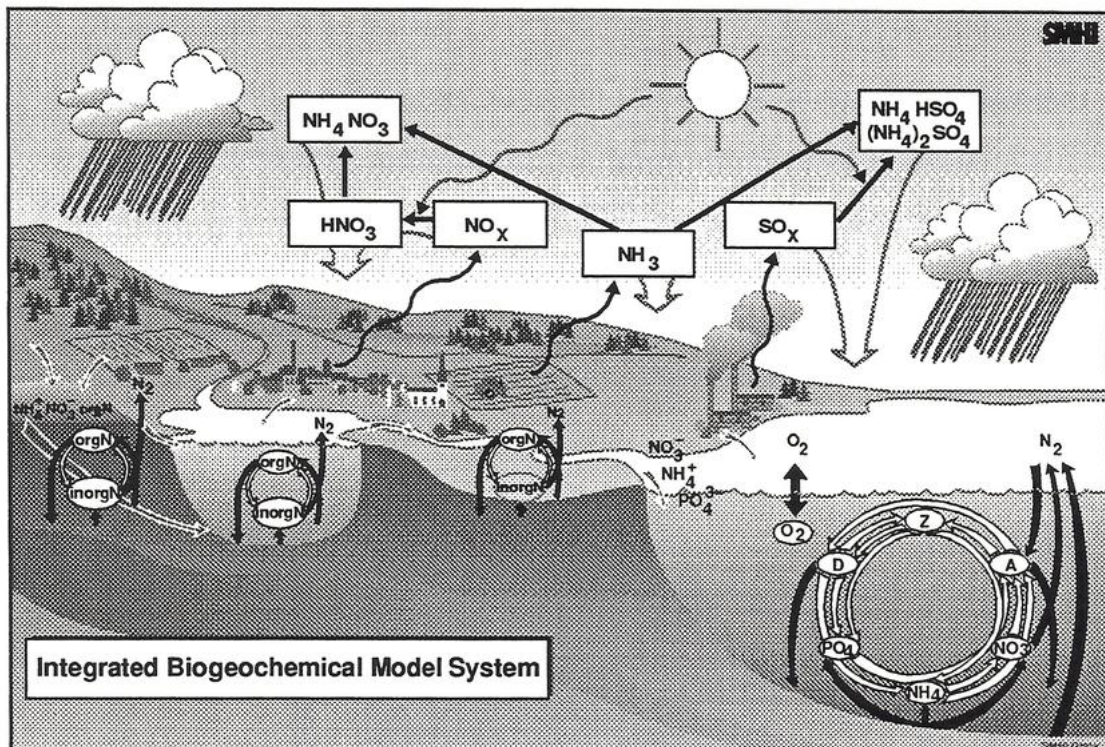


Figure 1 The integrated biogeochemical model system that is under development at the SMHI.

The Swedish Meteorological and Hydrological Institute is developing an integrated biogeochemical model system for the Baltic Sea, which includes marine, atmospheric as well as riverine biogeochemical processes. This presentation focuses on the marine biogeochemical model (the SCOBI model). The present version of the SCOBI model is coupled to the hydrodynamical model PROBE. Together they form a one dimensional model with high vertical resolution. The SCOBI model will however be developed into a three dimensional version in the near future.

The SCOBI model is a general biogeochemical model, but has under its development been applied in the Baltic Proper. It therefore takes into account the very special Baltic Proper conditions, where for example the nitrogen fixation by cyanobacteria plays an important role for the biological production. The nine variable SCOBI model deals with inorganic nitrogen and phosphorous, primary phytoplankton production nitrogen fixation and secondary zooplankton production.

The hydrodynamical PROBE model is a so called $k\epsilon$ -model, which determines the vertical diffusion by turbulent kinetic energy and its dissipation. The PROBE model can easily be set up in a system with coupled subbasins wherever the horizontal variations of the hydrodynamics so requires. A thirteen basin version of the PROBE model has been run operationally in the Baltic Sea for several years. It is coupled to the SCOBI model via the turbulence and via the horizontal and the vertical advection

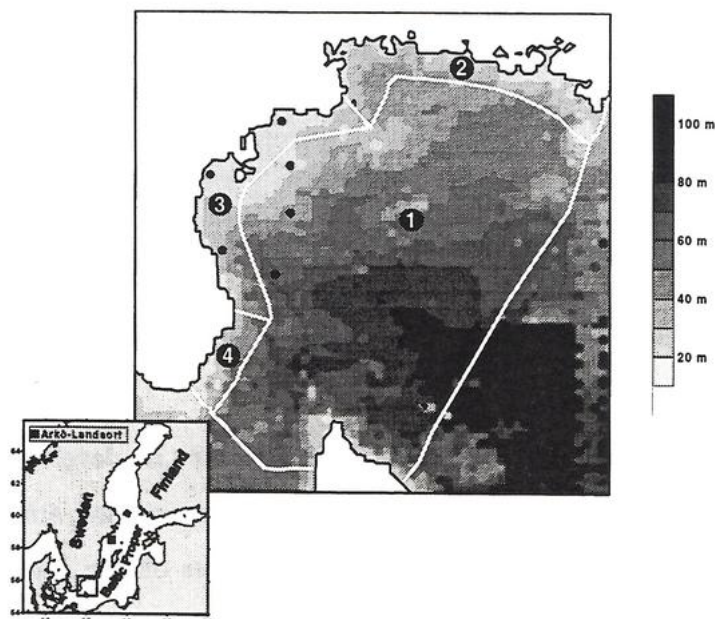


Figure 2 Bathymetric chart of the Hanoe Bight illustrating the division of the area into smaller subbasins.

The coupled SCOBI/PROBE model has in its present version been applied to the coastal zone in a limited area in the south western part of the Baltic Proper, the Hanoe Bight. The Hanoe Bight is a dynamically interesting area with upwelling and a southwards

coastal current along the coast line and a deep water current with incoming Kattegat water passing through the central part of the Bight on its way further into the Baltic. The application of the SCobi model in the Hanoe Bight is to be regarded as a pilot study for the coastal region of the entire Baltic Sea.

In the model set up of the Hanoe Bight, the area has been divided into four boxes. The central part of the bight is regarded as a representative for the open sea, this box is therefore regarded as infinite. The assumption has been made based on the fact that this study focus on the coastal zone. In order to avoid complex boundary conditions to surrounding waters, a simple form of data assimilation has been used in the central Hanoe Bight box. On a weekly basis, temperature, salinity, nutrients and oxygen in the model are simply replaced by data from a monitoring station (BY5), most representative for the box.

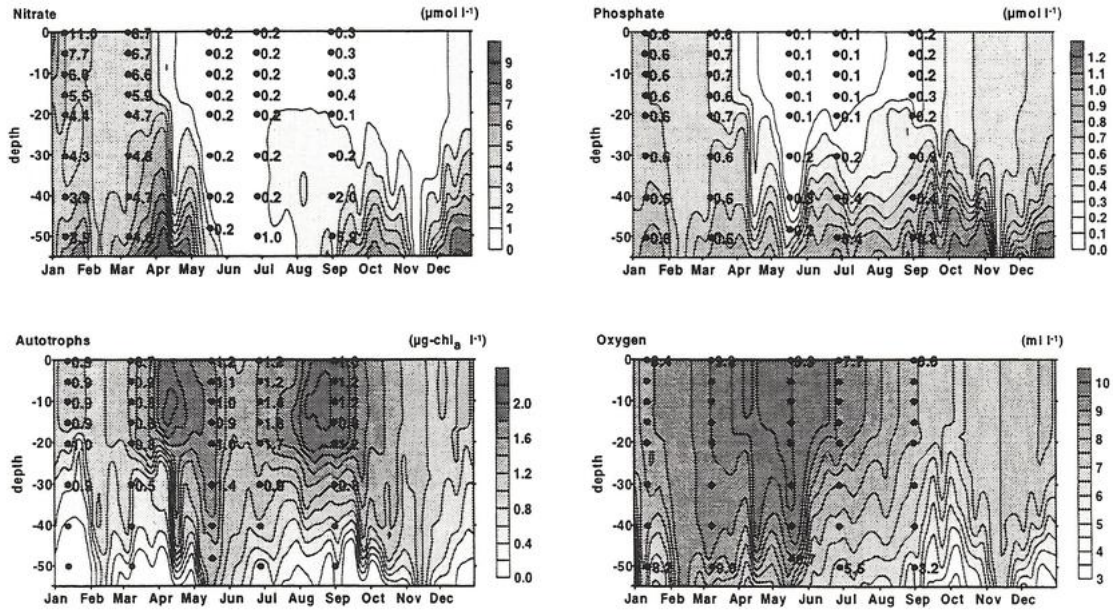


Figure 3 Isopleths of model simulations of nitrate, phosphate, autotroph and oxygen concentrations from the western part of the Hanoe Bight, box number 3. To be compared with monitored data from that area here illustrated as figures at discrete depths.

The horizontal advection is represented by the transports between the boxes. It is essentially forced by the riverine freshwater supply to the coastal boxes. Wind forcing is

also included in the model, but does not contribute to the water exchange between the boxes. It solely governs the upwelling within the coastal boxes. 1994 has for several reasons been chosen for the Hanoe Eight Year. Results from the model simulations will be shown for that year.

One of the primary ideas with the integrated biogeochemical model system is to serve as a tool for decision makers in aspects of environmental protection analyses. The model system has therefore been supplemented with a PC-based analysis and presentation system, which includes simulated data as well as monitoring data. It is also possible to make scenarios with the analysis system where effects of changes in the nutrient load to the coastal zone can be studied. Another aspect of the integrated biogeochemical model system is to form a forecasting model for e.g. the harmful cyanobacterial blooms to avoid harassments in affected areas.

Bio-optical model of Baikal phytoplankton: using for paleolimnological studies.

S.V.Semovski, M.A.Grachev, P.P.Sherstyankin, M.N.Shimaraev
Limnological Institute, Russian Academy of Science Siberian Branch,
Irkutsk

High vertical resolution bio-optical model of spectral underwater irradiance field and primary production based on Wozniak ideas is used for simulation of the Lake Baikal phytoplankton annual cycle. Phytoplankton pigments dynamics, biological and mineral suspended matter and dissolved organic matter consumption by bacteria is included for the optical field simulation. The physical part of the model consists of two-layer vertical mixing scheme with variable mixing rate in upper layer and climatic upper layer depth. Main Baikal autotrophic phytoplankton groups, namely, diatoms and picoplankton differs in biogens consumption and reaction on the temperature variability. Diatoms used silica for skeleton building, main silica source is rivers inlux. Picoplankton productivity increase with temperature growth.

Sediments records for the Baikal show great variability in biological silica content correlated with climate variability. For the cold periods diatoms skeletons in sediments almost completely disappear. One possible explanation of this fact is decreasing in silica supply from rivers during periods of cooling. We present a model studies of diatoms-picoplankton ratio reaction on silica content variability. Due to nonlinear population dynamics "smooth" variations in silica content tend to drastic changes of diatoms-picoplankton ratio.

The main spring diatoms bloom in the Baikal occurs under the ice. The model studies using real optical data on Baikal ice properties show the strong diatoms sring productivity dependence on the ice transparency. Another possible source of diatoms production variability in global scale can be influence of high aerosol content in atmosphere on Baikal ice optical properties and following picoplankton prevaling during summer. The dynamics of this processes is studies by the model using different scenarios on ice optical properties variability.

A physical-biological coupled model for algal dynamics in lakes

Ulrich Franke, Technische Universitaet Darmstadt

A coupled model is presented for physical and biological dynamics in fresh water lakes. The physical model rests upon the assumption that the turbulent kinetic energy in a water column of the lake is fully contained in a mixed layer of variable depth. Below this layer the mechanical energy content is assumed to vanish. Additionally, the horizontal currents are ignored. This one-dimensional two-layered model describes the internal conversion of the mechanical and thermal energy input from the atmosphere into an evolution of the mixed layer depth by entrainment and detrainment mechanisms. It is supposed to form the physical domain in which the simulation of the biological processes takes place.

The biological model describes mathematically the typical properties of phyto- and zooplankton, their interactions and their response to the physical environment. This description then allows the study of the behaviour of Lagrangian clusters of virtual plankton that are subjected to such environments. The essence of the model is the dynamical simulation of an arbitrary number of nutrient limited phytoplankton species and one species of zooplankton. The members of the food web above and below affect the model only statically. The model consists of different guilds of phytoplankton limited by an arbitrary number of nutrients and one zooplankton species. These guilds are modelled to resemble mean properties of the species composition in a lake.

Simulations calculated with this model show the influence of the biological system on the physical system, which results in a weak increase of the surface temperature due to the phytoplankton dynamics. As an example for the modeling of biological dynamics a scenario of exploitative competition between guilds of algae with different uptake kinetics under grazing pressure of zooplankton is examined. It will be shown that the model is able to reproduce the spring bloom and a summer bloom of algae corresponding to predator-prey dynamics, but still has problems with the prediction of the time of the spring bloom. Improvements in this case should be achieved by incorporating a more sophisticated k-epsilon turbulence model which has been developed by D. Ollinger (University of Constance).

The results of our calculations suggest that our coupled physical-biological model offers a general tool that is capable of simulating long-term algal dynamics in an arbitrary lake. It can be easily adapted to more special problems than the example mentioned above, e.g. to help predicting the delay of the system response and the changes of pool sizes during a re-oligotrophication process of an eutrophic lake.

A PROCEDURE TO DETERMINE THE PARTICULATE CONTENT OF SHALLOW WATER FROM THEMATIC MAPPER DATA

S.TASSAN

Space Applications Institute, Commission of the European Communities, Joint Research
Centre-Ispra Site, Ispra (VA), Italy

The knowledge of the particulate content (phytoplankton and organic/inorganic suspended sediment) in shallow water is of considerable interest in areas devoted to tourism, or used for, or potentially suitable for aquaculture activities, etc.. The estimation of this quantity from remotely sensed imagery in the visible-near infrared (VIS-NIR) range poses however a very difficult problem, because of the masking, and possibly dominant, effect of bottom-reflected light. A numerical exercise has been carried out to explore practical solutions to this problem. Being intended for present applications, the study considered only the information that may be provided by the Thematic Mapper (=TM) scanner onboard the NASA Landsat satellites.

Remote sensing yields the particulate concentration in the upper water layers (phytoplankton in terms of chlorophyll a concentration) by means of algorithms that operate on reflectance values (= R), derived from the radiance measured by the sensor and corrected for the effect of the atmosphere. The TM algorithms for chlorophyll (= C) and suspended sediment (= S) determination in infinite-depth water that are considered here have the form

$$C(\text{mg m}^{-3}) = a [R(486)/R(570)]^b \quad S(\text{g m}^{-3}) = c R(660)^d \quad (1)$$

where the numbers in brackets are the central wavelengths of channels 1, 2 and 3 of the scanner and a, b, c, d are numerical constants.

For this numerical study the reflectance was computed using a three-component optical model, with input data taken the literature. The numerical constants of the algorithms expressed by Eqs. 1 were determined by a least-squares fits to the reflectance

values computed for infinite-depth water. The shallow water reflectance was computed by a two-flow equation, that accounted for both water depth and light reflection by the sea bottom, for depths varying from 1 to 25 m, and bottom covered by sand or green algae. The same computation was used to generate look-up tables that convert the C, S concentration determined by the infinite-depth algorithm applied to the shallow water data to the two-flow estimate of the actual C, S concentration. A sensitivity analysis was performed to predict the concentration error, that is originated by realistic estimates of the uncertainty in water depth and bottom albedo, as well as in other computational parameters.

This study has shown that the use of the conversion nomograms yields a considerable reduction of the concentration error. With the chosen computational parameters, the sensitivity analysis predicts that for depths more than 5 m, respectively 2 m, 0.2-2 mg m⁻³ chlorophyll concentrations and 1-10 g m⁻³ sediment concentrations can be determined with relative error mostly lower than a factor of 2

The positive results obtained suggest a practical procedure for the determination of chlorophyll and suspended sediment concentration in shallow water, based on the use of computed look-up tables that convert the value yielded by the infinite-depth algorithm to the actual concentration. Clearly, the computation must be carried out with input data corresponding to the local situation. A sensitivity analysis, also using local statistical data (e.g. depth uncertainty) can provide an estimate of the quality of the results attainable, as well as the limits for the application of the procedure (e.g. minimum depth for determination of concentration with prefixed error).

Estimation and Direct Measurement of Remote Sensing Reflectance in Stratified and Mixed Water Bodies

Don Pierson & Niklas Strömbeck

Institute of Limnology

Uppsala University

Sweden

Remote sensing reflectance or the ratio of upwelling radiance (Lu) to downwelling irradiance (Ed) from a water body has often been approximated as an empirical function of two of the waters inherent optical properties (Kirk 1983).

$$Lu/Ed = 0.083 bb/a$$

Where bb is the back scattering coefficient and a is the absorption coefficient. As part of the EU SAtellite Remote Sensing For Lake MONitoring (SALMON) project we are collecting data to calculate Lu/Ed using the above equation, and are making direct measurements in of Lu/Ed in order to verify the theoretical calculations. Estimations of bb are made *in situ* using a Sequoia Scientific Hydroscat 6 backscattering sensor. Simultaneous measurements of Ed and Lu are made just above the surface and throughout the euphotic zone using two GER 1500 spectroradiometers. The absorption coefficient associated with dissolved and particulate matter was estimated from water samples as described in the SeaWiFS protocols (Muller and Austin 1995). In this paper we access the ability of the above equation to predict Lu/Ed in water bodies that are either stratified or well mixed in regards to phytoplankton, dissolved organic matter, and suspended particulate matter; the substances expected to strongly influence bb and a .

Kirk J. T. O. 1983. Light and Photosynthesis in Aquatic Ecosystems Cambridge University Press, New York. 401 pp.

Mueller, J.L. & R. W. Austin 1995. Ocean Optics Protocols for SeaWiFS Validation, Revision 1 SeaWiFS Technical Report Series. NASA Tech. Mem. 104566 Vol .25 pp 67.

Measurement of lake water absorption coefficients in order to support modelling of remote sensing reflectance and primary production

Niklas Strömbeck & Don Pierson
Institute of Limnology
Uppsala University
Sweden

We have initiated a sampling and analysis program in order to collect spectral absorption data of fresh water from different lakes. The data will be used primarily for supporting modelling work to predict the ratio of upwelling radiance (L_u) to downwelling irradiance (E_d) from the lakes (Kirk 1983), and secondly to support optical models for estimation of primary production (Kiefer and Mitchell 1983).

The measurements of the absorption coefficient follows the SeaWiFS protocols (Muller and Austin 1995), but some modifications are made according to the work of Allali et al. (1995) and Tassan and Ferrari (1995).

We will present some preliminary results form the work during the field season of 1997 together with results from the associated experiments.

Kirk, J. T. O., 1983. Light and Photosynthesis in Aquatic Ecosystems. Cambridge University Press, New York. 401 pp.

Mueller, J.L. & Austin, R. W., 1995. Ocean Optics Protocols for SeaWiFS Validation, Revision 1. SeaWiFS Technical Report Series. NASA Tech. Mem. 104566 Vol .25 pp 67.

Kiefer, D. A. & Mitchell, B. C., 1983. A simple steady state description of phytoplankton growth based on absorption cross spectra and quanta efficiency. Limnol. Oceanogr. 28: 770-776.

Allali, K., Bricaud, A., Babin, M., Morel, A. & Chang, P., 1995. A new method for measuring spectral absorption coefficients of marine particles. Limnol. Oceanogr. 40: 1526-1532.

Tassan, S. & Ferrari, G. M., 1995. An alternative approach to absorption measurements of aquatic particles retained on filters. Limnol. Oceanogr. 40: 1358-1368.

Algorithms for estimating some optically active substances and apparent optical properties from subsurface irradiance reflectance measurements in lakes.

A. Reinart, H.Arst, T.Kutser Estonian Marine Institute, Paldiski 1, EE0001 Tallinn, Estonia.

A.G. Dekker Vrije Universiteit Amsterdam, Institute for Environmental Studies De Boelelaan 1115, 1081 HV Amsterdam, The Netherlands.

INTRODUCTION

Deriving water quality information from irradiance reflectance spectra is especially complicated in turbid and algae-rich, multicomponent waters. Remote sensing of inland waters in Institute of Environmental Studies, Vrije University, Amsterdam the Netherlands has focused on developing multitemporally valid algorithms (Dekker 1993, Dekker *et al.* 1995). The main objective of this study is to test, whether these algorithms are suitable in conditions of Estonian and Finnish lakes.

MATERIALS AND METHODS

The irradiance reflectance just below the water surface is calculated as ratio of upwelling and downwelling irradiances. They are obtained from measurements by underwater spectroradiometer LI 1800 UW. From measured spectra R_{676} and R_{706} as irradiance reflectance at wavelengths 676 and 706 nm was calculated. Concentrations of total particulate matter, chlorophyll *a* and dissolved organic matter were determined from samples collected concurrently with irradiance measurements. Amount of dissolved organic matter is expressed by absorption coefficient $a(440)$ of filtered water at wavelength 440 nm. Subsurface reflectance spectra were obtained during 2 years in different seasons from 9 lakes. (Table1).

Table 1. Range, mean and standard deviation in water quality data and number of measurements in lakes where subsurface irradiance measurements were made for validation of algorithms.

Water quality	Measurements	Range	Mean	Stand. Dev.
Secchi disk transparency (m)	23	0.5-4.0	2.2	0.9
Diffuse attenuation coefficient (m^{-1})	25	0.5-4.2	1.24	0.7
Dry weight (mg/m^3)	22	1.5-22.0	6.8	6.1
Chlorophyll <i>a</i> ($\mu g/l$)	25	1.3-38.3	10.3	10.4
Dissolved organic matter (m^{-1})	25	1.2-53	8.1	12.7

For estimation of chlorophyll *a* concentration (CHLa) by remotely sensed reflectance the algorithm following the analytical approach was developed by Dekker (1993):

$$CHLa = \frac{a_{r676} - R_{706}/R_{676} a_{r706}}{b_{b676}^{**}(R_{706}/R_{676} - 1) - a_{676}^*} \quad (1)$$

Calculation were performed assuming average values of inherent optical properties for shallow eutrophic and deep lakes with chlorophyll α specific absorption $a^*_{676}=0.0164 \text{ m}^2\text{mg}^{-1}$; chlorophyll α correlated backscattering $b_b^*_{676}=b_b^*_{706}=0.0040 \text{ m}^2\text{mg}^{-1}$; and assuming an average absorption (a_r) of pure water, tripton and dissolved organic matter as measured in samples from Vecht lakes (Dekker 1993). Chlorophyll α could be derived from the actual remote sensing radiance with an accuracy of 9.5 mg/m^3 .

For estimating the seston dry weight (DW), diffuse attenuation coefficient (K_d) and Secchi disk depth (SD) Dekker (1993) obtained the following semi-empirical relationships:

$$DW=2.69+0.31R_{706} \quad (2)$$

$$K_d=-0.3457+1.6224 R_{706}/R_{676} \quad (3)$$

$$\ln SD=5.05-1.795\ln(R_{706}/R_{676}) \quad (4)$$

We tried to carry out some rough estimations of backscattering coefficient $b_b(\lambda)$ using irradiance measurement result in Estonian and Finnish lakes. The idea is based on Kirk's (1984) formula connecting the values of irradiance reflectance just below the water surface, absorption and backscattering coefficient. For $b_b(\lambda)$ we get:

$$b_b=aR(0-)/(0.975-0.629\mu_0) \quad (5)$$

values of μ_0 are easily determined by time and geographical coordinates of the measurements location. Absorption coefficient $a(\lambda)$ was estimated using relationship between scattering and beam attenuation coefficient, roughly estimated for waters of transparency between 1.5 and 7 m (Arst *et al.*, 1995).

RESULTS AND DISCUSSION

Results presented in Fig.1 demonstrate the suitability of Dekker's algorithms for Estonian and Finnish lakes. As is seen, the lines, obtained by algorithms, are very much describing the average trend of changing the parameters with the change of R_{706}/R_{676} . Taking into account that the differences between measured and calculated values may be to some extent caused by the errors of the measurements, one can conclude, that algorithms (1)-(4) are capable to give rather good results in different turbidity conditions. Amount of dissolved organic matter in Estonian and Finnish lakes is probably higher and the concentration of chlorophyll α in most cases lower than those in Dutch lakes.

Correlation between measured and calculated CHLa was 0.86 and linear regression line with forced intercept: $\text{CHLa}_{\text{cal}}=1.08\text{CHLa}_{\text{meas}}$. When the real amount of chlorophyll α was less

than 2 mg/m^3 , the algorithm yielded negative values. Our results show also, that in conditions of extremely high amount of dissolved organic matter in the water the results by Eq.(1) are rather far from measured chlorophyll values.

As is shown on the figure 1b, the correlation between measured and calculated by Eq.(2) values of DW is poor. The reasons can be the quality of water samples for DW laboratory estimations, but also the lack of information about DW-specific backscattering and volume scattering function necessary for deriving the analytical algorithm.

Using algorithms (3) and (4) for calculating the apparent optical properties of water we obtained the correlation coefficients of the ratio R_{706}/R_{676} with K_d and SD correspondingly 0.75 and 0.65. Separation of the points into water types (deep water, shallow water) increased both correlation coefficients (Fig.1c and 1d).

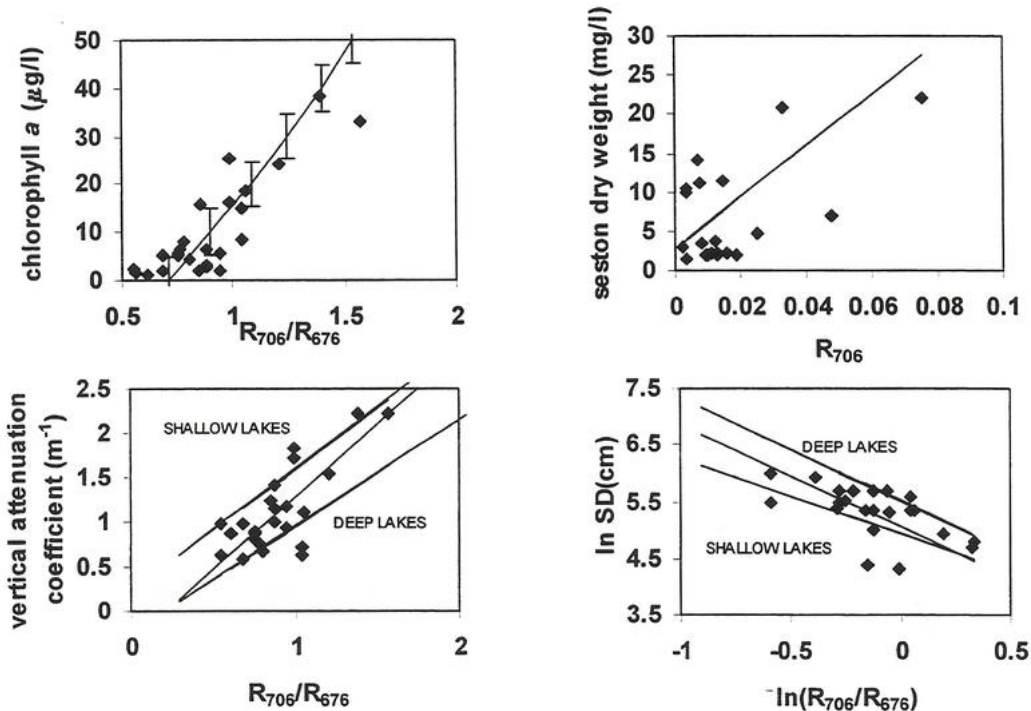


Figure 1. Results of applying the algorithms for estimating a) chlorophyll a concentration b) seston dry weight c) diffuse attenuation coefficient d) Secchi disk transparency by irradiance reflectance. Squares show *in situ* measured values in Estonian and Finnish lakes, lines calculated by Eq.(1)-(4) derived by Dekker for Dutch lakes.

Studies on the estimation of backscattering coefficient in Estonian and Finnish lakes showed the difference of backscattering spectra by almost two orders of magnitude and distinct maximums in spectra around 550 and 700 nm. In clear lakes waters the maximum values of

backscattering are close to the results obtained in oceanic waters (<0.01), but is significantly higher in the lakes with higher turbidity (up to 0.9) (Figure 2). It is hard to explain the maximum in the backscattering spectra of highly turbid waters, probably one reason is the low accuracy of the underwater irradiance measurements in the blue region of the spectrum.

The highest backscattering coefficient in The Netherlands (Dekker 1993) lakes occurred in very turbid and the smallest in deep clear lakes (Figure 2b). The spectral variability of $b_b(\lambda)$ is very weak, but in most cases backscattering decreases with increasing of wavelength.

Despite of differences in the shape of the spectra for turbid lakes, the variability limits of $b_b(\lambda)$ are similar for Estonian, Finnish and Netherlands lakes.

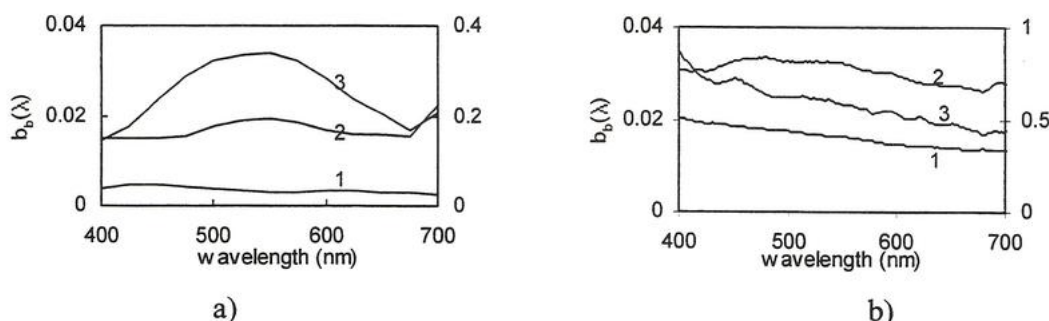


Figure 2. Some examples of estimated backscattering coefficients in Estonian and Finnish lakes (a) and in The Netherlands lakes (b). (Lines 1, 2 - left axe, line 3 - right axe)

Acknowledgements. This work has been supported by the Individual Mobility Grant of Tempus Phare program. The authors are indebted to A. Blanco Sequeiros and A. Herlevi from the University of Helsinki for kindly providing underwater measurements data on Estonian and Finnish lakes.

REFERENCES

- Arst H., S. Mäekivi, T. Lukk, A. Herlevi, (1995) "Estimation of the spectral distribution of the downward irradiance attenuation coefficient in the water by spectra of beam attenuation coefficient." Rep. Ser. Geophys. **32**, University of Helsinki, 29-35.
- Dekker A.G., (1993) Detection of optical water quality parameters for eutrophic waters by high resolution remote sensing." (Ph.D. thesis), Proefschrift Vrije Universiteit Amsterdam, 220.
- Dekker, A.G., Z. Zamurovic-Nenad, H.J. Hoogenboom and S.W.M. Peters, (1995) "Remote sensing, ecological water quality modelling and in situ measurements: a case study in shallow lakes." Hydrological Sciences **41**, 531-547.
- Kirk J.T.O., (1984) "Dependence of relationships between inherent and apparent optical properties of water on solar altitude." Limnol. Oceanogr., **29**, 350-357.

Averaging Techniques in Multi-Dimensional Water Quality Modeling of Vertically Stratified Lakes

Abstract

R. Kopmann and M. Markofsky ¹

Introduction

In multi-dimensional water quality modeling the spatial and temporal distributions of dissolved and suspended substances are simulated in order to account for non-homogeneities and non-linearities in the hydrodynamic transport and reactive processes. All of the exchange processes at and through the water surface e.g. photosynthesis, heat and oxygen transfer and at the sediment - water interface e.g. erosion, deposition and nutrient remineralisation are basically multi-dimensional.

It is well known, that with the increase in model dimensionality, the data requirements both for generating boundary conditions, and determining reaction rates drastically increases thus reducing their practicable applicability. For this reason it is useful to compare the results of different dimensional models in order to determine the appropriate parameterization for modeling heterogeneous processes.

A parameterization of heterogeneous processes is only possible when a clear differentiation is made between the numerical consequences of the averaging step and the biology, chemistry and physics of the process under consideration. For example, exponential growth is a description of undamped biological reproduction. In aquatic systems, this is, among others, also a function of the light intensity which is further a function of depth, shadowing and time. In order to simulate this process in a model of lower dimension it is therefore necessary to include extra terms which account for spatial and temporal averaging. Similar statements can be made for sedimentation, density stratification and wind induced flows and mixing processes.

Empirical Constants

Water quality models generally include different reaction functions which incorporate numerous empirical constants. These constants are normally determined from controlled laboratory experiments and comparison with normally sparse field measurements. This is the case since field measurements are not only costly but also have to be extremely complex in order to isolate particular processes. It is also seldom that the physical data necessary for determining the hydrodynamics and mixing processes are simultaneously measured. As such, it is not uncommon, that empirical constants range over factors of 10 and more since in reality they include all of the unmeasured effects affecting the process in question.

Mathematical Example

¹ I.f. Strömungsmechanik und ERiB, Universität Hannover, Appelstr. 9a, 30167 Hannover, Germany

A simple example is used to demonstrate the effect of averaging on the numerical results and the necessity for additional terms to correctly simulate spatial averaging.

The temporal change in the phytoplankton concentration is represented by a first order reaction in which the coefficients are both a function of time and space. In this example, the respiration rate ρ is constant but the growth rate $\mu(z,t)$ is light limited and is represented by a Michaelis-Menten reaction involving the maximum growth rate μ_{max} , a light dependent term $I(z,t)$ and a half saturation constant k_i .

$$\frac{\partial \text{Phy}(z,t)}{\partial t} = (\mu(z,t) - \rho)\text{Phy}(z,t)$$

$$\mu(z,t) = \mu_{\text{Max}} \frac{I(z,t)}{k_i + I(z,t)}$$

In 0-dimensional models the phytoplankton concentration , the growth rate and light intensity are only a function of time, t .

$$\frac{d\text{Phy}(t)}{dt} = (\mu(t) - \rho)\text{Phy}(t)$$

$$\mu(t) = \mu_{\text{max}} \frac{I_i(t)}{k_i + I_i(t)}$$

Figure 1 shows the time dependent spatially averaged phytoplankton concentration resulting from the 1-D calculations in comparison with that of the 0-D calculation using both a spatially averaged growth rate and light intensity. The light intensity was assumed to be sinusoidal during the day and 0 at night. The vertical dependence was exponential following Beer's law.

This figure shows that the 1D-model generates significantly higher concentration during the daylight hours. In other words, the integration over the water depth in the 0-D model considerably damped the maximum values and thus, the growth rate in the 0-D model is too low. Additional terms are needed to correct for the spatial averaging.

Correction Techniques

The following demonstrates two techniques for correcting for spatial averaging. These are then compared for the above given test case.

First the function $\bar{f}(t)$ which represents the depth average value is defined as:

$$\bar{f}(t) = \frac{1}{H} \int_z f(z,t) dz$$

The first method is based on the exact integration of the 1-D equation. Additional terms arise when the integration of a term containing two depth dependent terms is

made since $\int_z fg dz \neq \int_z f dz \int_z g dz$. A coefficient β is introduced in order to determine the degree of inhomogeneity in the averaged value, i.e.

$$\beta = \frac{\int_z f(z, t)g(z, t)dz}{\int_z f(z, t)dz \int_z g(z, t)dz}$$

The 0-D Equation includes this coefficient in the form

$$\frac{d\overline{Phy(t)}}{dt} = (\mu(t)\beta - \rho)\overline{Phy(t)}$$

In this relatively simple method the effect of vertical averaging is distinguished from the biological growth coefficient. The effect of averaging can thus be included by a parameterization of β .

The second technique is similar to that used in turbulence modeling. The function $f(z, t)$ is separated into a mean value and the deviation from it: $f(z, t) = \overline{f(t)} + f'(z, t)$. Then this is expanded in a Taylor series:

$$\frac{\partial f(z, t)}{\partial t} = \Theta(f(z, t), g(z, t))$$

and results in additional terms whose values are different from zero for which closure equations are needed:

$$\frac{\partial \overline{f(t)}}{\partial t} = \Theta(\overline{f(t)}, \overline{g(t)}) + \frac{1}{2} \overline{f'^2} \frac{\partial^2 \Theta}{\partial \overline{f(t)}^2} + \dots$$

The time dependent Phytoplankton concentration is given by:

$$\frac{d\overline{Phy(t)}}{dt} = (\mu - \rho)\overline{Phy(t)} + \overline{l(t)^2} \left(\frac{\overline{\mu(t)Phy(t)}}{k_1 + \overline{l(t)^2}} - \frac{\overline{\mu(t)Phy(t)}}{(k_1 + \overline{l(t)})l(t)} \right) + \frac{\overline{\mu(t)}}{l(t)} - \frac{\overline{\mu(t)}}{k_1 + \overline{l(t)}}$$

and requires a closure for $\overline{l(t)^2}$. Since in this example the light intensity function is known, the above equation can be solved analytically. In general, the additional terms are not known analytically and must be parameterized as in the first method.

An exact parameterization of the coefficient β in the first method leads to identical results for both the 0-D calculation and the vertical average of the vertically distributed information from the 1-D calculation. The results of the Taylor Series method always have some error due to the neglect of the higher order terms in the Taylor expansion. This is illustrated in Figure 2.

Literature:

Schellenberger, G., Behrend, H., Kozerski, H.P., Mohaupt, V.: Ein mathematisches Ökosystemmodell für eutrophe Flachgewässer, Acta Hydophysica 28 ½ S. 109-172, Berlin, 1983.

The Enhanced Stream Water Quality Models QUAL2E and QUAL2E-UNCAS, Documentation and User Model, EPA, 1987.

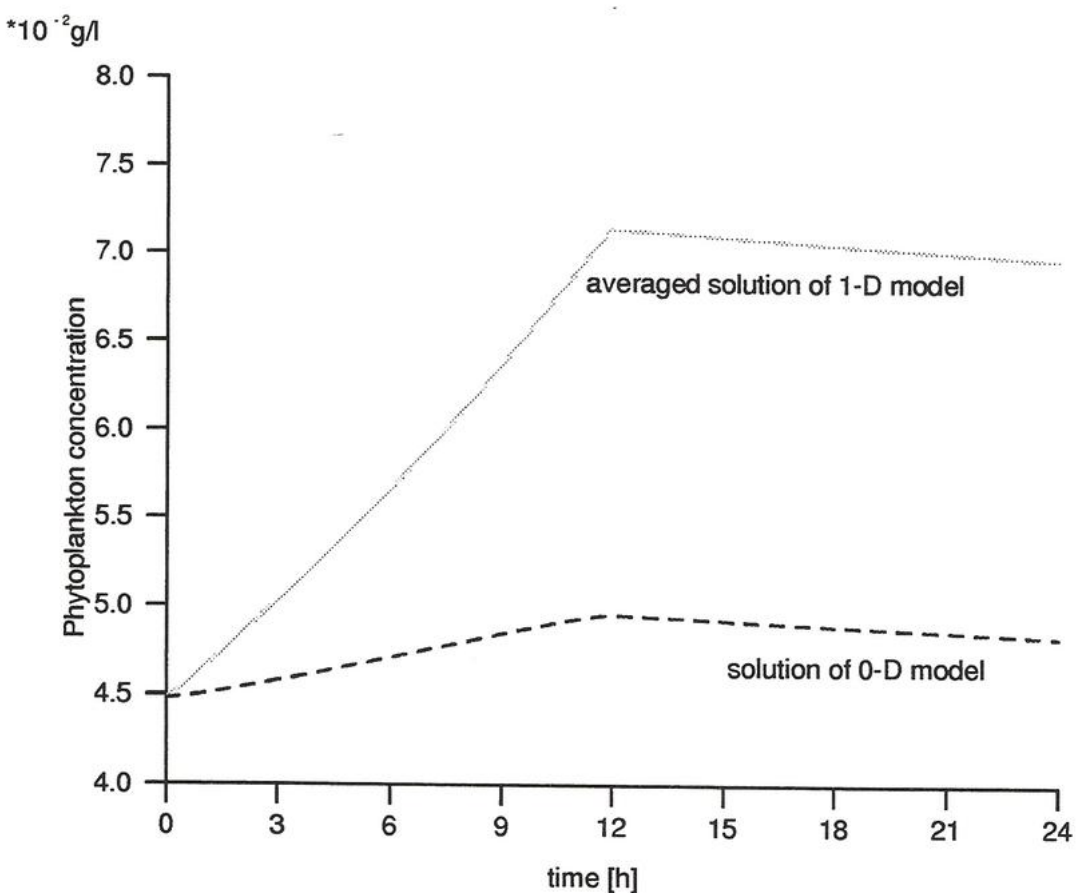


Figure 1: Phytoplankton concentration calculated with a 0-D model without an extra term for averaging in comparison with the averaged solution of a 1-D model.

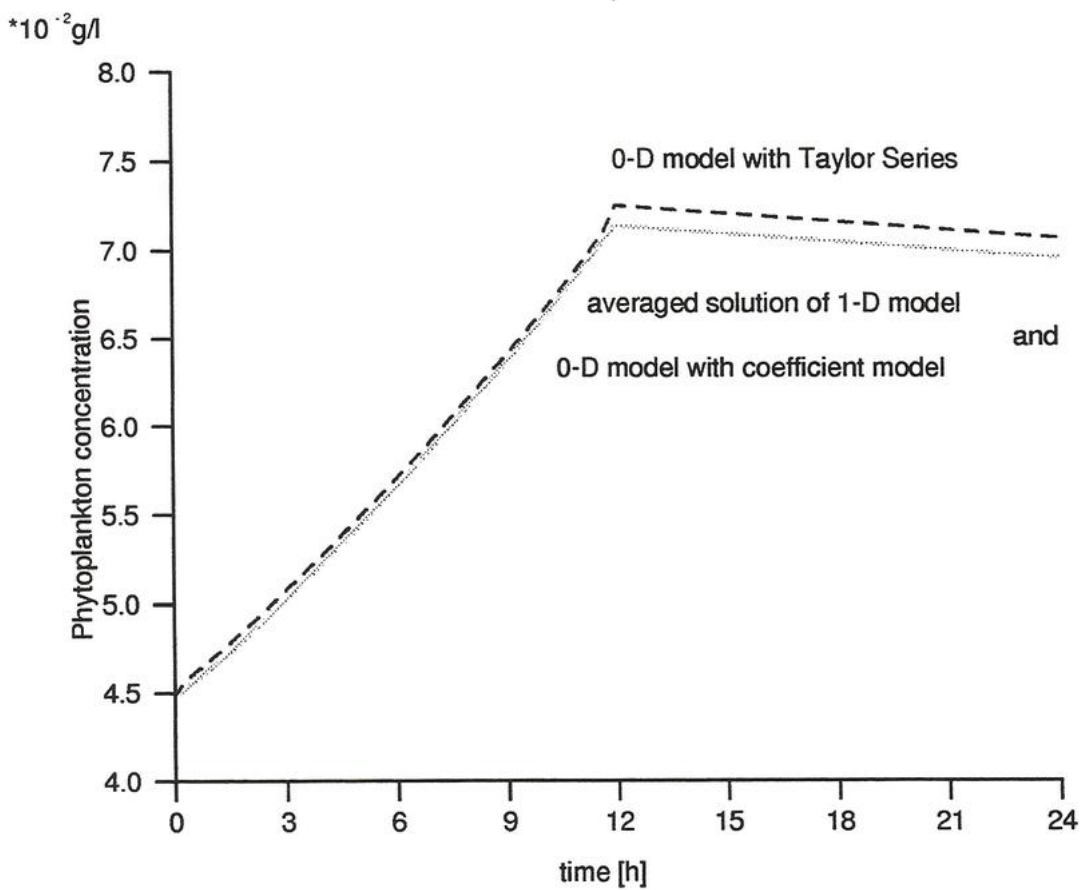


Figure 2: Phytoplankton concentration calculated with 0-D models using (1) a Taylor Series (---) and (2) a coefficient correction term (---) in comparison with a spatially averaged solution of a 1-D model

Michael Schimmele

UFZ Centre for Environmental Research Leipzig-Halle, Germany

Influence of dissolved substances on the physical properties of lignite mining lakes

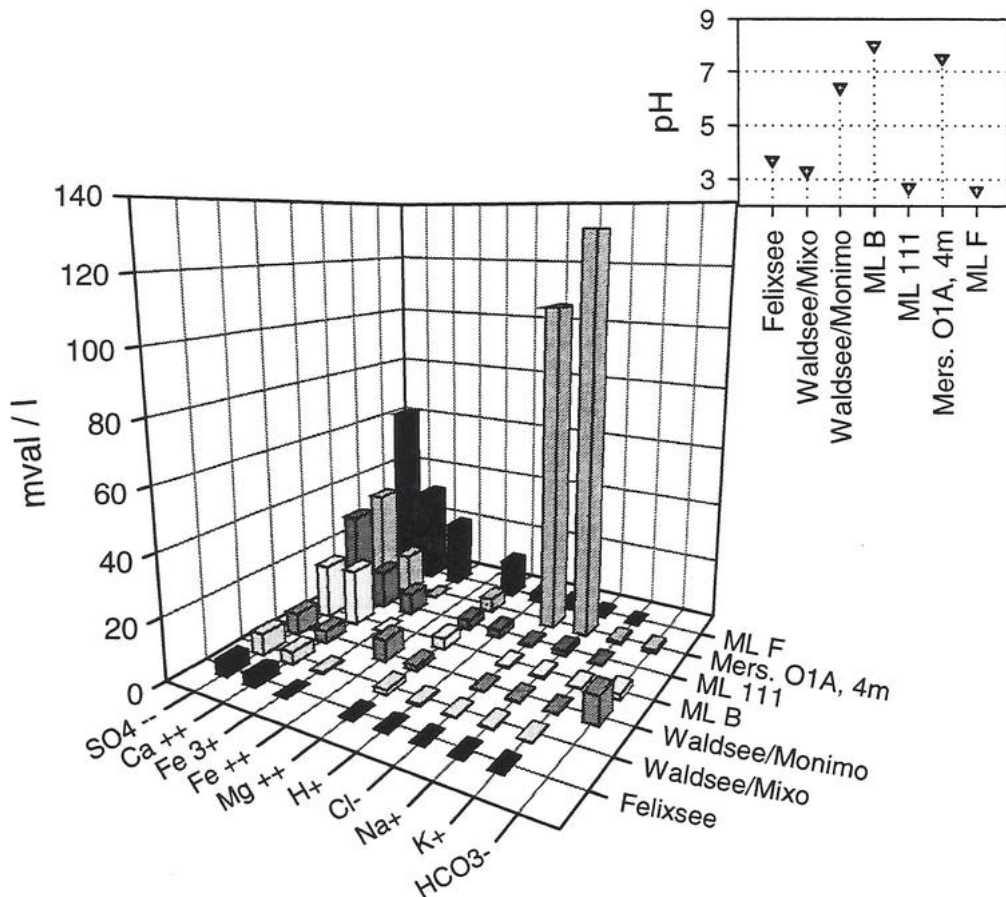
Extended Abstract: Over hundred of post-mining pit lakes are already existing or will come into being in former GDR. These lakes vary in their content of dissolved substances depending on the kind and origin of the filling water, the pits location in the groundwater field and the nature of the geological substratum. Especially the strongly acidified lakes ($\text{pH} < 3$) show high concentrations of sulfate and iron. Their color is brown to red. The geogenic acidification is caused by oxidation of pyrite and markasite in the aerated overburden. The resulting acidity is then transported by groundwater into the lake. Typical el. conductivities (κ_{25}) of such lakes are in the range of 1 to 4 mS/cm.

Another phenomenon is salinization, which may occur when the mining is in close proximity to salt layers. Inflowing groundwater can form layers, in which salt concentrations exceed oceanic values, e.g. in mining lake Merseburg Ost by a factor of 3.

These processes are indirectly caused by humans, but natural. In some cases additional impact on the water quality arises from the dumping of industrial and municipal waste and sewage nearby or even directly into the lake.

Therefore there is a relatively broad variability of the chemical composition in mining lakes. The chemical composition influences the measurement of some properties, e.g. electrical conductivity, in these waters. Some examples of the distributions of the main ions, which contribute to electrical conductivity is given in fig 1. El. conductivity normally is taken as a measure of dissolved and ionized substances, e.g. for the calculation of salinity. For a direct comparison it has to be corrected to a reference-temperature, which is 25°C in most cases. The temperature coefficient itself is a function of the chemical composition. It is relatively well known for freshwater, buffered by calcium carbonate, and for seawater.

Fig. 2 shows the factors for the correction of el. conductivity to 25°C for various mining lakes in comparison with standard methods (Bührer&Ambühl 1975, UNESCO 1978, APHA 1992, DIN 1993). It can be seen that there is a broad range of factors at low temperatures.



Unfortunately in mid to high latitudes low temperatures are very common in lakes. These implies errors of over 10% for some lakes.

fig. 1: Examples of distributions of the main ions, which contribute to electrical conductivity

Dissolved substances furthermore affect directly the density structure and therefore the stratification, the biological development and the formation of oxic/anoxic layers. These substances are not necessarily ionic. In lake Vollert Sued for example waste from a coking plant was dumped. Therefore it has a high content on highly polymerized phenols and humic acids. These (and others) contribute to density, but less to el. conductivity. Fig. 3 shows the comparison of measured and calculated densities of water from Vollert Sued from 0.5m and 22m depth. Density was calculated with the Chen&Millero (1986) equation of state for freshwater with salinities of $S=0.6$ and $S=1.2$, respectively (please note that $S=1.2$ is already outside the validity range given by Chen&Millero). These salinities would be the outcome of a

Michael Schimmele Influence of dissolved substances on the physical properties of lignite mining lakes calculation from temperature and el. conductivity after UNESCO recommendations (1978) for seawater. It can be seen that there is an offset in density caused by non-ionic substances, whereas the temperature dependency seems to be similar in this case.

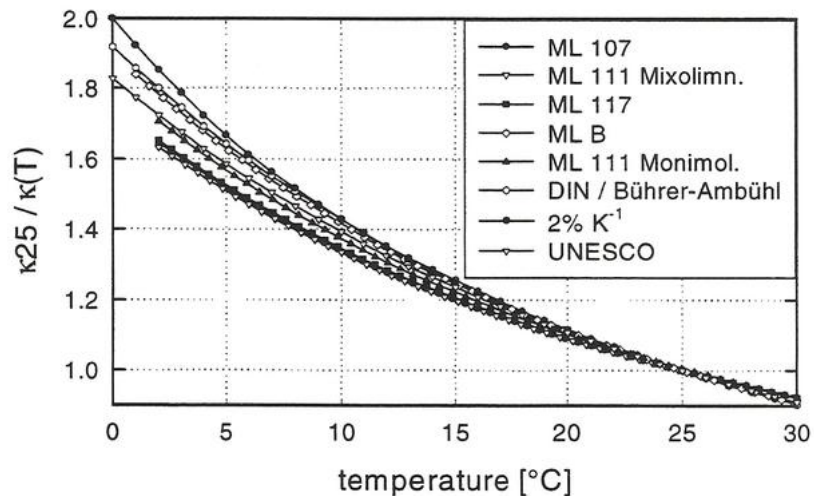


fig. 2: Factors for the correction of el. conductivity to 25°C

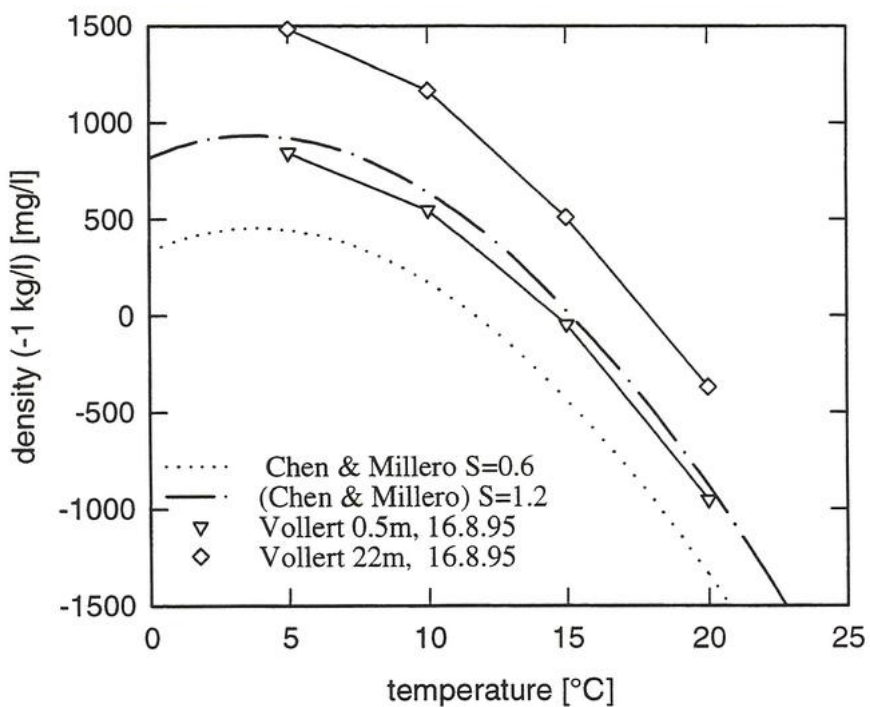


fig. 3: Densities in 0.5m and 22m depth, lake Vollert Sued, 16.8.95

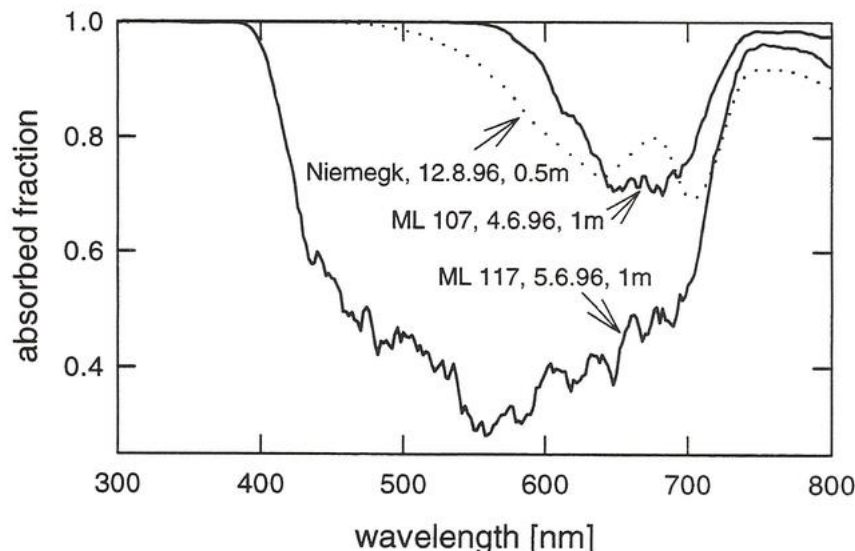


fig 4: Spectra of light absorption in three acidified lakes

The light climate is affected by the dissolved substances too. Three examples from acidified lakes (ML 107 pH 2.4, Niemegk pH 2.7, ML 117 pH 3) are given in fig. 4. There is high absorption in the short-wave range by dissolved iron in lakes Niemegk and 107. In contrast ML 117 had relatively low iron content and secchi depth > 14m (ground). These different absorption influences stratification and biological development as well.

In conclusion the influence of dissolved substances on physical properties may not be neglected in mining lakes. Because of the variability in the composition the influence on certain parameters has to be determined carefully. Standard methods are not sufficient to describe these influences. Furthermore neutralization of acidified lakes, for example with the help of sulfur reducing bacteria, would change the ion content and hence the equation of state and the light climate. These changes have to be taken in account when monitoring the restoration efforts.

Workshop on „Physical Processes in Natural Waters“, 3-5/11/1997, Ispra, Italy

Michael Schimmele Influence of dissolved substances on the physical properties of lignite mining lakes

DIN 1993: EN 27888 / ISO 7888 . Bestimmung der elektrischen Leitfähigkeit. Deutsches Institut für Normung e.V.

UNESCO 1983: Algorithms for computation of fundamental properties of seawater. UNESCO technical papers in marine science 44

Nutrient and heat fluxes and two dimensional advection in density stratified Lake Lugano

Ch. Mattenberger¹, A.Wüest¹, G. Goudsmit¹, A. Barbieri²

¹⁾ Swiss federal Institute for Environmental Science and Technology (EAWAG) and Swiss federal Institute of Technology (ETH), CH-8600 Dübendorf

²⁾Laboratorio di Studi Ambientali, CH-6900 Lugano-Paradiso

Introduction

In a steady density-stratified water body the turbulent eddy diffusion is normally one of the most important transportation processes for nutrients and heat. The discreet determination of its coefficients over the whole water column is essential for calculating the fluxes at any point and over the stratified hypolimnion into the well mixed epilimnion and vice versa.

If there are some multi-parameter profiles available to a higher resolution, e.g. temperature or κ_{20} -data, the diffusion-coefficients (K_z) may be determined by the budget-gradient-method.

In lakes it is known that advective fluxes in a 1D particular or diluted form enter the system by sedimentation, solar radiation and redissolution and exit it by outflow and embedding. In many cases a one-dimensional analysis is usually sufficient. Lake Lugano a steep perialpine lake is an exception to this norm, where like oceans, lateral intrusions of density- and turbidity-currents have been observed. As measurements and budgets of nutrients and temperature show, lateral advective contributions of heat, particles and connected nutrients can't be neglected. The discussion about diffusion, advection and heat and nutrient budgets within this steepbordered freshwater-lake should show the amount of those lateral contributions.

Eddy diffusion and vertical heat flux

Between 1990 and 1996 there have been 13 campaigns for measurements of temperature, conductivity and light-transmission. The influence of the internal seiche has been eliminated by averaging profiles of one campaign and by corrections with thermistor-chain data in the years '94, '95 and '96.

By the assumption of horizontal homogeneity, heat content (W) below depth z_0 and time t_1 can be determined in a first step as:

$$W(z_0, t) = \rho \cdot c_p \int_{z_0}^{z_{\max}} A_z \cdot T(z, t) dz \quad (1)$$

Fig. 1 shows temperature profiles with continuous temperature-increases in the hypolimnion of Lake Lugano during the last 6 years with an observed increase in temperature of $0.025 \text{ }^{\circ}\text{C a}^{-1}$. ΔW has been calculated as $5.0 \cdot 10^{12} \text{ J}$.

If it is assumed that a temperature-increase can only be accounted for by vertical diffusion, the internal heat is given by Fickian's first law, thus K_z can be calculated from:

$$K_z = \frac{\frac{\partial W}{\partial t}}{A_0 \cdot c_p \cdot \rho \frac{\partial T}{\partial z}|_{z_0}} = \frac{\int_{z_0}^{z_{\max}} A_z \cdot \frac{\partial T}{\partial t} dz}{A_z \frac{\partial T}{\partial z}|_{z_0}} \quad (2)$$

This method gives reasonable values for the topmost 70m (reduced to stratified hypolimnion), below this depth intrusions of warmer water occur regularly as it can be seen in Fig. 1. Below the regions where calculations by temperature fail, a parametrisation of bicarbonate HCO_3^- by conductivity profiles has been utilised to determine K_z by the same method. The distribution of bicarbonate seems to be less sensitive to local intrusions (Fig.2.).

Budgets and advection

Using the K_z -coefficients for determining the change in heat content at 250m reveals only a mean change in temperature in of $0.013 \text{ }^{\circ}\text{C a}^{-1}$ by diffusive inputs of $F_{\text{geo}} = 0.097 \text{ W m}^{-2}$ and $F_{\text{hypo}} = 0.109 \text{ W m}^{-2}$. If our calculations are correct, there should be a increase in temperature of $0.025 \text{ }^{\circ}\text{C a}^{-1}$. When the advection of lateral intrusions are not accounted within the budget-calculation, 0.9 % of heat-input is missing. That corresponds to $4.3 \cdot 10^8 \text{ m}^3$ of water or 10 % of lake water volume, renewed within 6 years.

To get further information about lateral intrusions we have to run a budget about each compartment in the lake. Phosphorus as the limiting nutrient is an appropriate parameter having been measured in particulate and dissolved forms assuming a steady state situation. Measurements in sediments of hypolimnetic traps and core-analysis gave the net-sedimentation-fluxes and the amount of redissolution or lateral input. Fig.3 shows fluxes and accumulations. Together with the diffusivities we get dissolutions of 74 % (28 t a^{-1}) of total particulate phosphorus. 26 % of total input (7 t a^{-1}) of PP come from lateral intrusions, while 72 % (26 t a^{-1}) of total input flows back to the epilimnion.

Lateral intrusions and diffusion account for 1-26 % and 72-98 % of input by heat and nutrients respectively. Nutrient budgets with steady state flow situations show backward general outflows of 68 % into the epilimnion by diffusion. Former measurement of Kz diminish the diffusive outflow and leads to an accumulation of 48 % of total particular inputs (15 t a^{-1}). In contrast the external budget shows a depletion of phosphorus in the lake of $30 \pm 42 \text{ t a}^{-1}$. That shows a better agreement with the internal budgets as shown in Fig.3 ($+ 4 \text{ t a}^{-1}$). Calculations in redissolution-chemical-reactions are only possible when comparing vertical and horizontal advective fluxes with vertical diffusion.

References

- Csanday G.T. (1973): Turbulent Diffusion in the environment. Reidel Publ. Company Dordrecht
- Fischer, H.B. List, E.J. Roh, R. Imberger, J. and Brooks, N. (1979): Mixing in inland and coastal waters, Academic Press New York
- Imboden, D.M. and Wüest, A. (1995): Mixing Mechanism in Lakes; in Lerman A. (edit.) Physics and Chemistry of Lakes. Springer New York
- Reichert, P. (1994): AQUASIM- a tool for simulation and data analysis of aquatic systems. Water Sci. Tech., 30: 21-30.
- Wüest, A. Imboden, D.M. and Schurter, M. (1988): Origin and size of hypolimnetic mixing in Urnersee, the southern basin of Vierwaldstättersee (Lake Lucerne). Schweiz. Z. Hydril. 50: 40-70

Temperature-Increase '90-'96

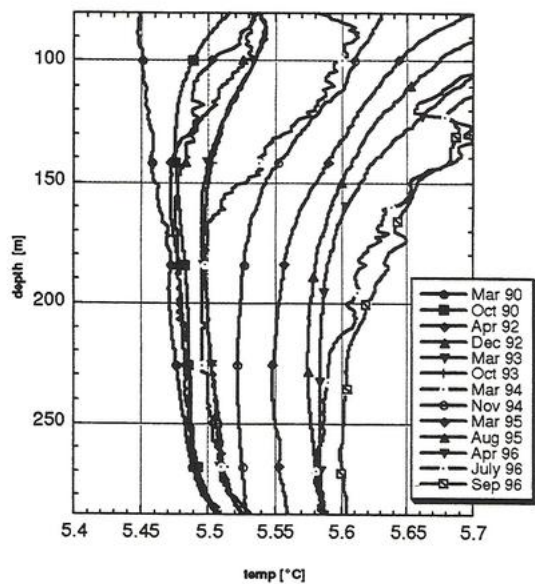


Fig.1: temperature-profiles with continuous temperature-increases in the hypolimnion of Lake Lugano during the last 6 years with a mean increase of 0.025 °C a¹. Relicts of deepwater-intrusions in july and september 1996

Diffusion-coefficients '90-'96

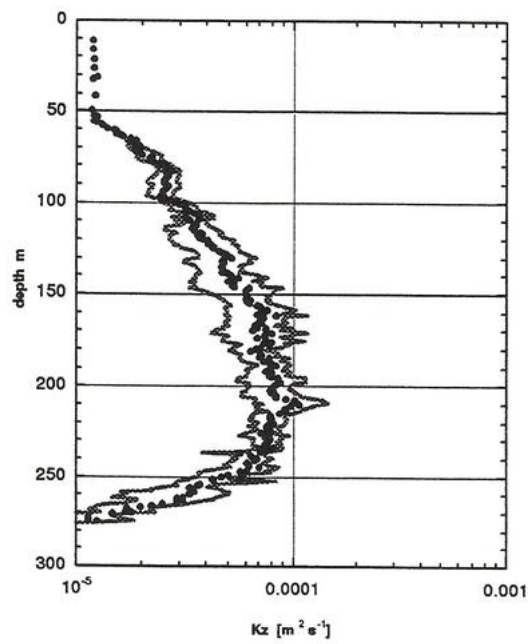


Fig.2: Kz-diffusion-coefficients of κ_{20} - (70-288 m) and temperature- (10-70 m) data

P-Fluxes 1985-1996

italic: g m⁻² a⁻¹
 normal: t a⁻¹

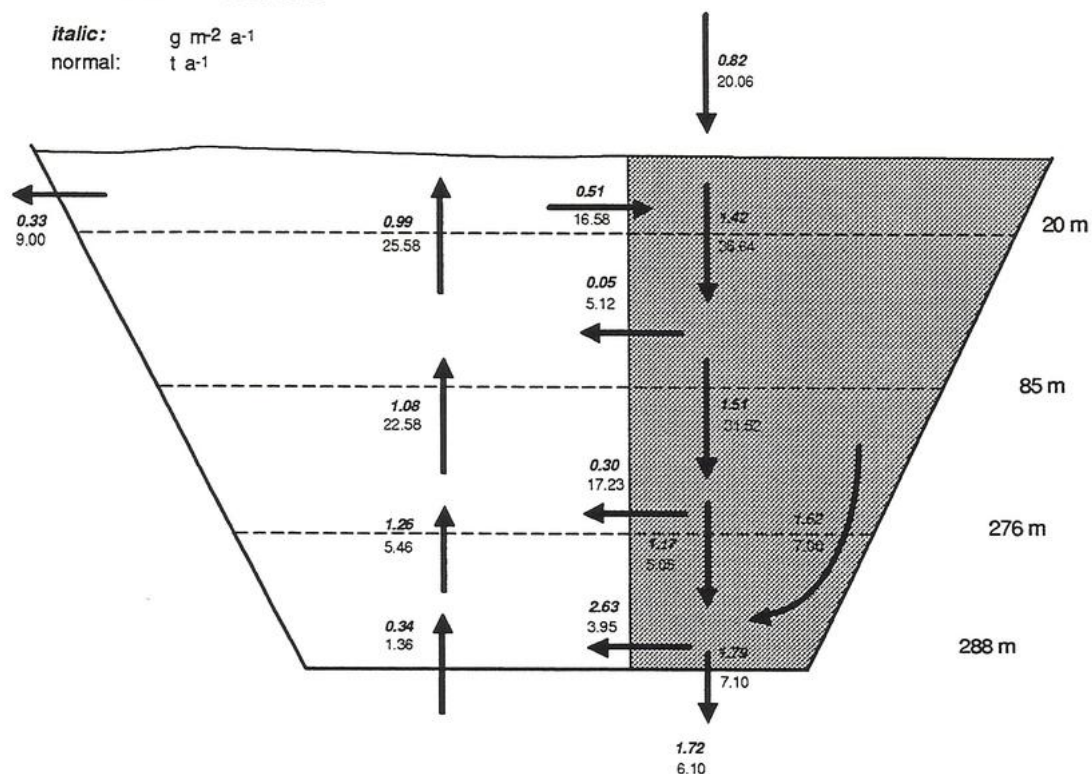


Fig.3: accumulations and fluxes of particular and dissolved phosphorus. The shaded area: particular forms.

